A SINGLE-PIXEL GHOST SHADOW IMAGING WITH THE INFLUENCE OF THE CHARACTERISTICS OF LIGHT SOURCE PROFILES AND A THEORETICAL DISCUSSION ON ENTANGLEMENT GENERATION USING LINEAR-OPTICAL ELEMENTS

THEERAPHOT SRIARUNOTHAI

A THESIS SUBMITTED IN PARTIAL FULFILLMENT
OF THE REQUIREMENTS FOR
THE DEGREE OF MASTER OF SCIENCE (PHYSICS)
FACULTY OF GRADUATE STUDIES
MAHIDOL UNIVERSITY
2012

Thesis

entitled

A SINGLE-PIXEL GHOST SHADOW IMAGING WITH THE INFLUENCE OF THE CHARACTERISTICS OF LIGHT SOURCE PROFILES AND A THEORETICAL DISCUSSION ON ENTANGLEMENT GENERATION USING LINEAR-OPTICAL ELEMENTS

THEERAPHOT SRIARUNOTHAI

.....

Mr. Theeraphot Sriarunothai
Candidate

.....

Mr. Wisit Singhsomroje,
Ph.D. (Physics)
Major advisor

.....

Mr. Asawin Sinsarp,
Ph.D. (Engineering)
Co-advisor

.....

Mr. Withoon Chunwachirasiri,
Ph.D. (Physics)
Co-advisor

B. Mahaisavariya

.....

Prof. Banchong Mahaisavariya,
M.D., Dip Thai Board of Orthopedics
Dean
Faculty of Graduate Studies
Mahidol University

S. Dangtip

.....

Mr. Somsak Dangtip,
Ph.D. (Applied Nuclear Physics)
Program Director
Master of Science Program
in Physics
Faculty of Science
Mahidol University

Thesis

entitled

A SINGLE-PIXEL GHOST SHADOW IMAGING WITH THE INFLUENCE OF THE CHARACTERISTICS OF LIGHT SOURCE PROFILES AND A THEORETICAL DISCUSSION ON ENTANGLEMENT GENERATION USING LINEAR-OPTICAL ELEMENTS

was submitted to the Faculty of Graduate Studies, Mahidol University
for the degree of Master of Science (Physics)
on
January 30, 2012

THEERAPHOT SRIARUNOTHAI
.....
Mr. Theeraphot Sriarunothai
Candidate

.....
Mr. Worawarong Rakreungdet,
Ph.D. (Physics)
Chair

.....
Mr. Wisit Singhsomroje,
Ph.D. (Physics)
Member

.....
Mr. Withoon Chunwachirasiri,
Ph.D. (Physics)
Member

.....
Mr. Asawin Sinsarp,
Ph.D. (Engineering)
Member

.....
Prof. Banchong Mahaisavariya,
M.D., Dip Thai Board of Orthopedics
Dean
Faculty of Graduate Studies
Mahidol University

.....
Prof. Skorn Mongkolsuk,
Ph.D. (Biological Science)
Dean
Faculty of Science
Mahidol University

ACKNOWLEDGEMENTS

I would like to express my sincere gratitude to all those who give me the possibility to complete this thesis.

I would like to express my gratitude to my supervisor, Dr. Wisit Singhsomroje, for his supervision, encouragement, wise suggestion, and all kind helps all the time of research. He gave me his precious time sharing his experience and guidance to work on this research. I am also highly grateful to Dr. Worawarong Rakreungdet, Dr. Asawin Sinsarp, Dr. Sujin Suwanna, and Dr. Withoon Chunwachirasiri for giving their invaluable suggestions. I gratefully acknowledge Development and Promotion of Science and Technology Talent Project (DPST) for all supports.

I greatly appreciate LaTeX template by Asst. Prof. Michael Allen, Mr. Tawat Rung-arunwan and Mr. Nattapong Kamyan.

For practical help and encouragement, I would like to thank the members of Collaborative Research Unit on Quantum Information, Mahidol University, especially Mr. Ekkarat Pongophas for exchanging ideas.

Finally, it is a pleasure to express my gratitude wholeheartedly to everyone whose support me to complete this work.

Theeraphot Sriarunothai

A SINGLE-PIXEL GHOST SHADOW IMAGING WITH THE INFLUENCE OF THE CHARACTERISTICS OF LIGHT SOURCE PROFILES AND A THEORETICAL DISCUSSION ON ENTANGLEMENT GENERATION USING LINEAR-OPTICAL ELEMENTS .

THEERAPHOT SRIARUNOTHAI 5237425 SCPY/M

M.Sc. (PHYSICS)

THESIS ADVISORY COMMITTEE : WISIT SINGHSOMROJE, Ph.D. (PHYSICS), ASAWIN SINSARP, Ph.D. (ENGINEERING), WITHOON CHUNWACHIRASIRI, Ph.D. (PHYSICS)

ABSTRACT

This thesis is divided into two parts. The first part presents an imaging technique, called "Ghost Shadow Imaging (GSI)". The second part consists of a theoretical discussion on entanglement generation using linear-optical elements.

In GSI, an image can be constructed by light without any information on the spatial resolution of an object. This image construction is inspired by Quantum Imaging, or the Ghost Imaging (GI) as described by Pittman *et al* (1995). The difference between GSI and GI is the construction process. GSI uses intensity correlations instead of the coincidence registers of two-photon states in the detection system used by GI. The experimental study demonstrates the GSI scheme with the resulting constructed images. The extended study shows the possibility for using a non-spatial-resolution detector solely in the imaging system. Additionally, the quality of the constructed images is also considered through a computer model simulating the experimental scheme. It has been found that there is an influence on the constructed images caused by the light source in the system. By this consideration, an optimal parameter is obtained to achieve the best constructed image.

The theoretical portion of the thesis discusses the schemes for entanglement generations based on linear-optical elements is discussed. The schemes result in the generation of four-photon entangled states and the heralded generation of biphoton entangled states. The entanglement generations in these schemes can be achieved with high efficiencies compared to some of the other schemes involving nonlinear-optical elements.

KEY WORDS : GHOST SHADOW IMAGING/CORRELATED IMAGING/
SINGLE-PIXEL DETECTOR IMAGING/
HERALD ENTANGLEMENT/MULTIPARTITE ENTANGLEMENT

89 pages

การสร้างภาพโกสต์ชาโดว์ (Ghost Shadow) แบบจุดภาพเดี่ยวและผลกระทบของรูปแบบแหล่งกำเนิดแสงและการศึกษาการกำเนิดสภาวะพัวพันด้วยอุปกรณ์ทัศนศาสตร์เชิงเส้น
A SINGLE-PIXEL GHOST SHADOW IMAGING WITH THE INFLUENCE OF THE CHARACTERISTICS OF LIGHT SOURCE PROFILES AND A THEORETICAL DISCUSSION ON ENTANGLEMENT GENERATION USING LINEAR-OPTICAL ELEMENTS

ธีรพจน์ ศรีอรุโณทัย 5237425 SCPY/M

วท.ม. (ฟิสิกส์)

คณะกรรมการที่ปรึกษาวิทยานิพนธ์ : วิศิษฐ์ สิงห์สมโรจน์, Ph.D. (PHYSICS), อัศวิน สินทรัพย์, Ph.D. (ENGINEERING), วิทูร ชื่นวชิรศิริ, Ph.D. (PHYSICS)

บทคัดย่อ

วิทยานิพนธ์ฉบับนี้แบ่งเป็นสองส่วนใหญ่ด้วยกัน ส่วนแรกนำเสนอเทคนิคการถ่ายภาพที่เรียกว่า “Ghost Shadow Imaging” ส่วนที่สองคือการพิจารณาเชิงทฤษฎีสำหรับการก่อกำเนิดสถานะพัวพันโดยใช้อุปกรณ์ทัศนศาสตร์เชิงเส้น

ในการถ่ายภาพแบบ Ghost Shadow Imaging ภาพจะถูกสร้างด้วยแสงที่ไม่มีข้อมูลการจำแนกเชิงตำแหน่งของวัตถุ ซึ่งการถ่ายภาพแบบนี้ได้รับแรงบันดาลใจจากการถ่ายภาพเชิงควอนตัม หรือ Ghost Imaging โดย Pittman *et al* (1995) ความแตกต่างระหว่างการถ่ายภาพทั้งสองคือขบวนการสร้างภาพ โดย Ghost Shadow Imaging จะใช้วิธีสหสัมพันธ์เชิงความเข้มแทนที่โฟตอนที่มาถึงพร้อมกันของสถานะโฟตอนคู่ที่ใช้ในระบบของ Ghost Imaging ในส่วนแรกของวิทยานิพนธ์แสดงการศึกษาเชิงการทดลองของระบบ Ghost Shadow Imaging พร้อมผลของการสร้างภาพ และยังขยายการศึกษาสู่โอกาสในการถ่ายภาพด้วยเซลล์รับแสงเดี่ยวนิ่ง และคุณภาพของภาพที่ถูกสร้างโดยศึกษาผ่านแบบจำลองทางคอมพิวเตอร์ที่สอดคล้องกับรูปแบบการทดลอง ซึ่งพบว่าแหล่งกำเนิดแสงมีผลต่อการสร้างภาพในระบบ ด้วยการพิจารณานี้ทำให้ได้เงื่อนไขภาพที่ดีที่สุดมา

สำหรับส่วนที่สองของวิทยานิพนธ์ ทำการศึกษาเชิงทฤษฎีของรูปแบบการก่อกำเนิดสถานะพัวพันด้วยพื้นฐานระบบทัศนศาสตร์เชิงเส้น ระบบที่ได้คือ ระบบการสร้างสถานะสี่โฟตอนพัวพันและระบบการก่อกำเนิดแบบประกาศสำหรับสถานะโฟตอนคู่พัวพัน ระบบการก่อกำเนิดเหล่านี้ให้ประสิทธิภาพดีกว่าเมื่อเทียบกับระบบอื่นที่ใช้อุปกรณ์ทัศนศาสตร์ไม่เชิงเส้น

89 หน้า

CONTENTS

CONTENTS (cont.)

CONTENTS (cont.)

LIST OF TABLES

LIST OF FIGURES

LIST OF FIGURES (cont.)

LIST OF FIGURES (cont.)

LIST OF FIGURES (cont.)

LIST OF FIGURES (cont.)

PROJECT I
GHOST SHADOW IMAGING

CHAPTER I
INTRODUCTION

1.1 Overview

A physical object can be interpreted and represented by the information of itself. Information that is stored a physical appearance of the object is projected by its image. In order to store information of an image, an imaging system was developed through an understanding of classical optics. Thus, an image is the information that can be obtained by an imaging system representing a physical appearance of the object. In general, an image can be constructed by the illuminating light reflecting from or passing through the object which has to arrive at a sensible sensor like eyes or a spatial-resolution detector. The most common and simple imaging is the optical imaging whose theory has been well developed classically. An image formation is constructed from the point-to-point relationship between the object and the image at the image plane.

Recently, there is another imaging system that cannot be described by classical optics. This imaging was demonstrated by Pittman *et al* in 1995 (Pittman *et al.* 1995). It is called "Ghost imaging" (GI). This technique has difference from what we have known. An image can be constructed indirectly not using the light from the object. In summary, GI is an imaging technique utilizing correlation measurements. According to Shih's article (Shih 2008), GI can be characterized into two types. Type-one GI is demonstrated by entangled photon pairs as a light source. Type-two GI is demonstrated by a chaotic light source. Type-one GI was understood to be a direct result from the behavior of the entangled state of the source, while Type-two GI has to be thought in a different manner. Thus, the interpretations of the process as being a classical (Gatti *et al.* 2004a,b; Wang & Cao 2004; Cao *et al.* 2005; Cai & Zhu 2005; Erkmen & Shapiro 2008) or quantum (Scarcelli *et al.* 2007; Shih 2007) phenomenon are still under discussion.

GI give us an inspiration to another imaging system using its concept. The same idea is the correlation between two detectors, but arrival times of photons at each detector are changed to intensity. The intensity of two detectors are correlated to construct an image. The new imaging system is called "Ghost Shadow Imaging" (GSI), which is studied in this thesis.

1.2 Objectives

The first part of this thesis focuses on another imaging system, which is called GSI. The main proposes of this thesis are:

1. To demonstrate another imaging system for an image construction of an object.
2. To make possible the use of only one non-spatial-resolution detector for constructing an image of an object.
3. To study the influence of the light source in GSI.
4. To study the optimal parameters to give the best constructed image.

1.3 Outline

The first part of this thesis is organized into four chapters. Chapter 2 introduces imaging systems. There are short concepts for each mentioned imaging system including the image formation of GSI. Chapter 3 is an experimental study of GSI. It contains (i) a basic construction of an image by GSI system with experimental results, (ii) making possible the use of a single-pixel detector for constructing an image with experimental results, and (iii) showing an example to describe why an image can be construct using GSI scheme. Chapter 4 is a simulation study of GSI. It focuses on intensity profiles of the GSI system. It contains (i) an imitation of the light source profiles by Gaussian convolution model, and (ii) the influence of varying these profiles on the image formation of GSI. Finally, chapter 5 discusses the conclusions.

CHAPTER II
BACKGROUND KNOWLEDGE

In this chapter, the concept of imaging systems is given. An optical imaging, a ghost imaging, and a ghost shadow imaging are described here along with the background behind a construction of an image in each system.

2.1 Optical Imaging

An image is constructed from the point-to-point relationship between the object and the image at the image plane according to Fig 2.1. The light of a single point of the object goes to a single point in the imaging plane. This image is like a mapping of the object because of the constructive interference of the waves from the electrodynamics point of view. In quantum physics point of view, a photon, the quantization of a light wave, from each point of the object has the largest probability to arrive at a specific point on the image plane. Between those two points, a photon has many possible routes to take. Therefore, the interference of the wave function of photon has to be considered. On the image plane, this is the constructive interference of the wave function of photon, thus the image is constructed at the image plane.

Simply, optical imaging, see Fig. 2.1, can be described by the "Gaussian thin lens equation"

$$\frac{1}{f} = \frac{1}{s_o} + \frac{1}{s_i} \tag{2.1}$$

where s_o is the distance between the imaging lens and the object, s_i is the distance between the imaging lens and the image plane, and f is the focal length of the imaging lens.

In the case of any plane out of the image plane (or off-image plane), each electromagnetic field comes to this plane distinguishably. Thus, an interference effect

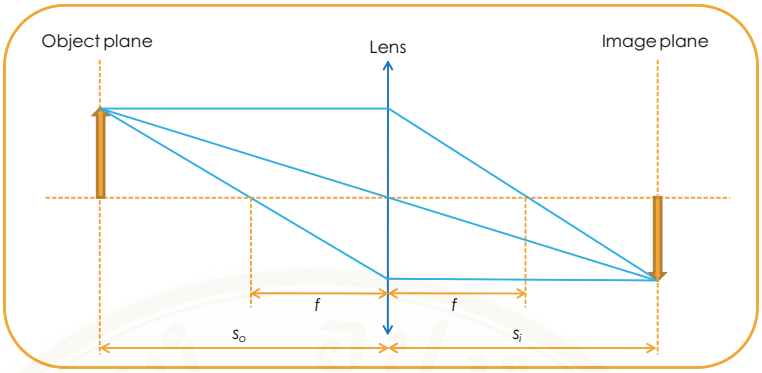

Figure 2.1: Optical imaging. A simple description is followed by the Gaussian thin-lens equation, $\frac{1}{f} = \frac{1}{s_o} + \frac{1}{s_i}$. Classically, an image formation is constructed from a point-to-point relationship between the object and the image. According to the figure, light from a certain point of the object is projected to another certain point at the image plane. For example, if the image is found to be the head of the arrow at the image plane, then the light that is gathered here must come from only the head of arrow. This is similar to the other points of the image.

does not take place. A point on this plane fills up with the intensity from any point of the object plane. This situation has to be considered as a summation of intensities in electrodynamics point of view. In quantum physics point of view, the wave function of photon has to interfere with itself (Dirac 1982). Thus, an image of any off-image plane is constructed from all added up probabilities of photons which can go to a considered plane; these are summations of the probabilities of photons. The summations cannot obtain the image of the object from this formation. In this work, this optical imaging is called "conventional imaging" (CI) .

2.2 Ghost Imaging

In 1995, the first GI was demonstrated by Pittman *et al.* (Pittman *et al.* 1995) Originally, an image of an object through GI scheme can be constructed using two detectors, which are a detector without any spatial resolution to collect the light behind the object and a detector with spatial resolution to collect the light from the given light source. These two detectors must have the ability to know numbers of photons in the measuring time.

An image was constructed in the setup schematically shown in Fig. 2.2.

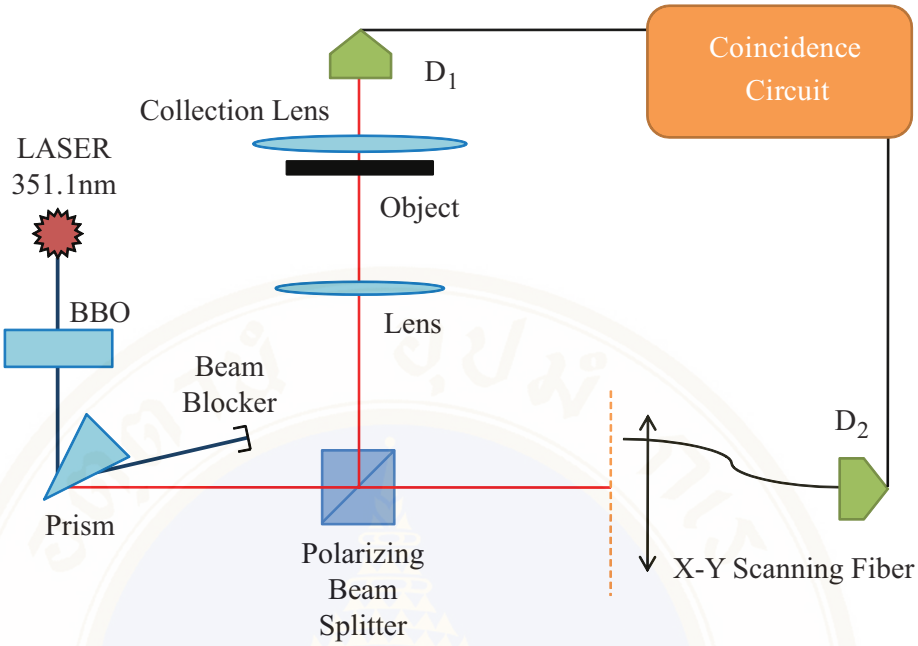

Figure 2.2: The first experimental setup of ghost imaging was demonstrated by Pittman *et al.* They used entangled photon pairs as a light source which is produced by a BBO type-II crystal.

This demonstration was performed and achieved based on the quantum nature of the light source. The entangled photon source, a quantum light source, was a nonlinear beta-bariumborate (BBO; β-BaB_2O_4) type-II crystal in the spontaneous parametric down-conversion (SPDC) process. The BBO crystal was pumped by a continuous wave (CW) laser and gave pairs of daughter photons. These daughter photons were set to be an entangled pair of orthogonally polarized photons. The entangled photon pairs were then separated by a polarizing beam-splitter (PBS) . The reflected photons, namely the signal, passed through an aperture to be collected by a bucket detector package D_1. The aperture was the object whose image was to be constructed. The transmitted photons, namely the idler, passed through the beam-splitter and were directly collected with a spatial resolution detector D_2. The collection time and numbers of photons on the detector D_1 or D_2 did not give any information about the image of the object. Certainly, there was no image to be constructed from either one of the detectors alone. However, an image was constructed by joint-detections between detector D_1 and detector D_2. This image construction was explained by using the behavior of the entangled state of the

entangled photon pair.

Joint-detection was also known as "coincidence detection". It means that two (or more) photon-counters register two (or more) photons simultaneously. In the image construction of GI scheme, joint-detection counts come from pairs of photons passing the object because of the properties of the entangled photon. The generation of entangled photon pairs indicates that the photon pairs are generated simultaneously.

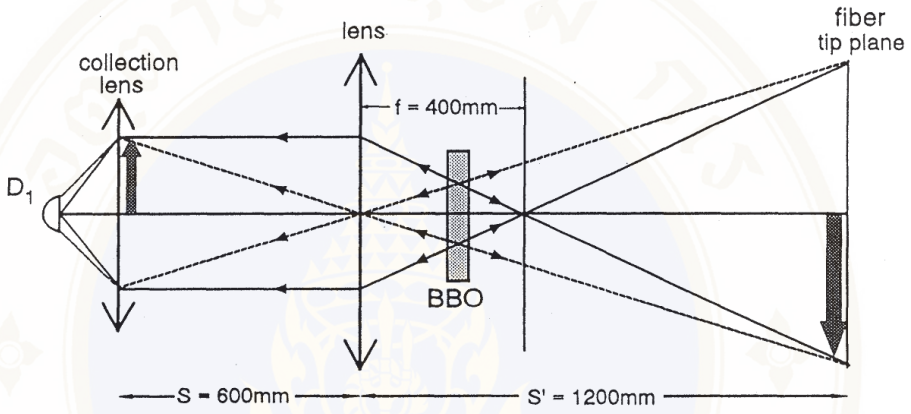

Figure 2.3: Conceptual "unfolded" version of the setup shown in Fig. 2.2.

GI scheme with entangled photon source can be described and shown in Fig. 2.3. The entangled photons were selected in case of degenerate case of SPDC process. Photon pairs were separated with the same magnitude of angle oppositely. With the angle of this splitting, each direction of photons can be represented by a straight line in the unfolded diagram. The trajectories of photons were consistent with the Gaussian thin lens equation. Therefore, GI scheme with entangled photon source can be understood by the generation of entangled photon and the Gaussian thin lens equation.

2.3 Ghost Shadow Imaging

The idea of GI gives an inspiration to another method for image formation, namely GSI. This is the work in the first part of this thesis. GSI is demonstrated in the following chapter to construct an image by the correlations between intensity behind the object and the intensity profiles of the light source.

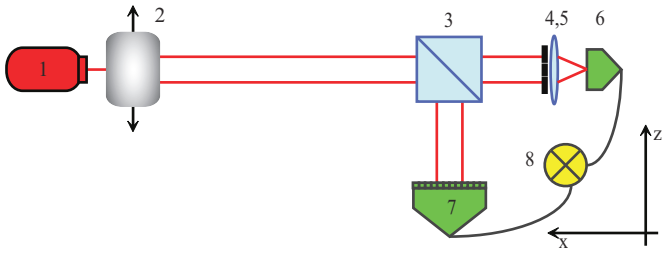

Figure 2.4: The Schematic setup. (1) Laser, (2) Intensity modulator, (3) Beam-splitter, (4) Double slit (Object), (5) Collection lens, (6) Single-pixel detector, (7) Spatial-resolution detector, and (8) Correlator.

The experimental setup of GSI is shown in Fig. 2.4. The laser beam is randomly modulated by an intensity modulator such that source becomes a pseudothermal light. The beam is split into two paths by a polarization-independent beam-splitter. The reflected path is collected by a spatial-resolution detector, which is placed at a certain distance from the beam-splitter. (A spatial-resolution detector can be either one-dimensional or two-dimensional.) By the collection, the spatial-resolution detector can only provide the spatial intensity profile of the source. The transmitted path of the laser beam passes through double slits, the object to be imaged, placed at the same distance from the beam-splitter as that of the spatial-resolution detector. The beam after the slits is then collected by a bucket detector, which has no spatial information. Generally, the bucket detector can only provide information about the total intensity of the light beam after the object. To form an image of the object, the correlation of two parts of information, one from the spatial-resolution detector and one from the bucket detector, is calculated according to the equation

$$G(x) = \frac{1}{N}\sum_{i=1}^{N} I_i(x)(B_i - \langle B\rangle), \tag{2.2}$$

where i is the step of the intensity modulation, $I_i(x)$ is the intensity at the x^{th} pixel of the spatial-resolution detector at the step i^{th}, B_i is the intensity reported by the bucket detector at the step i^{th}, and $\frac{1}{N}\sum_i \cdot$ denotes an ensemble average over the N steps of the intensity modulation.

In GSI scheme, an image of an object can also be constructed by correlations between two detectors, according to Eq. 2.2. The image of GSI scheme is obtained indi-

rectly by correlation like GI. The image can be either one-dimensional or two-dimensional depending on a spatial-resolution detector in the system.

CHAPTER III
EXPERIMENTAL METHODS AND RESULTS

This chapter focuses on the experimental study of an image construction of GSI system. It contains (i) a basic construction of an image by a GSI system with corresponding experimental results, (ii) an investigation of conditions of the successfully constructed images, (iii) a modification of the system to use a single-pixel detector in the system, and (iv) an image construction mechanism model describing how an image is constructed by the calculation of correlation.

3.1 Basic Ghost Shadow Imaging

In this section, the proposed imaging technique is shown with corresponding results of the constructed images. According to the concept of GSI given in Sec. 2.3, GSI experimental scheme requires two set of data from two detectors. The first detector, which is a spatial-resolution detector, records an intensity profile per step of a spatial intensity modulation. In this experiment, the spatial-resolution detector is a linear-arrays CCD detector. It can collect one-dimensional intensity profiles. The second detector, which is a non-spatial-resolution detector integrating with a convex lens, acts as a bucket detector. It records all unblocking light behind the object per step of a spatial intensity modulation. In this experiment, a step-moving ground glass is used as a spatial intensity modulation in the system.

3.1.1 Preparation of Intensity Profiles

In GSI imaging system, a spatial intensity modulation is expected to be random on each spatial element of light plane recorded by a linear-arrays CCD detector. This randomness is consistent with the creation of photon pairs from BBO in GI scheme.

Normally, a spatial intensity modulation is done by a rotating diffuser or a computer-controlled spatial light modulator (Bromberg *et al.* 2009). However, a step-moving ground glass is chosen as a modulator in this experiment, because it can be used to control light patterns by referring to the position of the ground glass and it is cheaper than a computer-controlled spatial light modulator. For the structure of a piece of ground glass, a grain size of the ground glass has to be considered. This size corresponds to an output of spatial light pattern that passes through a piece of ground glass. The disadvantage of using a piece of ground glass as a modulator is the fact that a step size must be greater than a grain size of ground glass to achieve variation of intensity patterns to be collected intensity profiles.

The consideration of ground glass is demonstrated by the following. A laser is aligned and focused on a piece of ground glass, which is standing on a motor-controlled translation stage. The light is collected by a linear-arrays CCD detector. This scheme is shown in Fig. 3.1. The recorded light as light source profiles come from each translation

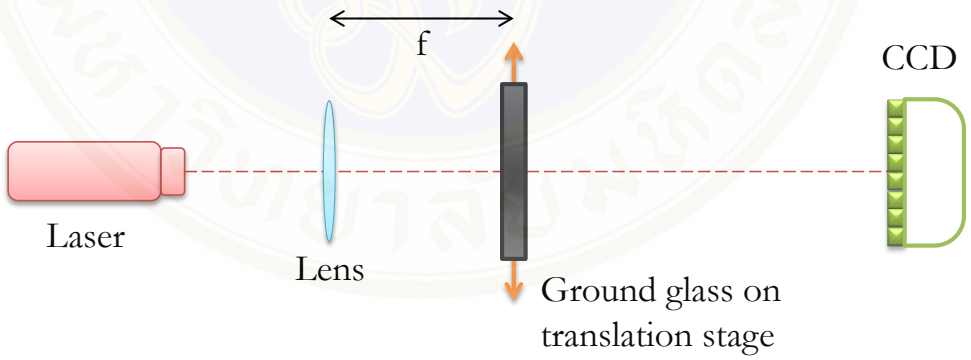

Figure 3.1: The schematic setting of collection intensity profiles from a piece of ground glass. A laser focuses on the ground glass, which is standing on a motor-controlled linear-translation stage. By moving a position of the ground glass, the focusing light of the laser projects on another region on the ground glass, thus the light intensity is modulated spatially. The records of profiles come from steps of translation of the ground glass, which give patterns of intensity.

step of the ground glass. By using 0.02 mm step size, the intensity profiles are shown in Fig. 3.2. To determine whether the step size is enough for varying patterns in the intensity profile, the correlations[1] between two patterns in the same intensity profiles

[1]This is calculated by a correlation function. See more in appendix B.

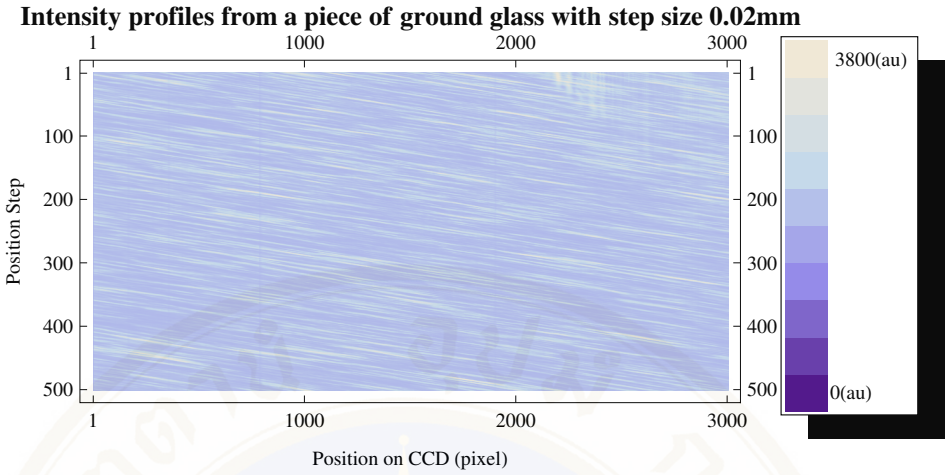

Figure 3.2: An example of intensity profiles collecting from a piece of ground glass with step size 0.02 mm. For each step, an one-dimensional pattern is recorded to 3,000 pixels of CCD. 500 intensity patterns are recorded in this intensity profile.

are calculated. The calculation is obtained from all combinations of two patterns out of 500 recorded patterns in the intensity profile and shown in Fig. 3.3, when the correlation mean is 0.005596 and the correlation standard deviation is 0.1077. The correlation function has a range between -1 to 1. The correlation value 1 shows completely correlated trend between two considering patterns. The correlation value -1 shows completely anti-correlated trend between two considering patterns, which is correlated conversely. If the absolute value of the correlation value is calculated, the completely correlated trend and the completely anti-correlated trend give 1. When the correlation value equals 0, two considering patterns are uncorrelated. When the absolute correlation value is calculated, the value lies between 0 to 1, which show uncorrelated two considering trends to correlated two considering trends. The correlation results of any two patterns in the intensity profile show the absolute value of correlation mean is 0.08320 and the absolute value of correlation standard deviation is 0.06863. These reported values, which are close to 0, show the uncorrelation between any two intensity profiles.

3.1.2 Experimental Scheme

The experimental scheme is set following the ideal concept as shown in Sec. 2.3 of chapter 2. It is shown in Fig. 3.4. In this experiment, a double slit is

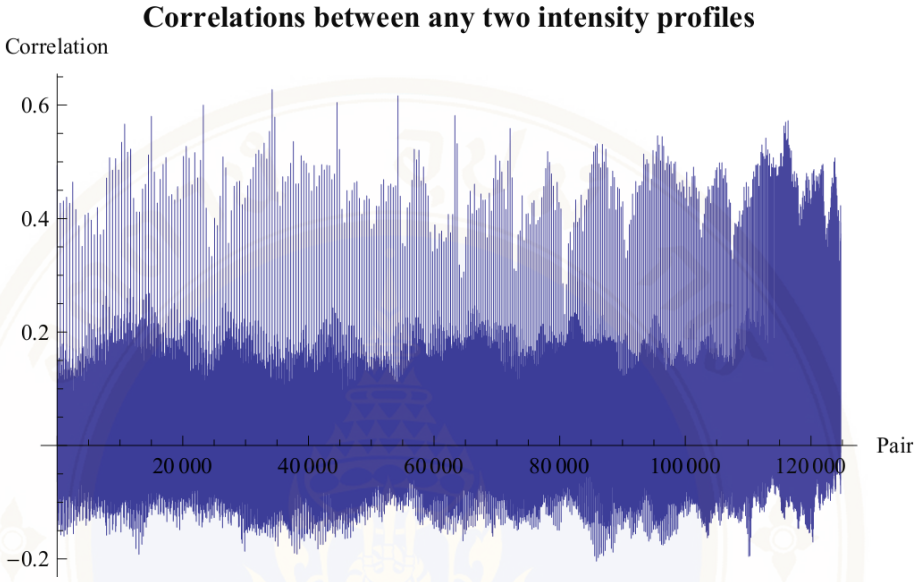

(a) Correlation

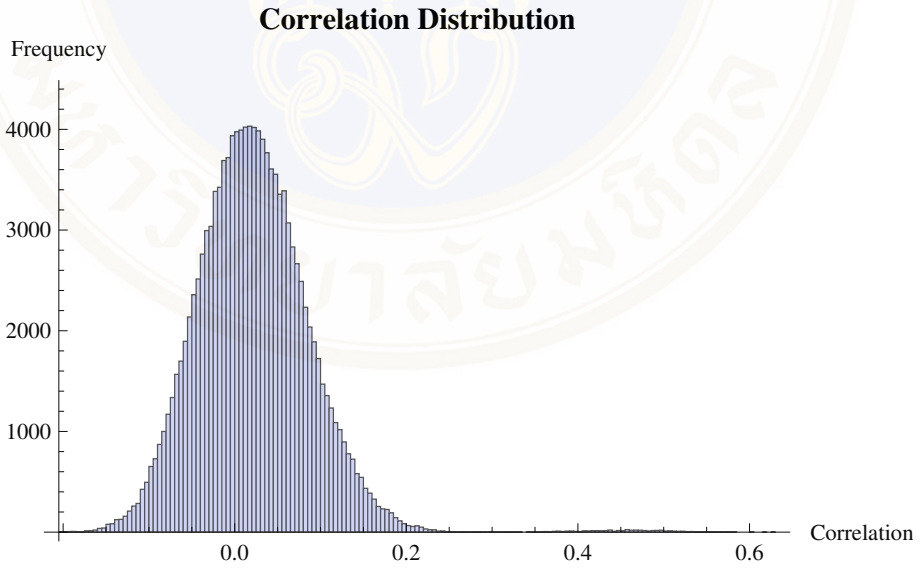

(b) Correlation Distribution

Figure 3.3: (a) The calculation results of correlation between all combinations of two intensity profiles out of 500 recorded intensity profiles, when the correlation mean is 0.005596 and the correlation standard deviation is 0.1077. (b) Correlation distribution.

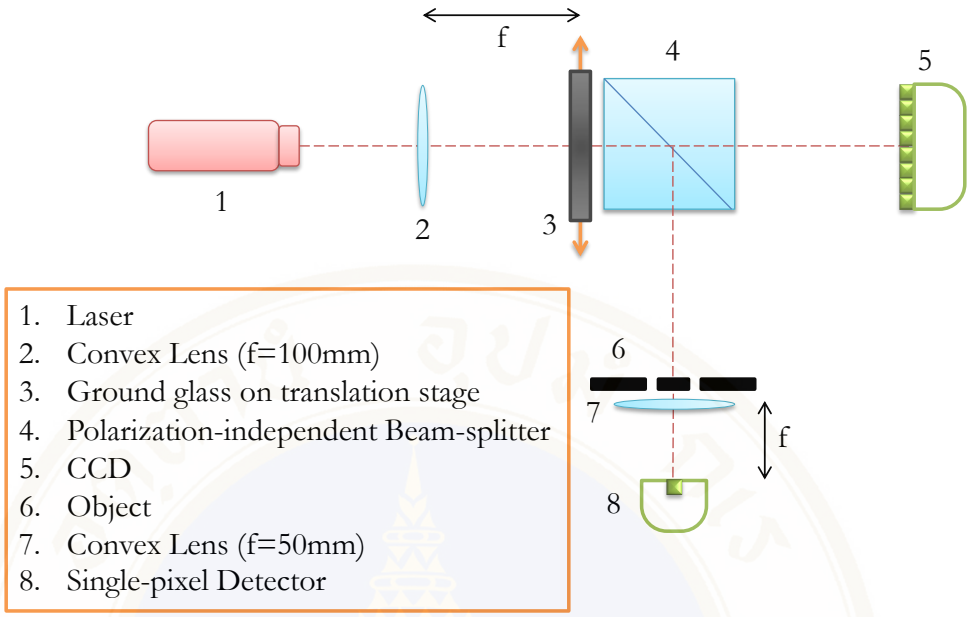

Figure 3.4: The experimental scheme of GSI. The system consists of (1) a laser, (2) a convex lens ($f = 100$ mm), (3) a piece of ground glass on translation stage, (4) a polarization-independent beam-splitter, (5) a spatial resolution detector (a linear-arrays CCD), (6) an object, (7) a convex Lens ($f = 50$ mm), and (8) a single-pixel detector (a non-spatial resolution detector)

chosen as an object, see Fig. 3.5. The double slit has an aperture size of 0.1 mm and an aperture separation of 0.5 mm. Laser, a narrow monochromatic light source, passes through and focuses on a piece of ground glass. The ground glass stands on a motor-controlled linear-translation stage. After passing through the ground glass, the light is split into two directions by a polarization-independent beam-splitter. In the first direction, the light is collected by a linear-arrays CCD detector as intensity profiles or light source profiles. In the second direction, the light is projected onto the object. All passing light through the object is focused and collected by a single-pixel detector.

3.1.3 Ghost Shadow Image Construction

According to the previous section, the experimental result is obtained by collections of two data; intensity profiles and intensity of the bucket detector. In this result, the data is collected 300 sets of modulation. The image construction is obtained by calculating with Eq. 2.2. The image is shown in Fig. 3.6. In this result, the image of

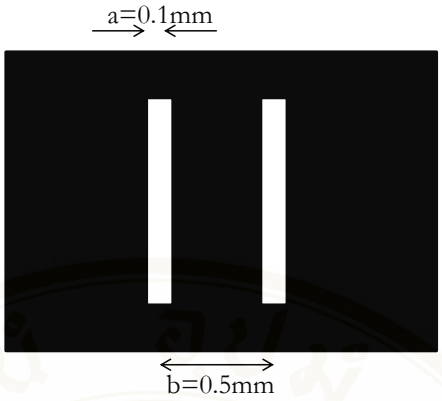

Figure 3.5: Double slit is chosen as an object in the system. The double slit has an aperture size of 0.1 mm and an aperture separation of 0.5 mm.

the double slit is not found distinctively.

In order to measure the quality of the constructed image, two quantities are defined. The first quantity is a discrepancy level, which is given by

$$\text{Discrepancy Level}(X,Y) = 1 - |\text{Corr}_{X,Y}(x_1, y_1)|\,, \tag{3.1}$$

in which the correlation function is made between the expected image of the object and the constructed image. X (or Y) is a list of one-dimensional data with elements $\{x_i\}$ (or $\{y_i\}$). The correlation $\text{Corr}_{X,Y}(x_1, y_1)$ is calculated by starting at the same sequence. Discrepancy level lies between 0 to 1. Discrepancy level 0 shows the absolute consistence between the object and the constructed image. The other quantity is noise-ratio which is given by

$$\text{Noise-Ratio} = \left|\frac{\text{error of background}}{\text{image level}}\right|, \tag{3.2}$$

where the error of background means the absolute value of standard error of background and the image level means the mean of values in the expecting image region related to the object. Noise-ratio also lies between 0 and 1. Noise-ratio 0 shows the greatest difference between image level and background level. The best image is expected to have discrepancy level 0 and noise-ratio 0.

The first constructed image in Fig. 3.6 gives discrepancy level 0.82829 and noise-ratio 0.0104915.

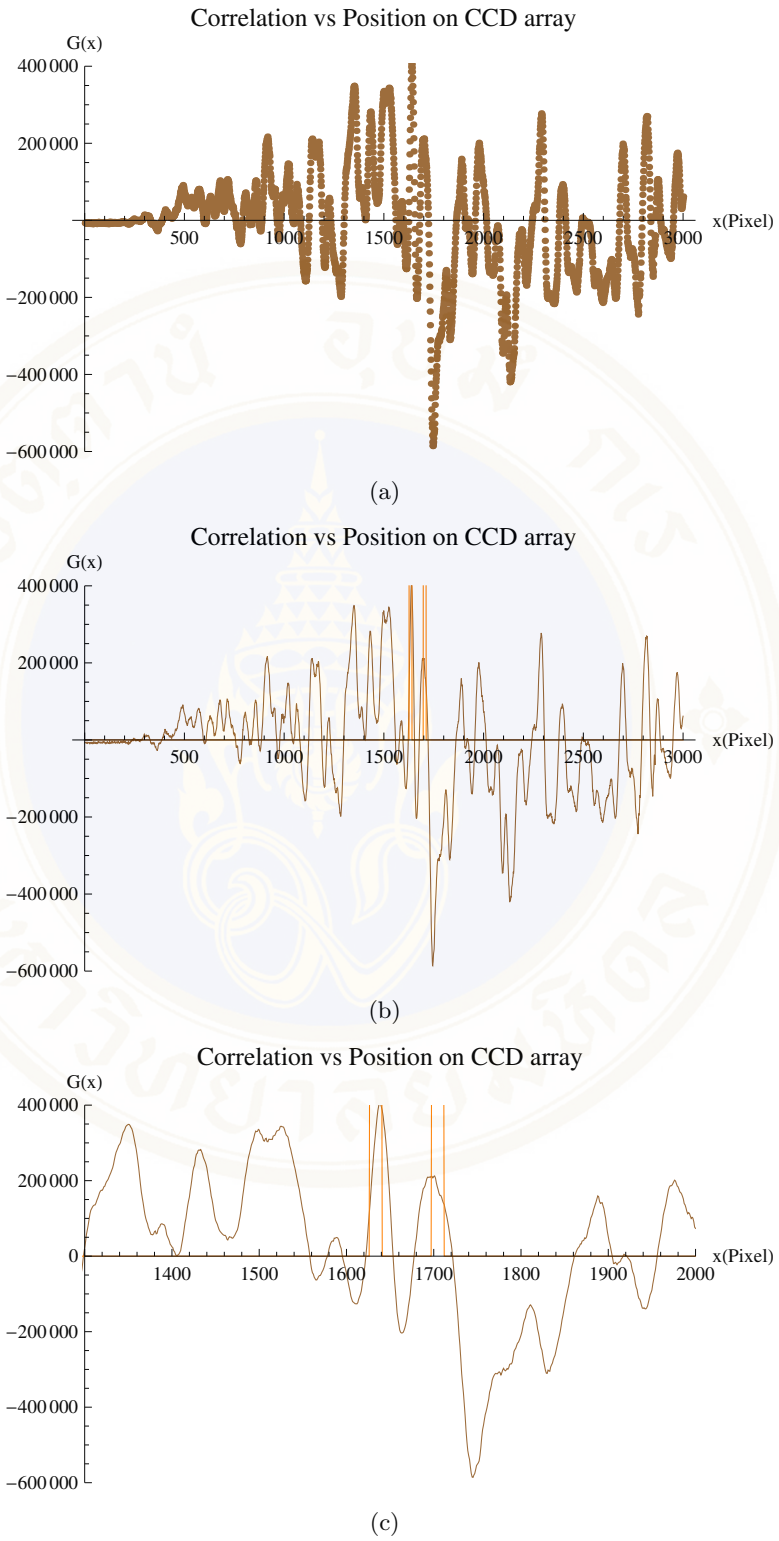

Figure 3.6: The constructed image with 300 sets of collected intensity profiles and intensity of the bucket detector. (a) Point plot of the constructed image. (b) Line plot of the constructed image comparing to the expected image of the double slit. (c) the zoom-in of the expected region of the constructed image. The constructed image shows discrepancy level 0.82829 and noise-ratio 0.0104915.

Next, the bucket detector, the lens and the single-pixel detector, is replaced by a linear-arrays CCD detector. Therefore, the experimental scheme is according to Fig. 3.7. In this experimental scheme, the constructed image is shown in Fig. 3.8.

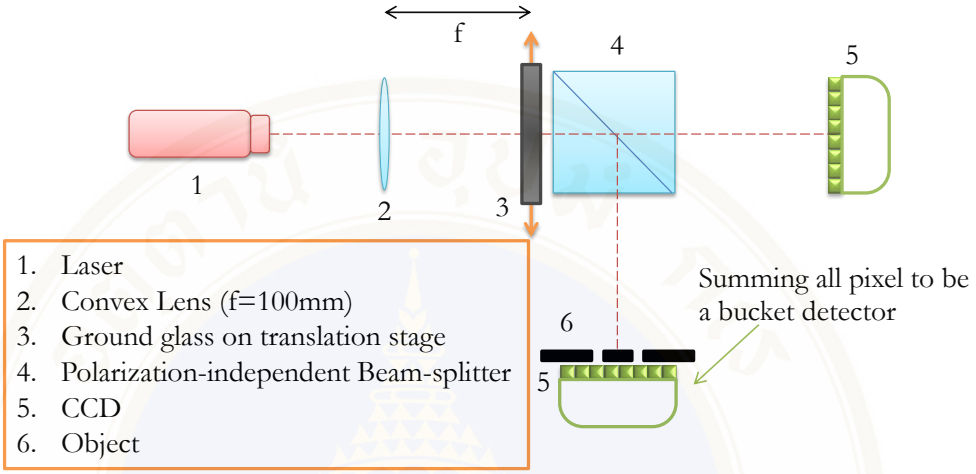

Figure 3.7: The second experimental scheme of GSI. The bucket detector is replaced by a linear-arrays CCD detector.

According to the result, the image can be constructed. The constructed image obtains discrepancy level 0.513537 and noise-ratio 0.0031292.

Comparing these two results together, they are obviously significantly different. Numerically, the second image gives a better quality parameters, which means it is a better-constructed image than the first image. For more detail, the changing of the detection method will be given in the next section.

3.1.4 Investigation of Conditions of the Successfully Constructed Image

According to the results of Fig. 3.6 and Fig. 3.8 in the last section, the same conditions are set except the bucket detector. The bucket detector from a single-pixel detector integrating with a lens is changed to a summing over all pixels of a linear-arrays CCD, which is also a non-spatial-resolution detector. An assumption is stated here from these two results of the constructed images. The assumption is any light out of the collecting area of intensity profiles, which are considered by the size of the CCD, are

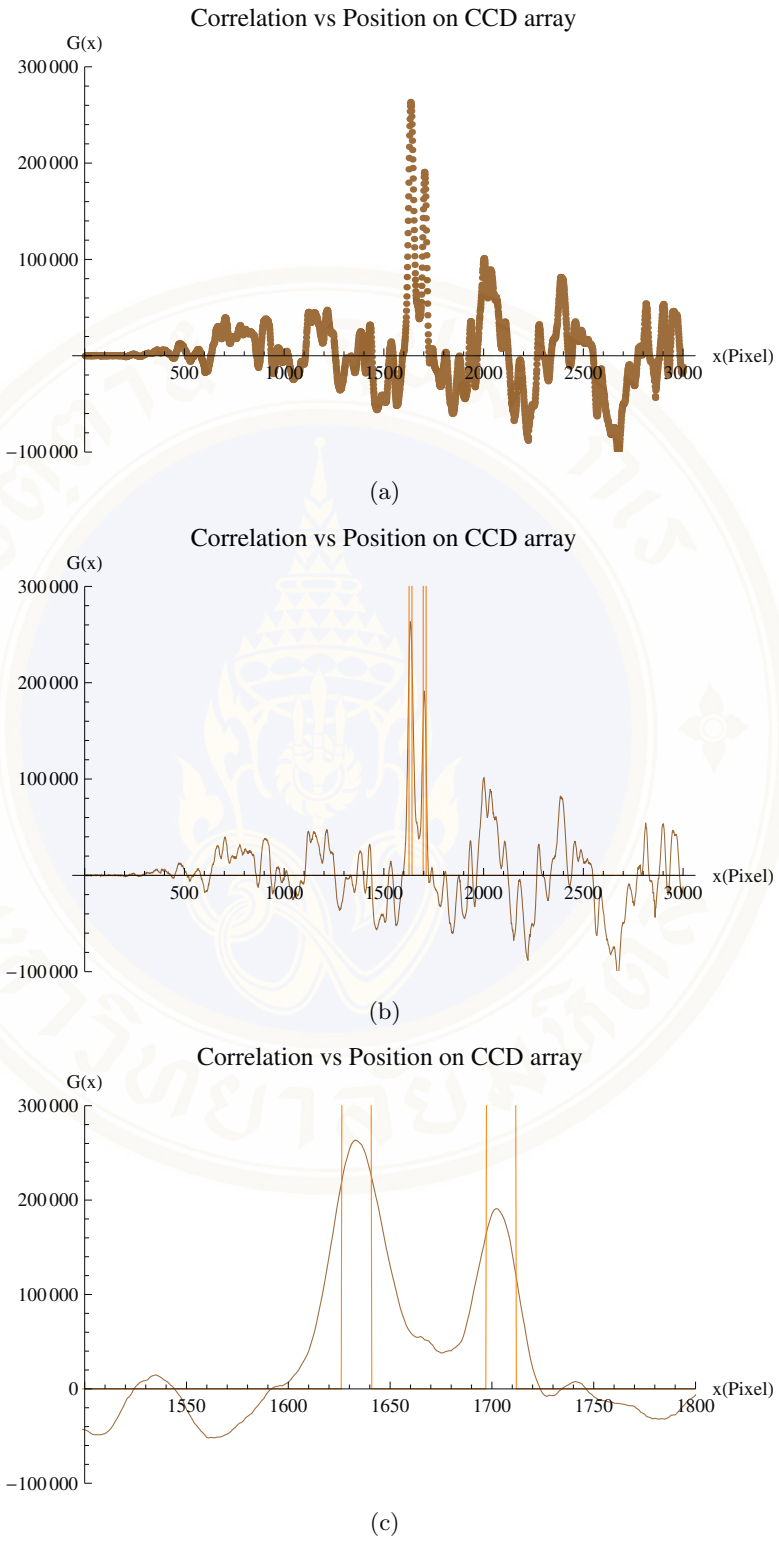

Figure 3.8: The constructed image with the same parameters as in the result of Fig. 3.6. The difference is the changing of the bucket detector to be a summing over all pixel on the linear-arrays CCD. (a) Point plot of the constructed image. (b) Line plot of the constructed image comparing to the expected image of the double slit. (c) The zoom-in of the expected region of the constructed image. The constructed image obtains discrepancy level 0.513537 and noise-ratio 0.0031292.

recognized as noise in the intensity of the bucket detector of the image construction. Because the intensity profiles is split from the source, two directions have to be the same pattern, and these profiles are projected through the object to the bucket detector. Thus, the light from another direction must be excluded. In order to select light in the expected direction, an opaque mask is chosen to block the unnecessary light at a collecting lens of bucket detection, shown in Fig. 3.9. The mask is a single aperture in

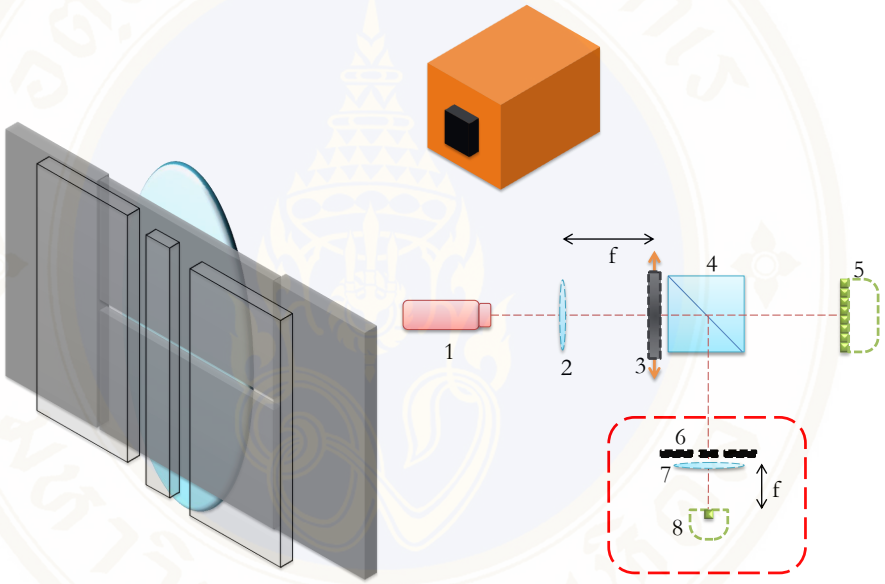

Figure 3.9: The location of the horizontal mask.

horizontal axis. Therefore, the constructed image from the imaging system integrating the horizontal mask is obtained and shown in Fig. 3.10. In this constructed image, the quality parameters are discrepancy level 0.516325 and noise-ratio 0.00309477. The mask makes the constructed image appears. When the mask is inserted, the image can be seen according to the result of Fig. 3.6 to the result of Fig. 3.10. Numerically, quality parameters show the result of Fig. 3.10 closing to the result of Fig. 3.8. It indicates that the blocking light affects the collecting data of the bucket detection part.

For further investigation, more results are collected. This experimental

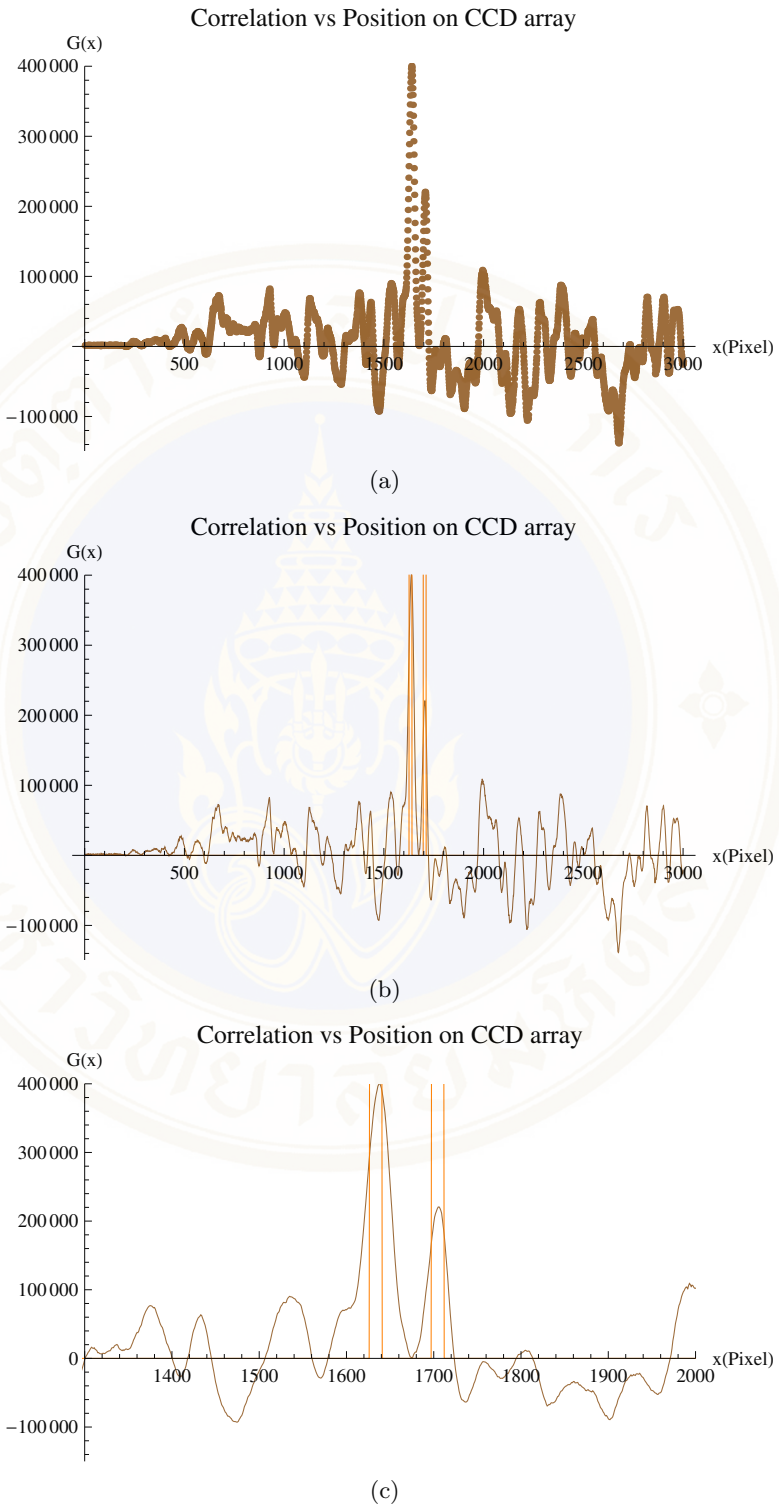

Figure 3.10: The constructed image with the mask choosing light from the consistent set between the intensity profile and the bucket intensity. (a) Point plot of the constructed image. (b) Line plot of the constructed image comparing to the expected image of the double slit. (c) The zoom-in of the expected region of the constructed image. The constructed image obtains discrepancy level 0.516325 and noise-ratio 0.00309477.

scheme is going to explain the noise effect from the blocking light in the GSI system integrating the horizontal mask, according to the assumption that was mentioned in the previous paragraph. The experiment considers constructed images by a fixed intensity profile and other planes of bucket intensity sets. The other planes can be done by shifting the horizontal mask up and down relative to the ground. These planes are called shift off plane. The results of the constructed images from these varying planes of bucket intensity are shown in Fig. 3.11. The first line has the constructed image of the nor-

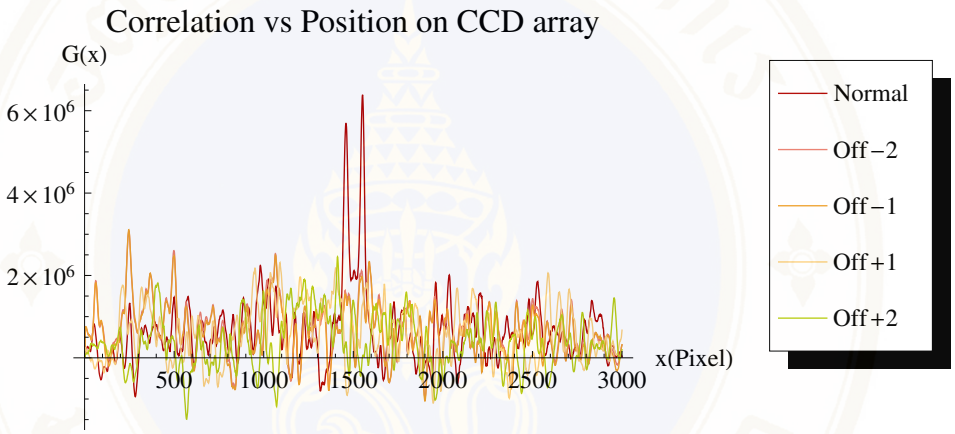

Figure 3.11: The constructed images. These are results from considering a fixed intensity profile and other planes of bucket intensity sets (by shifting the horizontal mask at collecting lens).

mal condition, which is the consistent set between the intensity profile and the bucket intensity. The second line has the condition of shifting off plane away from ground 1.0 mm. The third, fourth, and fifth lines have the conditions of shifting off plane away from ground 0.5 mm, toward to ground 0.5 mm, and toward to ground 1.0 mm, respectively. According to the results of the constructed images, they can be obviously said that the off plane of bucket intensity sets cannot construct any image. Without the horizontal mask, all planes of light, even they are out of the intensity profile area, are focused by the collecting lens in the bucket detection. The expecting light plane is influenced by all other planes because of the behavior of the collecting lens. Therefore, these off-planes are noise in the system. The constructed image disappears. To make the appearance

of the constructed image in the one-dimensional system, the image construction need a horizontal mask as an extra element in the detection system. If an image is constructed by GSI in two dimensions, these influences do not occur. Light of all planes has to be collected in order to construct an image. Therefore, there is no need a horizontal mask.

3.1.5 Properties of Constructed Images

After an image is constructed, properties of constructed images are shown in this section. The first condition is to try the translation of the object. The results are shown in Fig. 3.12 and Table 3.1. These two constructed images in Fig. 3.12 come from

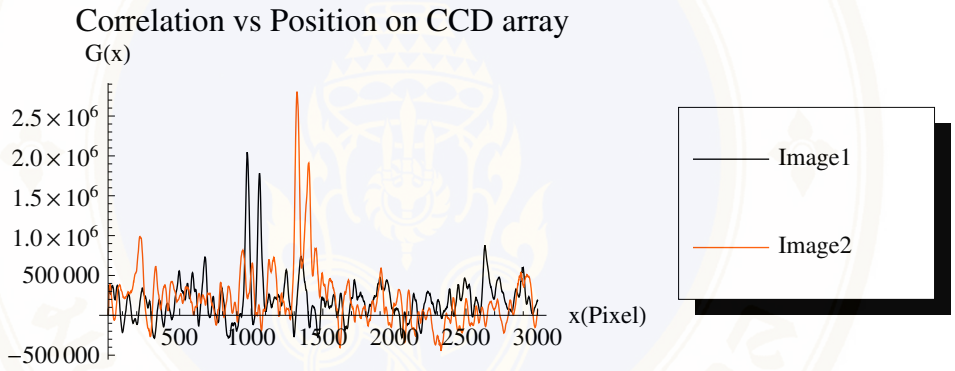

Figure 3.12: The constructed images. These are results from considering two positions of the object. The object is moved by 2.00 mm relatively to each other.

	Position				
	Left peak (pixels)	R-squared	Right peak (pixels)	R-squared	Center (pixels)
Image1	973.326	0.999551	1,058.23	0.994535	1,015.78
Image2	1,321.55	0.990493	1,395.77	0.990493	1,358.66

Table 3.1: These are results considering two spatial positions of the object. The object is moved by 2.00 mm relatively to each other. The positions of images are shown from a left peak, a right peak, and a center of image (a center between two peaks). According to the center positions of these two images, the relative position is 342.88 pixels. Each pixel has width 7 μm, thus the translation is 2.4002 mm.

the condition that the object is moved 2.00 mm relative to each other. Considering in details, the first image has the significant peaks in the region as shown in Fig. 3.13a, and the second image has the significant peaks in the region as shown in Fig. 3.13d. By fitting

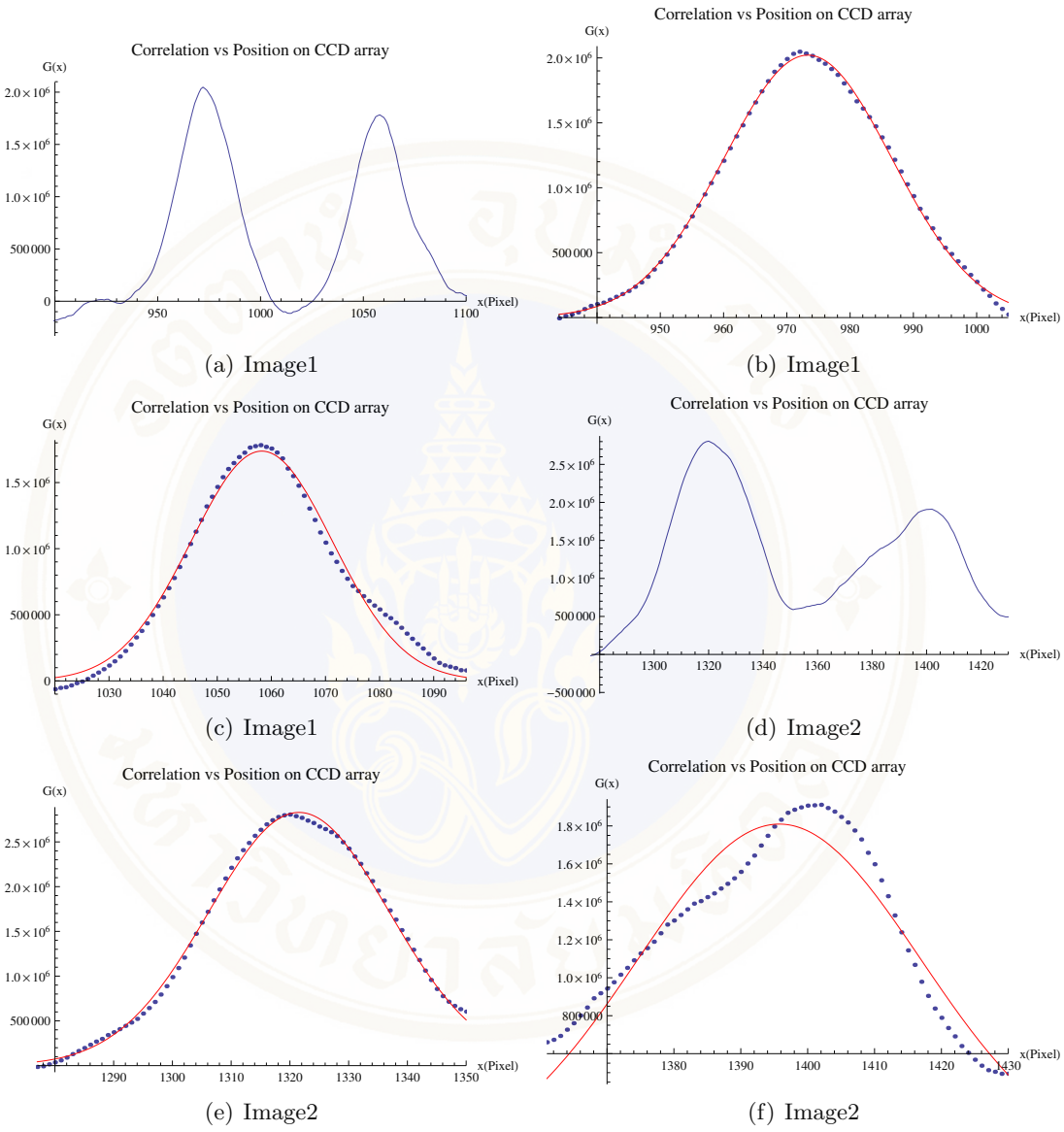

(a) Image1 (b) Image1

(c) Image1 (d) Image2

(e) Image2 (f) Image2

Figure 3.13: The zoom-in of the results of Fig. 3.12. (a) Show the region of the significant peaks of the first considering image. (b) Show the Gaussian function fitting of the first peak of the first considering image with mean at 973.326 pixels and R-squared 0.999551. (c) Show the Gaussian function fitting of the second peak of the first considering image with mean at 1,058.23 pixels and R-squared 0.994535. (d) Show the region of the significant peaks of the second considering image. (e) Show the Gaussian function fitting of the first peak of the second considering image with mean at 1,321.55 pixels and R-squared 0.999276. (f) Show the Gaussian function fitting of the second peak of the second considering image with mean at 1,395.77 pixels and R-squared 0.990493.

these peaks with the Gaussian function, Fig. 3.13b and Fig. 3.13c give positions of the aperture of the double slit of the first image in Fig. 3.12 at 973.326 pixels (with R-squared confidence 0.999551) and 1,058.23 pixels (with R-squared confidence 0.994535), and the positions of the second image, from Fig. 3.13e and Fig. 3.13f, are at 1,321.55 pixels (with R-squared confidence 0.999276) and 1,395.77 pixels (with R-squared confidence 0.990493). The center positions of each image are found at 1,015.78 pixels and 1,358.66 pixels, respectively. The translation of these two constructed images is 342.88 pixels. Each pixel of the CCD has width 7 μm. Therefore the translation is 2.4002 mm. The real translation of the object is 2.00 mm. This value shows that the difference between the translation of the object and the image is 20%.

3.1.6 Summary

Ghost shadow imaging technique is shown here along with the corresponding results. The imaging scheme requires two set of data from two detectors; a spatial-resolution detector measuring intensity patterns and a bucket detector after the object. The consideration was begun with the preparation of an intensity profile in case of changing a rotating diffuser or a computer-controlled spatial light modulator in experimental scheme. A rotating diffuser or a computer-controlled spatial light modulator is substituted by a step-moving ground glass. A generated intensity profile was considered by the correlation between two intensity patterns in the intensity profile. When the intensity profile was good, experimental data were collected with a double slit as an object. To obtain a constructed image corresponding to an experiment, Eq. 2.2 was calculated. Two indicators, which were discrepancy level and noise-ratio, were defined to show the quality of constructed images. For the normal configuration, the constructed image was very poor. The image is not close to the expected image. When the bucket detection is substituted by summing overall linear-arrays CCD, the constructed image is better than the constructed image from the normal configuration. The conditions to obtain the successfully constructed image are investigated focusing on the reason for the better

image in the modify system of the bucket detection. The investigation found that the bucket detector, which is the integration between a lens and a single-pixel detector, is not suitable for one-dimensional collection. The lens can obtain light out of the plane of the intensity profile, which can be considered a noise. When the noise is excluded by using an opaque mask together with the lens to select the plane of the intensity profile that is projected to the bucket detection, a constructed image appears. The last result shows a real position of the object relative to the position of an appearance constructed image. It has been found that the image moves relative to the moved object.

3.2 A Fixed Single-Pixel Detector Imaging

In this section, the conventional GSI system is modified to achieve a possibility to a fixed single-pixel detector imaging. The schematic setting is changed and shown in Fig. 3.14. In conventional GSI, an image is constructed by the correlation between

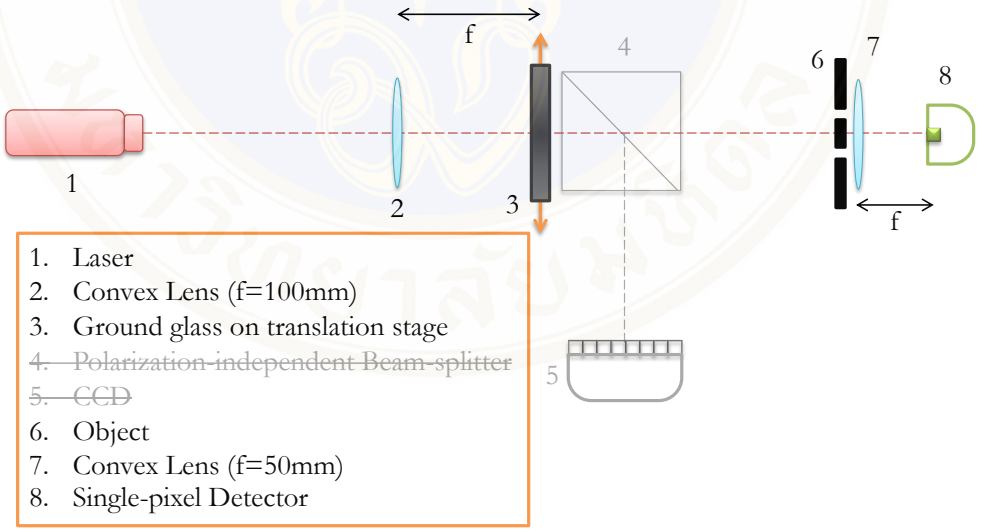

Figure 3.14: The experimental scheme of modify GSI to be a single-pixel imaging. According to the schematic setting, a polarization-independent beam-splitter and a spatial-resolution detector are removed from the system.

an intensity profile and intensities of a bucket detection. In this case, a beam-splitter and CCD are removed. However, by using the same concept to construct an image, the correlation between an intensity profile and intensities of bucket detection are necessary. To satisfy the necessary condition, an intensity profile has to be prepared in advance

according to the absent parts. This condition can be achieved by using our spatial intensity modulator, a piece of ground glass on a stepping-motor-controlled translation stage. The steps of modulation are recorded with respect to the position steps of the motor. By considering this reference, the precise position step has to be satisfied. The reliability can be considered by two intensity profiles as shown in Fig. 3.15. The error of the inten-

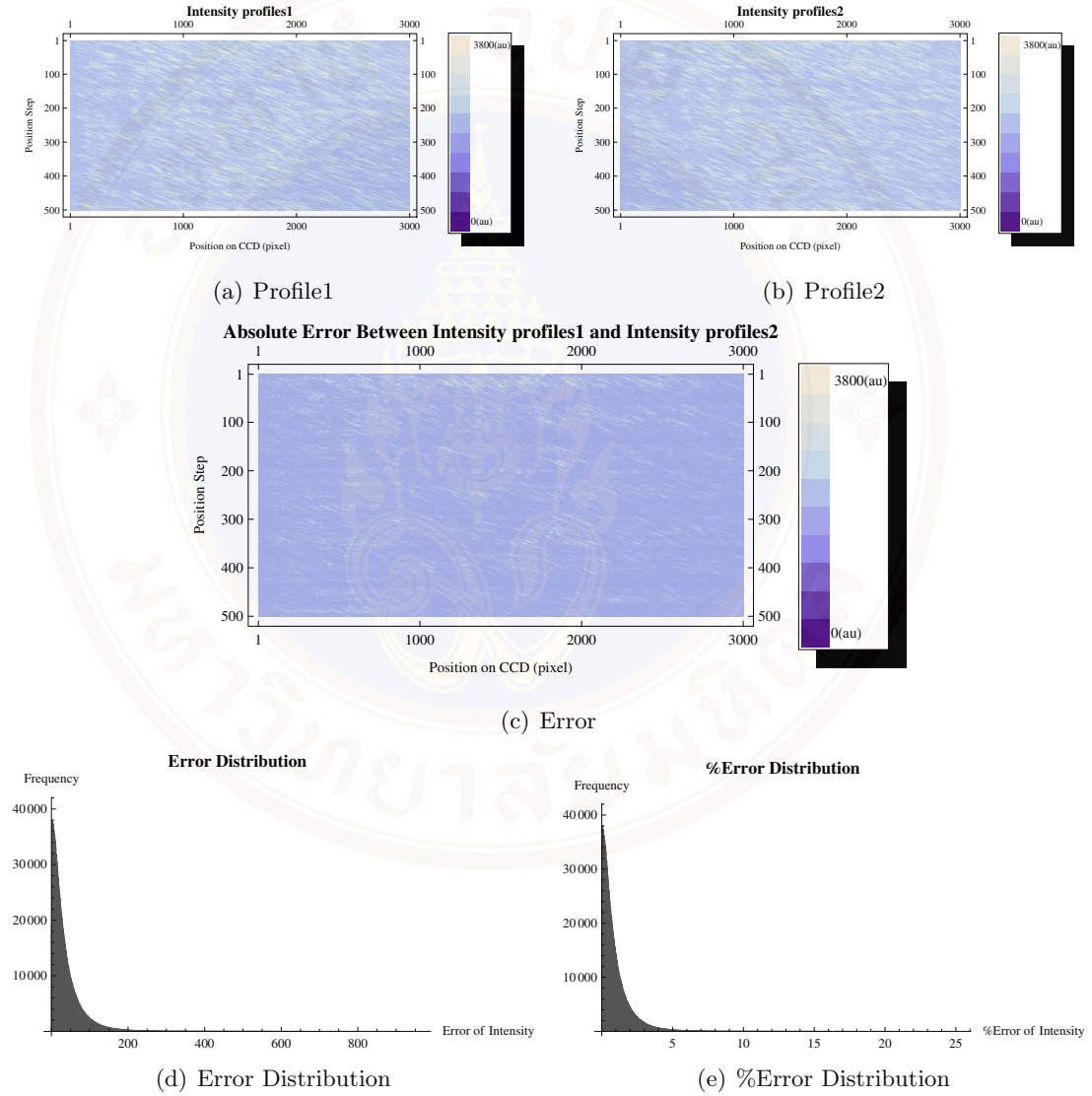

(a) Profile1 (b) Profile2

(c) Error

(d) Error Distribution (e) %Error Distribution

Figure 3.15: The intensity profiles collecting from steps-moving ground glass with motor-control. (a) The first considering intensity profile 500 steps. (b) The second considering intensity profile 500 steps. (c) The error consideration by the absolute of the different intensity of pixel-by-pixel with the absolute error mean 0.95%. (d) Error distribution. (e) %Error distribution. For (d) and (e), these histograms indicate the small number of high error.

sity profiles with the same set of position reference, shown in Fig. 3.15c, is considered by

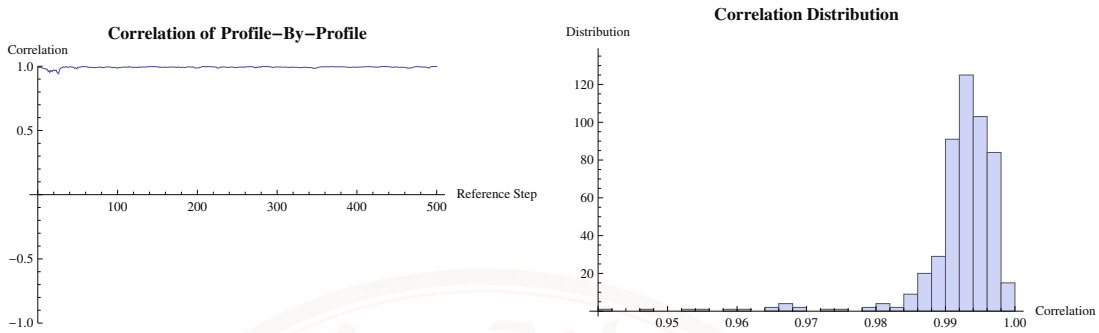

(a) Correlation of Profile-By-Profiel (b) Correlation Distribution

Figure 3.16: According to two intensity profiles in Fig. 3.15, (a) the correlations between these two profiles are calculated for the same reference step. The mean correlation is 0.9921 with the standard deviation 0.006551. (b) Correlation distribution.

the absolute different pixel-by-pixel of two considering profiles. The absolute mean error is 0.95%. In addition, for each position step, the intensity patterns from two profiles should be the same. For these pairs, the correlations are calculated, shown in Fig. 3.16. The mean correlation is 0.9921 with the standard deviation 0.006551. When using the same-recorded profile, these three images are constructed and shown in Fig. 3.17. As

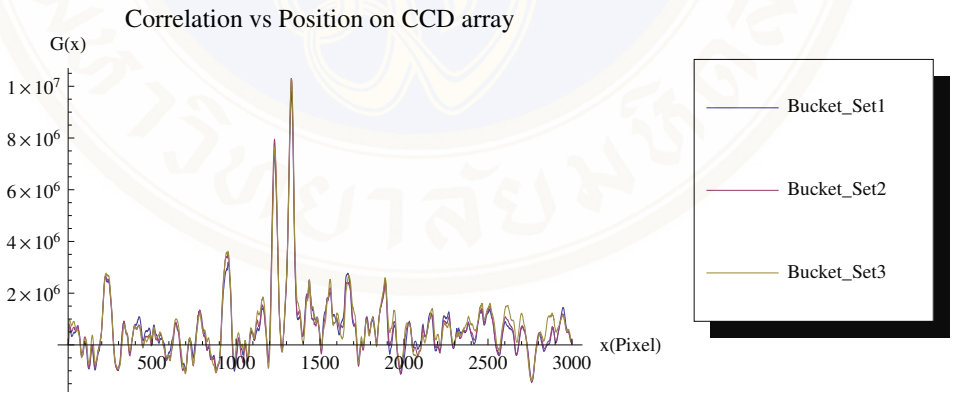

Figure 3.17: Three constructed images using the same recorded intensity profile.

they can be seen, the images look alike (with small errors). Numerically, by considering the correlation function between 2 of 3 images, the correlation between the first considering image and the second considering image is 0.9933, the correlation between the first considering image and the third considering image is 0.9750, and the correlation between the second considering image and the third considering image is 0.9869. These

three correlation values are not different in significance. In summary, if an intensity profile of the system is recorded before then an image can be constructed solely using a fixed single-pixel detector with a precise moving step respect to the intensity modulation step.

3.3 Image Construction Mechanism Model

In this section, the reason behind the correlation method of the image construction in the GSI scheme are given. The image construction is the accumulation of information. The description is shown by an example.

As it has already been seen, the image of GSI does not require the interference phenomenon. The image is constructed by the correlation between the intensity profile and the intensity of the non-spatial-resolution detector, and the correlation is calculated following the Eq. 2.2. What does it mean to calculate this correlation? The explanation is in the following.

The image formation will be described by the accumulation of the weighted information in the following example. Suppose that a 4×4 grid is considered. The object is a filling grid as shown in Fig. 3.18. Random numbers are generated into the grid. The

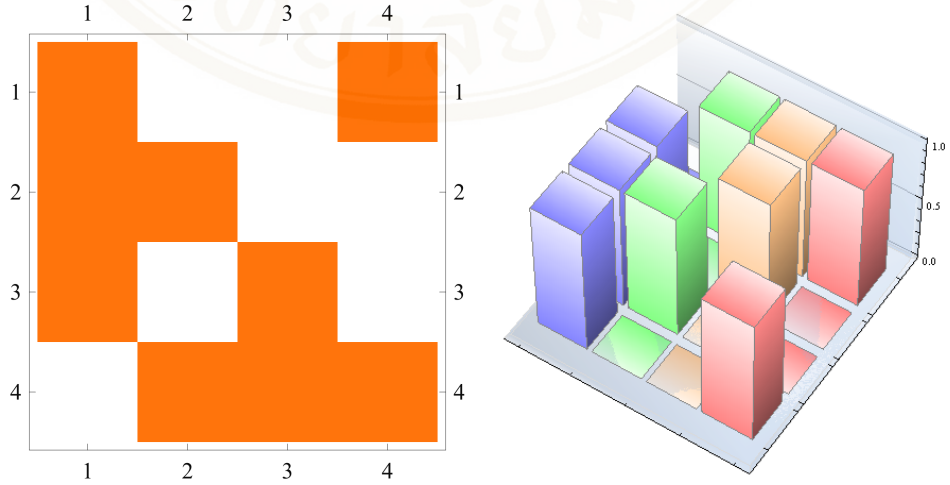

(a) Object (b) 3DObject

Figure 3.18: The 4×4-filling grid acts as an object in the model.

number of projected elements can be collected by comparing to the object. The number

of projected elements is the summation of points of a random grid that is in the same grid of the object. In this model, numbers of projected elements represent intensity of a non-spatial-resolution detector, bucket intensities, and grids of random numbers represents a set of intensity profile. The results of the calculation steps are shown in the Table 3.2. According to this table, the images are gradually constructed by accumulation of a random grid and weight in each step. After 1,000 steps, the constructed image is shown in Fig. 3.19. This constructed image has correlation 0.9821 comparing to the

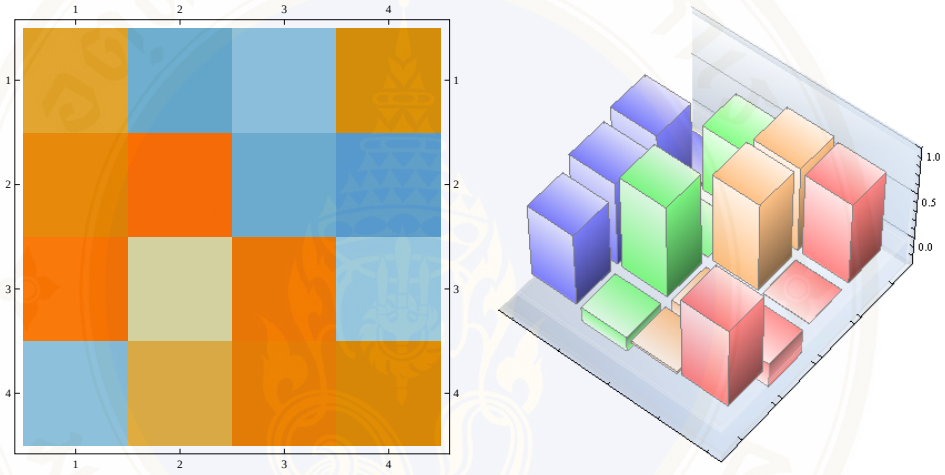

(a) Constructed Image(1,000Steps) (b) 3D-Constructed Image(1,000Steps)

Figure 3.19: The constructed images after 1,000 steps with correlation 0.9821.

expected image in Fig. 3.18. By consideration the calculation step, the correlation is developed according to Fig. 3.20. Similarly, GSI image construction is being the same. The intensity of the bucket detector is like a weight in each step of modulation. These weights come along with the intensity patterns accumulating to be a constructed image as it has already been shown.

In summary, this simulation model describe how accumulate the information in the image construction using the calculation of the correlation. The correlation function can be used to indicate the fidelity of constructed images. This simulation model leads to the study in the next chapter.

Step	Random Site	Constructed Image	Correlation
1	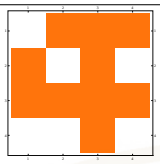	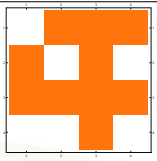	-0.1627
2	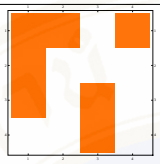	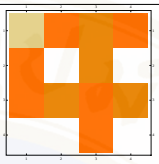	-0.1040
3	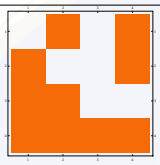	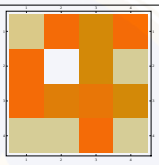	-0.0979
50	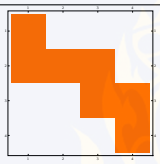	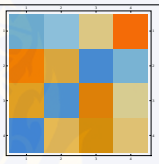	0.7425
100	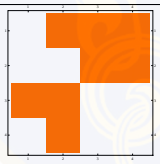	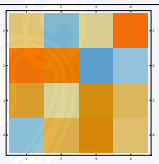	0.8157
200	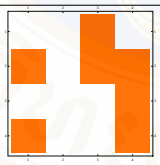	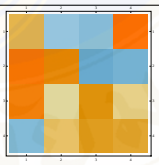	0.9116
500	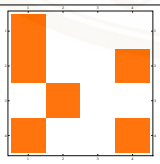	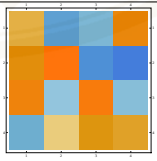	0.9647
1000	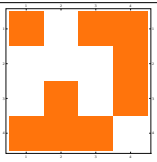	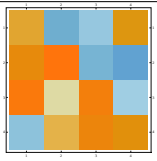	0.9821

Table 3.2: Image Construction. The second column shows the generation of the random grid at each step. The third column shows the accumulation of information to be an image. In these figures, the orange shade represents positive values and the blue shade represents negative values. The last column shows the correlation comparing to the expected image.

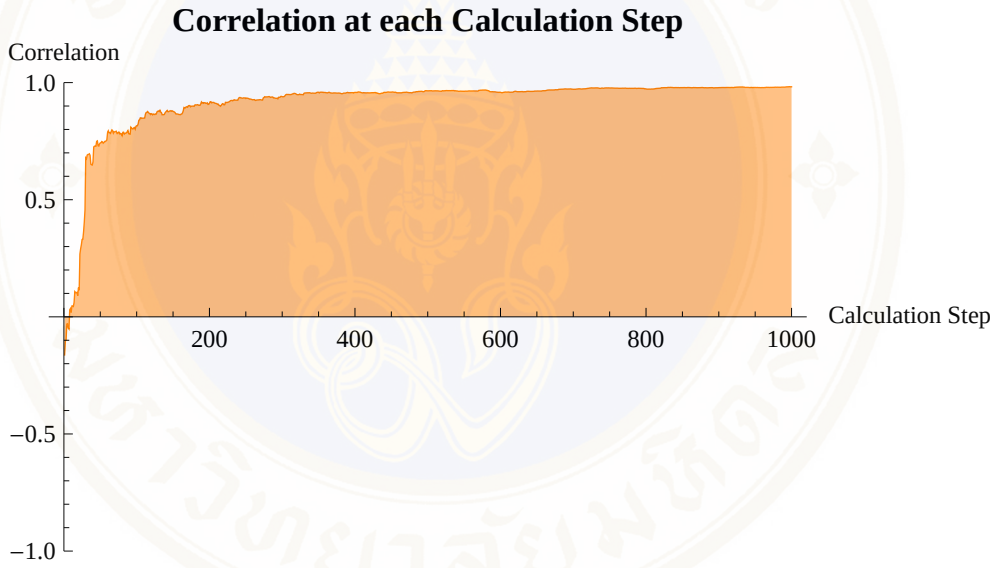

Figure 3.20: The correlation of the constructed image at each step comparing to the expected image.

CHAPTER IV
SIMULATION STUDY AND RESULTS

This chapter focuses on the extended study of the previous chapter. According to chapter 3, the experimental results of the constructed images from the GSI scheme were shown with not quite good quality. A simulation model in this chapter will be used to find out the best configuration in the scope of a parameter of an intensity profile, which describes in the following detail. At the end, the best configuration is obtained for using in the real experimental scheme. The chapter contains (i) a preparation of intensity profile using Gaussian convolution model, (ii) using the generated intensity profile to construct an image following the GSI scheme, (iii) changing a parameter of the profile to construct another image, and (iv) comparing the constructed images to find out the best construct image.

According to the concept of GSI given in Sec. 2.3, the image construction comes from the correlation between an intensity profile and series of intensity at a bucket detector. Certainly, a simulation tries to resemble the experimental study in the previous chapter. An intensity profile has to be prepared like the experiment. The generated patterns in the profile can be projected to an object to obtain series of the bucket intensity. The object is certainly the same object in the previous chapter. After that, an image of the GSI scheme is constructed by using the prepared intensity profile and the series of the bucket intensity. By changing a parameter in the intensity profile of the simulation model, which will be discussed in the following sections, the other constructed images of GSI scheme are obtained. The best configuration of the studied parameter is considered by considering the quality of constructed images.

4.1 Preparation of Intensity Profiles

In the experimental scheme, an intensity profile is generated by intensity patterns of the spatial intensity modulations of the light source. The profile is collected by a linear-arrays CCD, which has 3,000 pixels (with 7 μm for each pixel). In order to resemble a collected profile, random positions on the detection area with random magnitudes, represented intensity at positions, are generated. At this point, the random pattern is an intensity profile with the peak size of one pixel. To make the raw random pattern look alike the experimental intensity pattern, the random pattern is convoluted with the Gaussian distribution function,

$$k(x) = A \exp \frac{-(x-\mu)^2}{2\sigma^2}, \tag{4.1}$$

where A is a normalization constant, μ is the mean of the distribution function, and σ^2 is the variance. The convolution is given by

$$[f * k](x) \equiv \int_{-\infty}^{\infty} f(x')k(x-x')dx', \tag{4.2}$$

where $f(x)$ is an input function and $k(x)$ is a kernel function of the convolution. In Gaussian distribution, twice magnitude of the standard deviation is related to a full width at half maximum (FWHM) of the function, a transverse size of the source. Obviously, the input function is the random pattern, and the kernel function of the convolution is the Gaussian function.

The idea to use the Gaussian function as the kernel function comes from the fact of the source in the experimental part in the previous chapter. The source is a laser focusing on the step-translation ground glass. A laser has the Gaussian beam profile. Even it passes through the ground glass, it still has the Gaussian beam profile. Therefore, the kernel function must be the Gaussian function.

The simulation parameters are (i) 3,000 pixels for the linear-arrays CCD, (ii) an intensity pattern with 500 random positions, and (iii) 300 intensity patterns for each intensity profile.

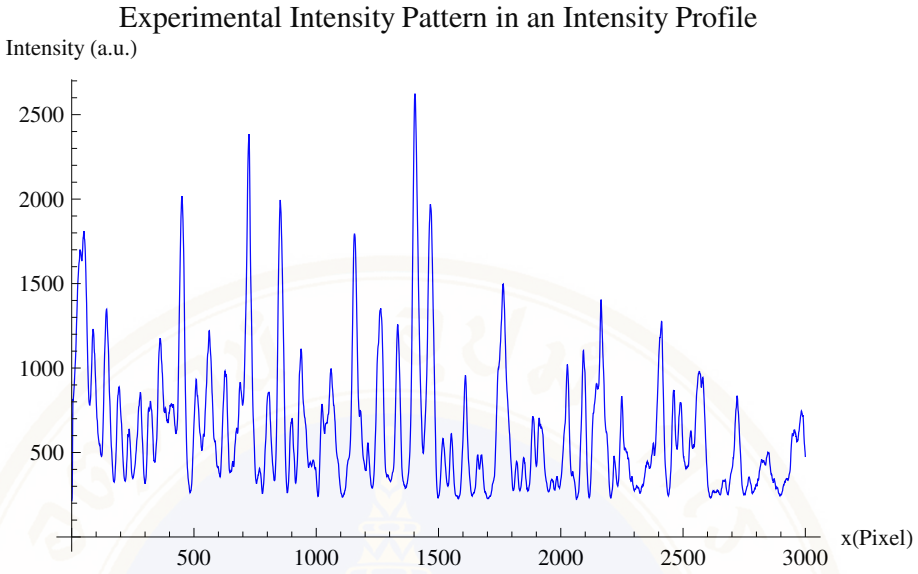

Figure 4.1: An intensity pattern in an experimental intensity profile.

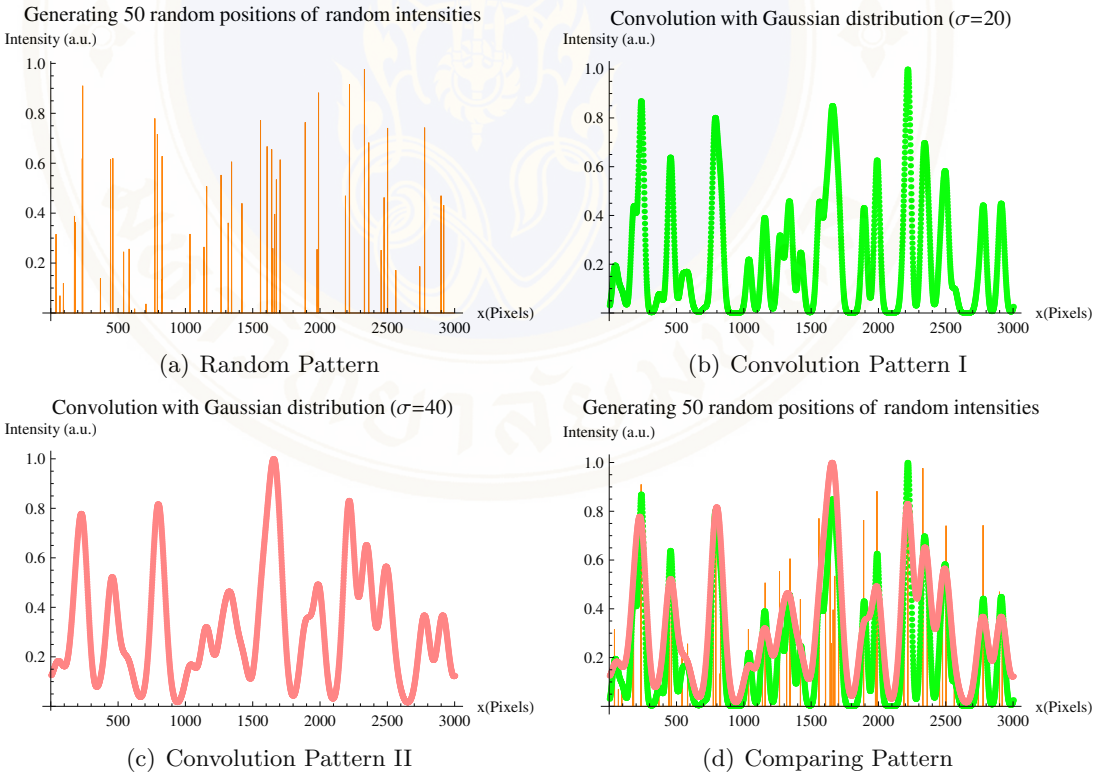

(a) Random Pattern

(b) Convolution Pattern I

(c) Convolution Pattern II

(d) Comparing Pattern

Figure 4.2: The example of the simulation pattern in the simulation model using Gaussian convolution model. (a) Random intensity at 50 random positions on the detection area as a base of an intensity pattern of an intensity profile. (b) The random pattern is convoluted with the Gaussian function as a kernel function. The kernel function in this result uses the half of peak size of 20 pixels ($\sigma = 20$). (c) The random pattern is convoluted with the Gaussian function with the half of peak size of 40 pixels ($\sigma = 40$). (d) Compared plots.

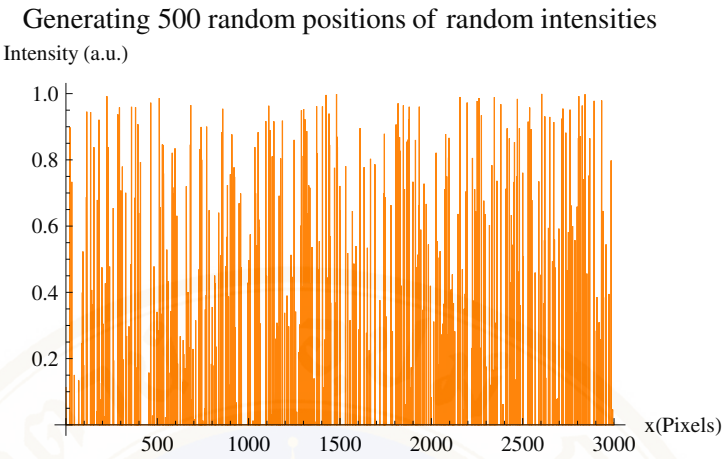

(a) Random Pattern

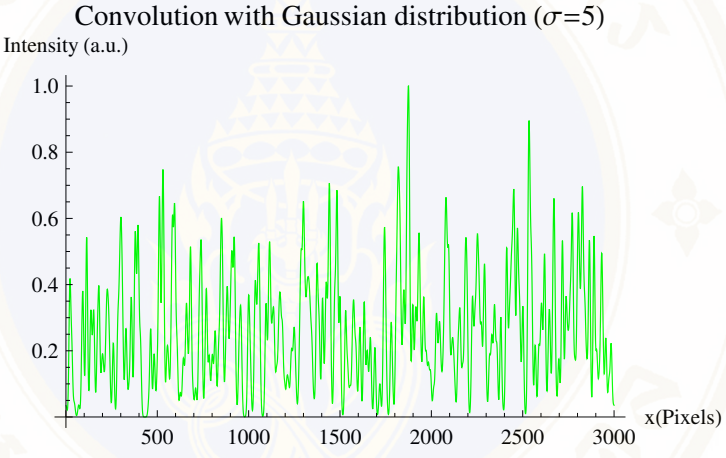

(b) Convolution Pattern I

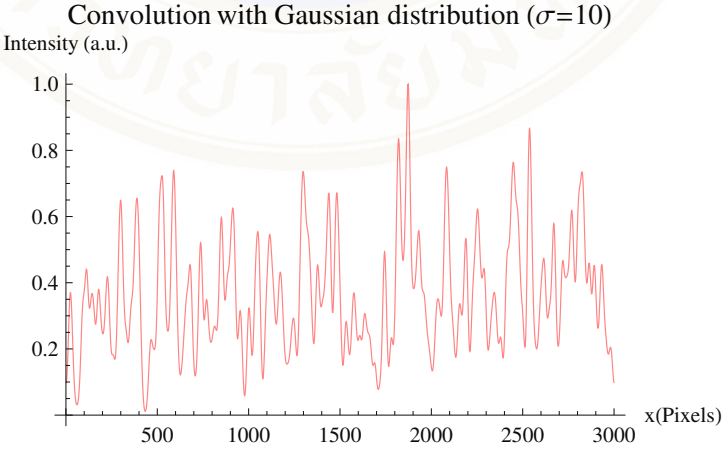

(c) Convolution Pattern II

Figure 4.3: The example of the simulation pattern in the simulation model using Gaussian convolution model. (a) Random intensity at 500 random positions on the detection area as a base of an intensity pattern of an intensity profile. (b) The random pattern is convoluted with the Gaussian function as a kernel function. The kernel function in this result uses the half of peak size of 5 pixels ($\sigma = 5$). (c) The random pattern is convoluted with the Gaussian function with the half of peak size of 10 pixels ($\sigma = 10$).

The expected result, shown in Fig. 4.1, is the same pattern that is generated in the experimental scheme. The example of the simulation result of an intensity pattern is shown in Fig. 4.2. For the real simulation of the study, the example of the simulation result is shown in Fig. 4.3. According to the simulation result, the results can be considered consisting to the experimental result of an intensity pattern. To prepare an intensity profile in GSI scheme, 300 simulation intensity patterns are generated and shown in Fig. 4.4. The intensity profile is used to construct an image in GSI scheme.

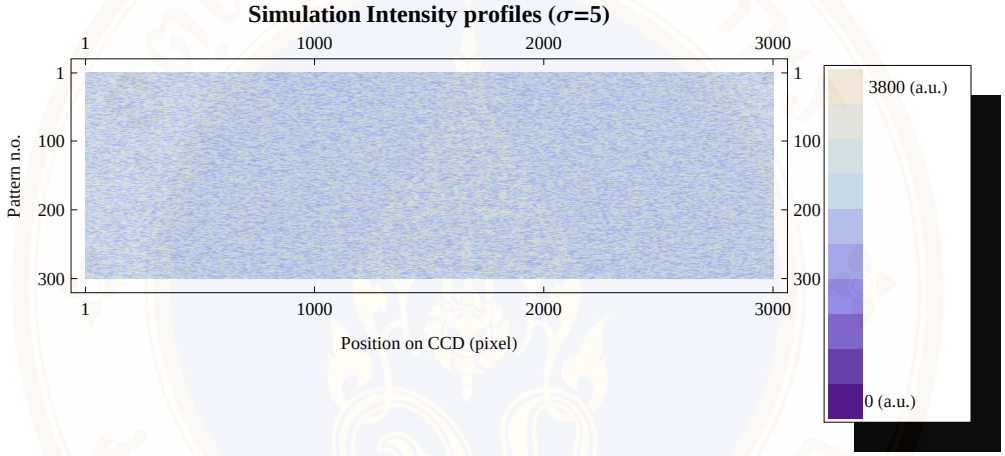

Figure 4.4: The simulation intensity profile from 300 generated intensity patterns with the half of peak size of 5 pixels.

In addition, the generated intensity profile is examined by the correlation function between two intensity patterns in the intensity profile to consider the non-duplication in the intensity profile. The correlation is shown in Fig. 4.5 with the mean -0.000593 and the standard deviation 0.0649. The correlation closes to zero, therefore the duplication between two intensity patterns in the example of the intensity profile does not exist significantly. The generated intensity profile is good enough to be used in the GSI scheme.

4.2 Ghost Shadow Image Construction

After obtaining an intensity profile, the corresponded intensity series of the bucket intensity have to be found out. With the same object as in the previous chapter (a double slit with an aperture size of 0.1 mm or 14 pixels and an aperture separation of 0.5

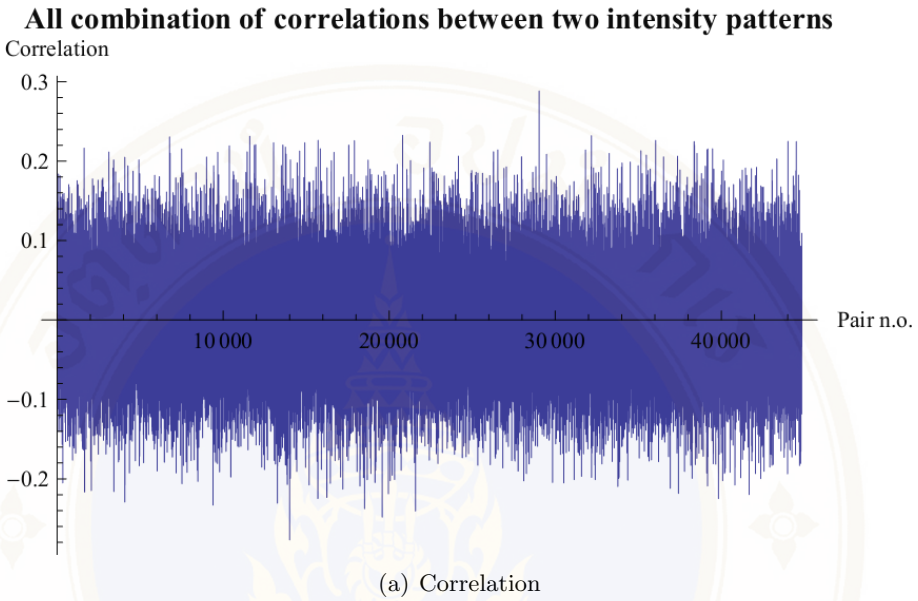

(a) Correlation

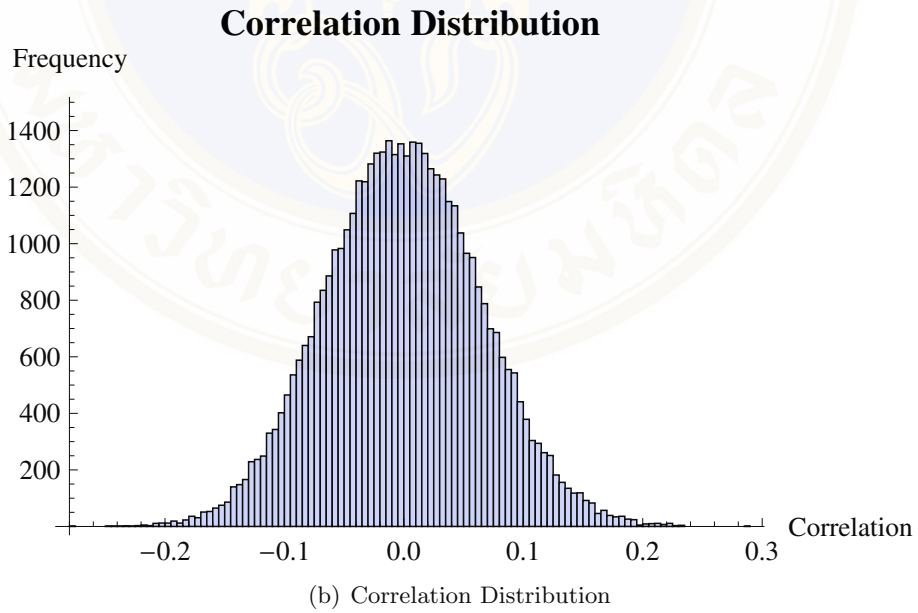

(b) Correlation Distribution

Figure 4.5: The calculation results of correlation between all combinations of two intensity patterns out of 300 generating intensity patterns in the intensity profile, when the correlation mean is -0.000593 and the correlation standard deviation is 0.0649.

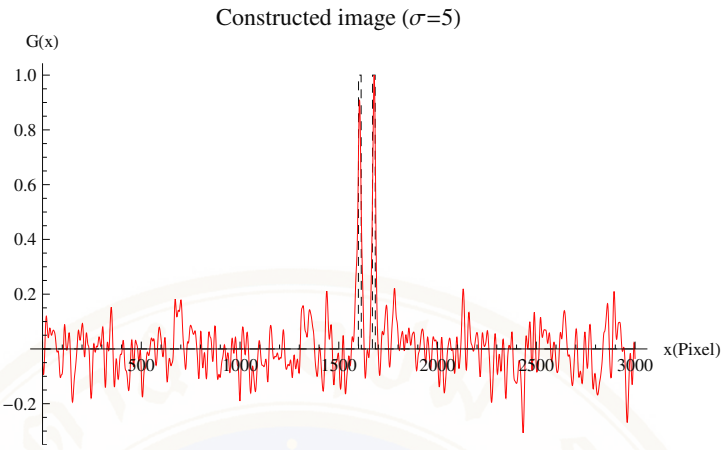

(a) Constructed Image

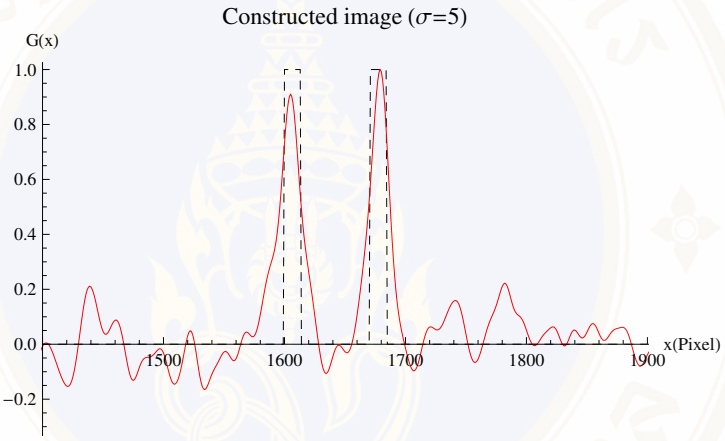

(b) Image Region

Figure 4.6: The constructed image using the intensity profile with the half of peak size of 5 pixels.

mm or 59 pixels), the corresponded intensity series can be calculated by the projection through the object. The accumulation intensity of the intensity pattern that matches the aperture area of the double slit is a corresponded intensity. For example, the intensity profile, shown in Fig. 4.4, that is generated by a set of intensity patterns with the half of peak size of 5 pixels constructs the corresponded image in Fig. 4.6. (The intensity pattern is shown in Fig. 4.3b.) Thus, an image can be constructed using the intensity profile from the simulation model.

4.3 The Influence of the light Source Profile

The intensity profiles with the half of peak size of 1 to 40 pixels are generated. Additionally, each standard deviation of the kernel function of an intensity profile is generated 30 times to consider the statistical result. These profiles are used in the image construction following the GSI scheme as shown in the previous section. Fig. 4.7

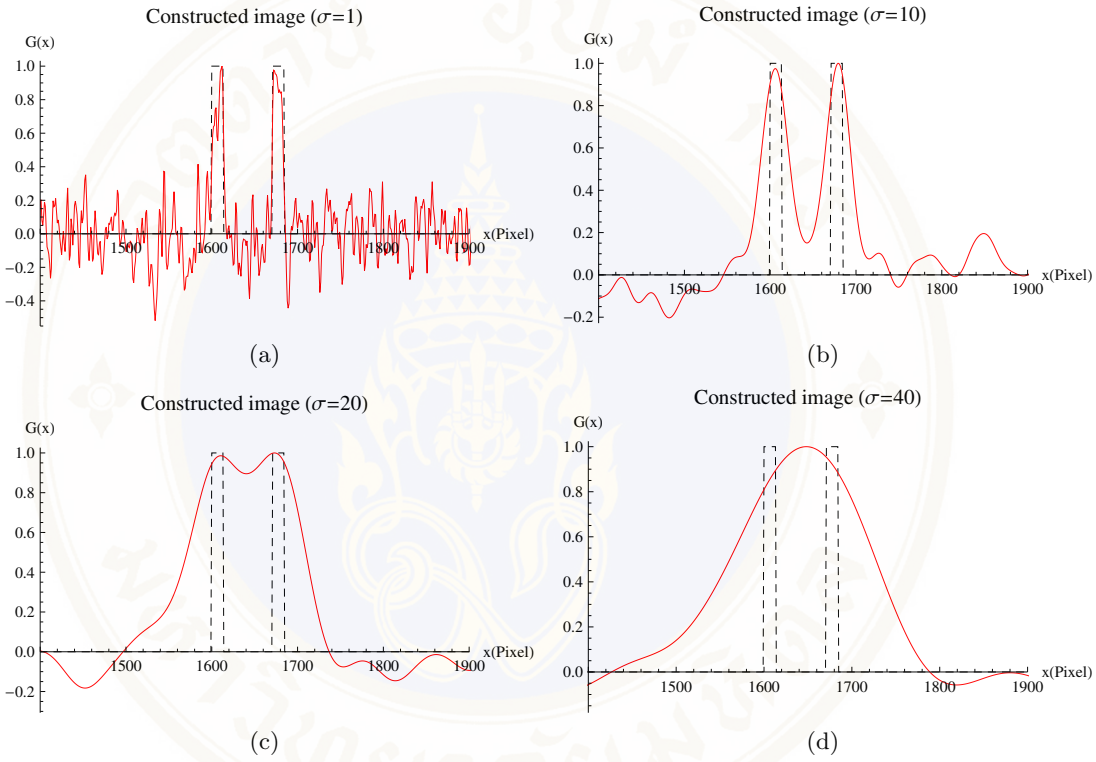

Figure 4.7: The examples of the constructed image using the intensity profile with the half of peak size of 1, 10, 20, and 40 pixels, respectively.

shows the examples of the constructed images with the half of peak size of 1, 10, 20, and 40 pixels, respectively. The examples show that the intensity profiles influence to the quality of the constructed images significantly. In order to measure the quality of the constructed images, discrepancy level and noise-ratio[1] are also considered. Thus, the discrepancy levels and noise-ratios of the simulation-constructed images are shown in Fig. 4.8. According to Fig. 4.8, the smallest ensemble average discrepancy level is obtained from the half of peak size of 4 pixels, and the smallest ensemble average noise-

[1]These two indicators were introduced before. See more in Sec. 3.1.3.

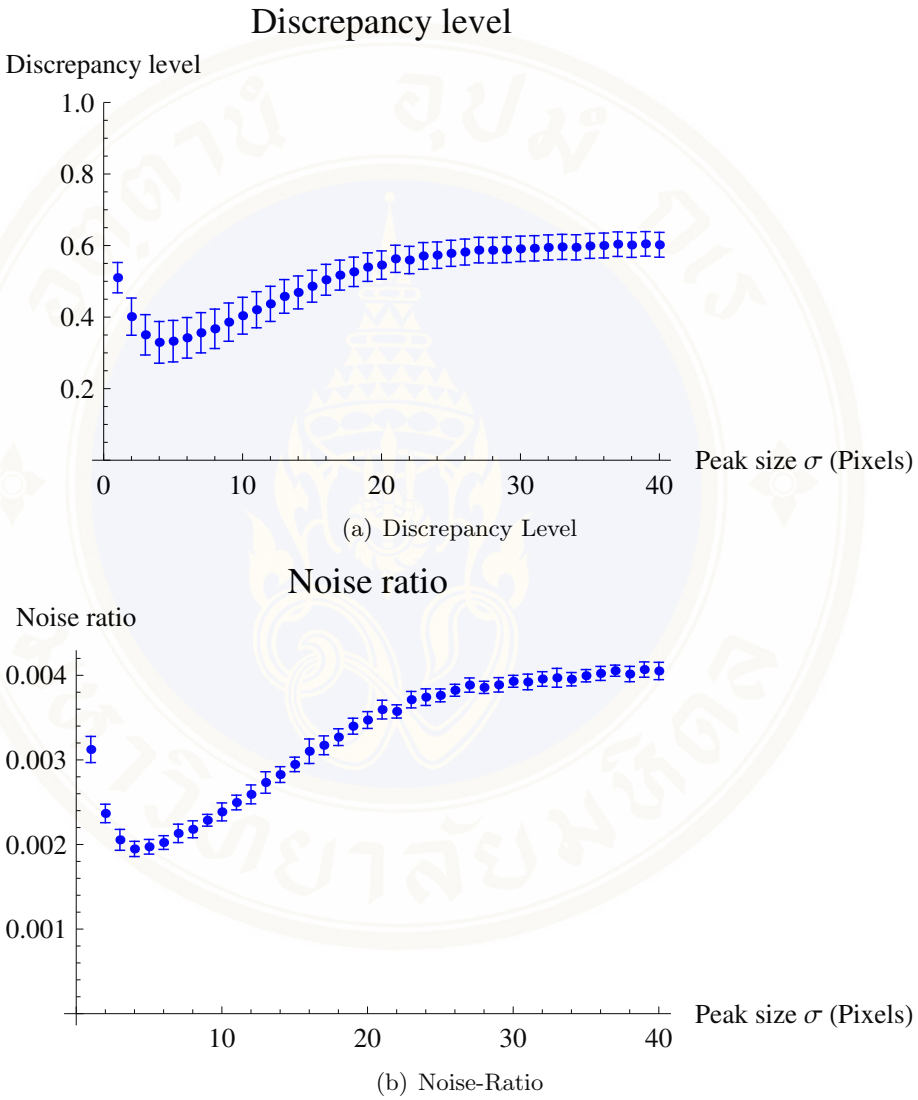

(a) Discrepancy Level

(b) Noise-Ratio

Figure 4.8: The results of discrepancy level and noise-ratio from ensemble average 30 times for each constructed image. (a) Graph of discrepancy level varying the peak size of the intensity profile. (b) Graph of noise-ratio varying the peak size of the intensity profile.

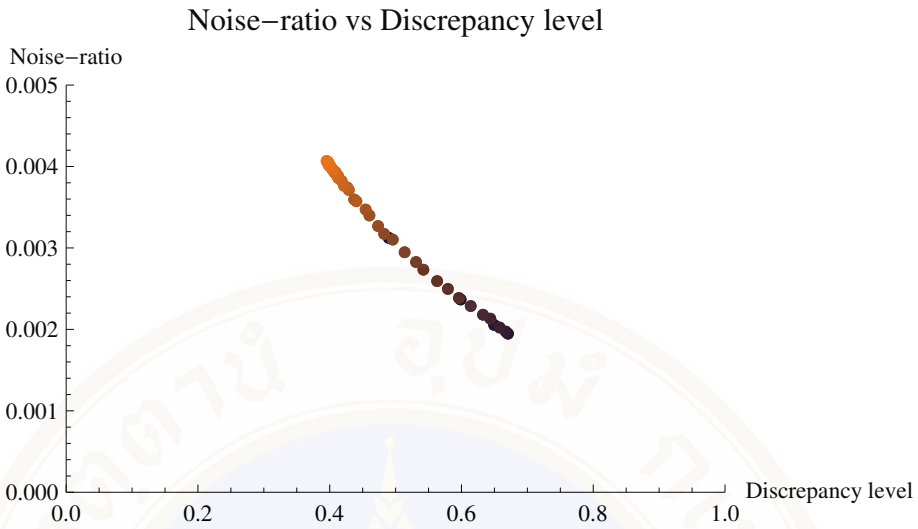

(a) Scatter Plot

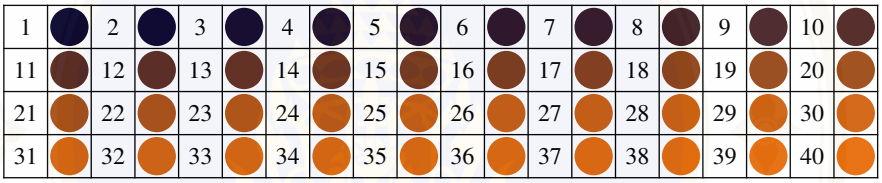

(b) Scatter Plot Legend

Figure 4.9: (a) The scatter plot between noise-ratio and discrepancy level. For each point on the graph, the coordinate is (discrepancy level,noise-ratio). (b) According to the legend, the darkest point represents the half of peak size of 1 pixel and the most light point represents the half of peak size of 40 pixels. The points lie in the scatter plot respectively.

ratio is also obtained from the half of peak size of 4 pixels. To combine two indicators considering simultaneously, the scatter plot is shown in Fig. 4.9a following the legend in Fig. 4.9b to represent the half of peak size of the constructed image. For each point on the scatter plot, the coordinate (x,y) is (discrepancy level,noise-ratio). The darkest point represents the half of peak size of 1 pixel and the most light point represents the half of peak size of 40 pixels, respectively. The best value for optimal quantity is obtained by choosing the point that close to the absolute value, which is lied at (0,0) in the scatter plot. Thus, the best value is found to be the half of peak size of 4 pixels or the peak size of 8 pixels. The constructed image using the intensity profile with the half of peak size of 4 pixels in the kernel function of the convolution is shown in Fig. 4.10. The mean discrepancy level is 0.329446, the mean noise-ratio is 0.0582549, and the quality

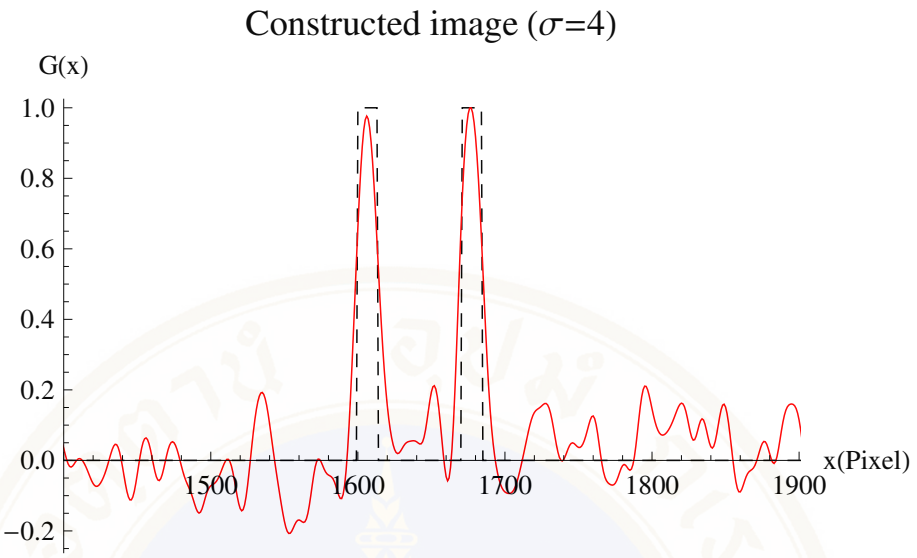

Figure 4.10: The constructed image using the intensity profile with the half of peak size of 4 pixels. The mean discrepancy level is 0.329446, the mean noise-ratio is 0.0582549, and the quality magnitude is 0.329452.

magnitude is 0.329452.

4.4 Summary

the simulation of GSI is calculated using the non-correlated intensity profiles. These intensity profiles are generated using Gaussian convolution model. The Gaussian convolution model is random intensity on random positions convoluted with Gaussian function as a kernel function. By changing the standard deviation of kernel function in Gaussian convolution model, an intensity profile is also changed. This changing indicates the relationship to varying the transverse size of intensity profile. By using different transverse sizes (or peak sizes) of intensity profile, different constructed images are obtained. In order to compare the quality of the constructed images, discrepancy level and noise-ratio are defined. For the object, it is defined consistent with the real experiment as in chapter 3. The object is a double slit with 0.1 mm for each aperture and 0.5 mm aperture separation. In CCD view, the double slit has 14 pixels for each aperture and 59 pixels aperture separation. The constructed image given the best quality comes from the standard deviation of 4 pixels (28 μm) in Gaussian convolution model. This

configuration means setting the transverse size (or the peak size) of 8 pixels (56 μm) in intensity profiles gives the best constructed image for this object. All of these results, there is an influence of the light source profile for the considered object in this thesis.

CHAPTER V
SUMMARY OF THE PROJECT I

Information without a spatial resolution and a light source profile are found a method to construct an image of an object by using the correlation between two data. Two data are the intensity information of the light source in the area of an image and the bucket intensity that passes through the object (intensity without the spatial resolution of the object). Thus, an image can be constructed indirectly. This imaging technique is called "Ghost Shadow Imaging". GSI technique is demonstrated by the experiment and the simulation. The experiment studies the preparation of an intensity profile by a step-moving ground glass as a spatial intensity modulator, the image construction with experimental technique to obtain an image, the extended study of the possibility for using a fixed single-pixel detector as a fixed single-pixel detector imaging, and mechanism model by accumulating the information. The simulation studies the preparation of an intensity profile by the Gaussian convolution model, the image construction following the idea of the accumulated information in the mechanism model, and the influence of the intensity profile by varying the transverse size of intensity profile.

PROJECT II
ENTANGLEMENT GENERATION

CHAPTER VI
INTRODUCTION

6.1 Overview

Entangled states have played essential roles in the development of quantum theory since early in its development, as indicated by the famous paradox of Einsten, Podosky, and Rosen (EPR) (Einstein *et al.* 1935). Furthermore, entanglement is generally accepted as a fundamental role in quantum information technologies such as quantum cryptography (Ekert 1991; Gisin *et al.* 2002; Jennewein *et al.* 2000), teleportation (Bouwmeester *et al.* 1997; Furusawa *et al.* 1998; Boschi *et al.* 1998), and quantum computing (Nielsen & Chuang 2000; Bennett & DiVincenzo 2000). For bipartite entanglement (entanglement of two-system state), a famous way to prepare the entangled states was demonstrated by Kwiat *et al* (Kwiat *et al.* 1995, 1999) basing on a nonlinear-optical process, known as a spontaneous parametric downconversion (SPDC). For multipartite entanglement, the entangled states were introduced by Greenberger, Horne, and Zeilinger (GHZ) (Greenberger *et al.* 2007), now called GHZ-states, and were first realized by Bouwmeester *et al* in an optical system with three particles (Bouwmeester *et al.* 1999). Indeed, Shih and Alley have demonstrated the entangled states by post-selection without any nonlinear-optical process (Shih & Alley 1988). It is more practical this way because of using simple linear-optical elements. This entanglement can be called position-time entangled states. Heralded states, which can be considered as multipartite entanglement, were introduced to enhance the accuracy of states detecting in low signal information (Podoshvedov 2006; Śliwa & Banaszek 2003; Pan *et al.* 2001; Barz *et al.* 2010). These heralded states have been generated by using multipairs of down-converted photons and post-selections of states (Walther *et al.* 2007; Barz *et al.* 2010), using some part of the states as a trigger for obtaining the information of the other states without

measurement. However, the multipairs of down-converted photons, expected as an input of the generating system, are difficult to obtain because of a very small efficiency of generations. Therefore, a more convenient way is considered by using only linear-optical elements.

6.2 Objectives

1. To show the entangled system without using any nonlinear-optical process.
2. To develop new idea by calculating theoretically an implementation of using the multipartite entanglement.
3. To show a practical implementation for entanglement generation.

6.3 Outline

The second part of this thesis is organized into three chapters. Chapter 7 introduces the background knowledge required for quantum entanglement. The given concepts consist of the action of beam-splitters by quantum optics, entanglement, multipartite entanglement, heralded entanglement, and basic system for linear-optical entanglement. Chapter 8 shows the theoretical study for the generation of entangled states using linear-optical elements. The calculation shows two systems of entanglement generation, four-photon entangled states and heralded generation of bipartite entangled states. Finally, the last chapter is conclusions.

CHAPTER VII
BACKGROUND KNOWLEDGE

In this chapter, the concept of entanglement is given together with the background knowledge for entangled systems. Moreover, heralded entanglement is given the idea here through multipartite entangled system. Finally, a basic system for generating entangled states by linear-optical elements is shown here.

7.1 The Action of Beam-splitters in Quantum Optics

Before the beam-splitter in a fully quantum mechanics is considered, the discussion returns back to a classical light field. A classical light field is considered with the complex amplitude ϵ_1 incident upon a lossless beam-splitter as shown in Fig. 7.1a. ϵ_2 and ϵ_3 are the amplitudes of the reflected and transmitted fields, respectively. If r and t are, respectively, the complex reflectance and transmittance of the beam-splitter, then it can be described as

$$\epsilon_2 = r\epsilon_1, \tag{7.1}$$

$$\epsilon_3 = t\epsilon_1, \tag{7.2}$$

Since the beam-splitter is lossless, it has to satisfy the condition $|\epsilon_1|^2 = |\epsilon_2|^2 + |\epsilon_3|^2$ which requires that

$$|r|^2 + |t|^2 = 1. \tag{7.3}$$

In quantum optics, annihilation and creation operators are directly proportional to field operators, which are classical analogies. Therefore, the field amplitudes are replaced by annihilation operators. At the unused port, even there is no inputting

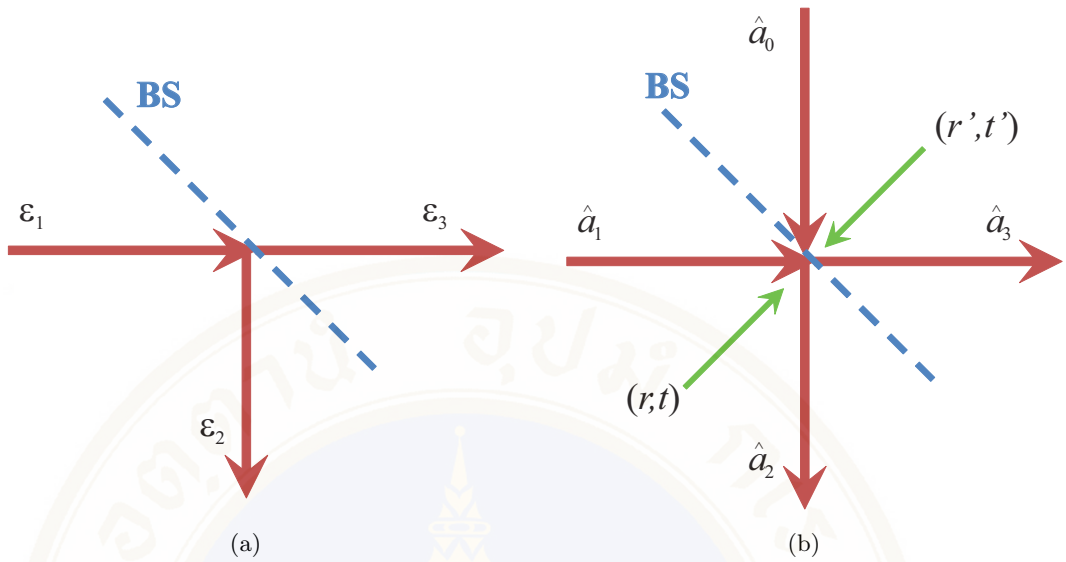

Figure 7.1: (a) Classical point of view of beam-splitter. A classical field of amplitude ϵ_1 is split into fields of amplitudes ϵ_2 and ϵ_3. (b) Quantum point of view of beam-splitter.

field in the classical picture, but there is a quantized field mode in the vacuum state in the quantum picture. Thus, the unused port has to have a vacuum state as an input. The transformations of states, see Fig. 7.1b, are going to be

$$\begin{pmatrix} \hat{a}_2 \\ \hat{a}_3 \end{pmatrix} = \begin{pmatrix} t' & r \\ r' & t \end{pmatrix} \begin{pmatrix} \hat{a}_0 \\ \hat{a}_1 \end{pmatrix}. \tag{7.4}$$

Let us investigate a further property of a beam-splitter. The phase shift of the reflected and transmitted light depends on the type of a beam-splitter (Hamilton 2000). If a single dielectric layer is used as a beam-splitter, the reflected and transmitted beams will differ by phase $\pi/2$, which is a phase factor of $\exp(i\pi/2)$. Another popular beam-splitter is used an asymmetry coating, a plated beam-splitter, so the reflected and transmitted beams will differ by phase π. In this work, beams-splitters are an asymmetry coating. In case of a 50:50 plated is according to

$$\hat{a}_2 = \frac{1}{\sqrt{2}}(\hat{a}_0 + \hat{a}_1) \tag{7.5}$$

$$\hat{a}_3 = \frac{1}{\sqrt{2}}(\hat{a}_1 + e^{i\pi}\hat{a}_0) \tag{7.6}$$

7.2 Entanglement

Entanglement is a property of correlations between two or more quantum systems, which cannot be satisfactorily accounted for by any classical theory. It has played an essential role in the development of quantum theory. This discussion (Barnett 2009) of entangled states begins by considering a pure state of two quantum systems, labeling a and b. This state can be described by the direct product as

$$|\psi\rangle = |\lambda\rangle_a |\phi\rangle_b . \tag{7.7}$$

The state can be considered separately. The state of system a alone can be written down as $|\lambda\rangle_a$ and, vice versa, the state of system b alone can be written down as $|\phi\rangle_b$. Considering, the superposition of Eq. 7.7 is also an allowed state of this two-system. The state can be shown as

$$|\psi\rangle = c_1 |\lambda_1\rangle_a |\phi_1\rangle_b + c_2 |\lambda_2\rangle_a |\phi_2\rangle_b . \tag{7.8}$$

This state is not possible to write as a product of each individual system. States having this property are entangled. Generally, Eq. 7.8 can be rewritten as

$$|\psi\rangle = \sum_n a_n |\lambda_n\rangle_a |\phi_n\rangle_b , \tag{7.9}$$

where the states $\{|\lambda_n\rangle\}$ and $\{|\phi_n\rangle\}$ are orthonormal sets for the system a and b, respectively.

A possibility to separate the mentioned system as a product state may be quite difficult. This possibility can directly tell the indicator having a property of entanglement. Similarly, this possibility can be provided by forming the density operator associated with the state. Considering, the density operator for the non-entangled state, mentioned in Eq. 7.7, is

$$\hat{\rho}_{ab} = |\lambda\rangle \langle\lambda| |\phi\rangle \langle\phi| . \tag{7.10}$$

Thus, the reduced density operator for the system a is

$$\hat{\rho}_a = |\lambda\rangle \langle\lambda| , \tag{7.11}$$

which is the density operator for the pure state. Obviously, $\mathrm{Tr}\left(\hat{\rho}_a^2\right) = 1$. Therefore, any non-entangled pure state has the condition $\mathrm{Tr}\left(\hat{\rho}_a^2\right) = 1$. Similarly, this condition can also consistent with any non-entangled state. If the trace is found that $\mathrm{Tr}\left(\hat{\rho}_a^2\right) \neq 1$ then the state is entangled.

The famous entangled states are the four Bell states, which are

$$\left|\Psi^-\right\rangle = \frac{1}{\sqrt{2}}\left(|0\rangle \otimes |1\rangle - |1\rangle \otimes |0\rangle\right), \tag{7.12}$$

$$\left|\Psi^+\right\rangle = \frac{1}{\sqrt{2}}\left(|0\rangle \otimes |1\rangle + |1\rangle \otimes |0\rangle\right), \tag{7.13}$$

$$\left|\Phi^-\right\rangle = \frac{1}{\sqrt{2}}\left(|0\rangle \otimes |0\rangle - |1\rangle \otimes |1\rangle\right), \tag{7.14}$$

$$\left|\Phi^+\right\rangle = \frac{1}{\sqrt{2}}\left(|0\rangle \otimes |0\rangle + |1\rangle \otimes |1\rangle\right). \tag{7.15}$$

7.3 Multipartite Entangled State

Generally, an entangled state is considered by a bipartite system. This section is going to discuss about a multipartite entanglement, which is an entanglement of a multipartite system and called GHZ-state. GHZ-state was introduced by Greenberger, Horne, and Zeilinger in 1989 (Greenberger *et al.* 2007). GHZ-state was known by a gedankenexperiment that tried to answer the question in conflict beyond Bell's argument.

In 1999, the experimental realization was demonstrated by Bouwmeester *et al.* (Bouwmeester *et al.* 1999). It took about ten years to accomplish. The polarization entanglement for three spatially separated photons was presented. The schematic setup is shown in Fig. 7.2. The scheme considered the case that "two pairs" of SPDC photons are generated by a single UV pulse on a nonlinear crystal. The state of four detectors, which are D_T, D_1, D_2, and D_3, was considered when D_T is trigged. This state is

$$|\psi_{T123}\rangle = \frac{1}{\sqrt{2}}|H\rangle_T\left[|H\rangle_1|H\rangle_2|V\rangle_3 + |V\rangle_1|V\rangle_2|H\rangle_3\right]. \tag{7.16}$$

For the conditional state on the trigger T, the state becomes

$$|\psi_{123}\rangle = \frac{1}{\sqrt{2}}\left[|H\rangle_1|H\rangle_2|V\rangle_3 + |V\rangle_1|V\rangle_2|H\rangle_3\right], \tag{7.17}$$

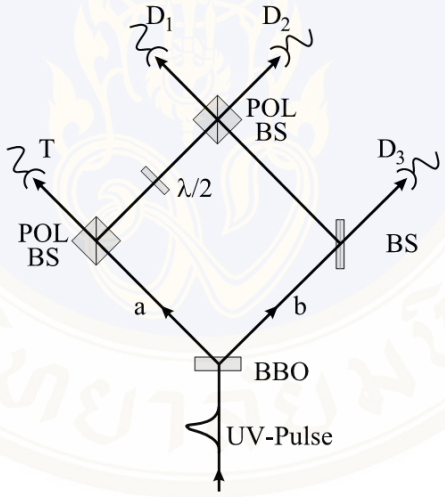

Figure 7.2: Schematic diagram of the experimental setup for the demonstration of the GHZ entanglement for spatially separated photons of Bouwmeester *et al.* (Bouwmeester *et al.* 1999).

which is a GHZ state (of three particles). The density operator of Eq. 7.17 is

$$\hat{\rho}_{123} = \frac{1}{2}\left[\begin{array}{l} |H\rangle_1|H\rangle_2|V\rangle_3\langle H|_1\langle H|_2\langle V|_3 + |V\rangle_1|V\rangle_2|H\rangle_3\langle H|_1\langle H|_2\langle V|_3 \\ +|H\rangle_1|H\rangle_2|V\rangle_3\langle V|_1\langle V|_2\langle H|_3 + |V\rangle_1|V\rangle_2|H\rangle_3\langle V|_1\langle V|_2\langle H|_3 \end{array}\right]. \quad (7.18)$$

The reduced density operator over D_1 is

$$\hat{\rho}_{23} = \mathrm{Tr}_1\left(\hat{\rho}_{123}\right) = \frac{1}{2}\left[|\mathrm{H}\rangle_2|\mathrm{V}\rangle_3\langle\mathrm{H}|_2\langle\mathrm{V}|_3 + |\mathrm{V}\rangle_2|\mathrm{H}\rangle_3\langle\mathrm{V}|_2\langle\mathrm{H}|_3\right], \quad (7.19)$$

which can be separated as

$$|\psi_{23}\rangle = \frac{1}{\sqrt{2}}\left[|H\rangle_2|V\rangle_3 + |V\rangle_2|H\rangle_3\right]. \quad (7.20)$$

Eq. 7.20 shows that the state from Eq. 7.17 can reduce to be like the EPR state. This reduction is done by taking the trigger T at whatever D_1.

7.4 Heralded Entangled Photon

Heralded states, which can be considered as multipartite entanglement, were introduced to enhance accuracy of states detecting in low signal information (Podoshvedov 2006; Śliwa & Banaszek 2003; Pan *et al.* 2001; Barz *et al.* 2010). Heralded states have been generated by using multipairs of down-converted photons and post-selections of states (Walther *et al.* 2007; Barz *et al.* 2010). Thus, heralded entangled states are based on multipartite entangled states with some part of the whole states used as a trigger for obtaining the information of the rest states without measurement. The exact states of the interest can be obtained without destroy. This method can be used to obtain on-demand entanglement.

7.5 Basic Linear-Optical Entanglement

Consider the two-photon interference of Hong-Ou-Mandel (HOM) effect, which was firstly constructed in 1987 (Hong *et al.* 1987), when two modes of a beam-splitter are input each mode with polarized single photons orthogonally, $|1,0\rangle_0\,|0,1\rangle_1$. The transformation of operators is according to Eq. 7.5 and Eq. 7.6. Thus, the output

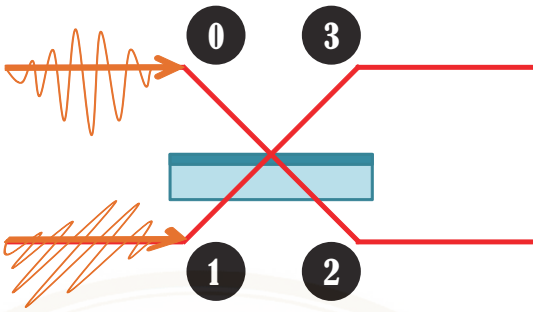

Figure 7.3: Two-photon interference by two orthogonally polarized single photons into two modes of a beam-splitter.

state is

$$\begin{aligned}
|\text{output}\rangle_{2,3} =& U|\text{input}\rangle_{0,1} = Ua^\dagger_{0H}a^\dagger_{1V}|0,0\rangle_0|0,0\rangle_1 \\
=& Ua^\dagger_{0H}U^\dagger Ua^\dagger_{1V}U^\dagger U|0,0\rangle_0|0,0\rangle_1 \\
=& \left(Ua^\dagger_{0H}U^\dagger\right)\left(Ua^\dagger_{1V}U^\dagger\right)U|0,0\rangle_0|0,0\rangle_1 \\
=& \frac{1}{2}\left[\left(a^\dagger_{2H}-a^\dagger_{3H}\right)\left(a^\dagger_{2V}+a^\dagger_{3V}\right)\right]|0,0\rangle_2|0,0\rangle_3 \\
=& \frac{1}{2}\left[a^\dagger_{2H}a^\dagger_{2V}-a^\dagger_{3H}a^\dagger_{3V}+a^\dagger_{2H}a^\dagger_{3V}-a^\dagger_{2V}a^\dagger_{3H}\right]|0,0\rangle_2|0,0\rangle_3 \\
=& \frac{1}{2}\left[|1,1\rangle_2|0,0\rangle_3-|0,0\rangle_2|1,1\rangle_3+|1,0\rangle_2|0,1\rangle_3-|0,1\rangle_2|1,0\rangle_3\right] \qquad (7.21)
\end{aligned}$$

The last line of Eq. 7.21 can be separated into two parts: the non-entangled part and the entangled part. The non-entangled state is the first two terms of the output state and the entangled state is the last two terms of the output state. If the joint-detection or coincidence detection is performed, then the post-selection is according to the following equation and the entangled part can be measured.

$$|\text{SelectedOutput}\rangle_{2,3} = \frac{1}{\sqrt{2}}\left[|1,0\rangle_2|0,1\rangle_3-|0,1\rangle_2|1,0\rangle_3\right] \qquad (7.22)$$

This measurement can select an entanglement out of the all-possible states. This selected state is the entangled state of photon polarization.

CHAPTER VIII

THEORETICAL CALCULATION

In this chapter, the theoretical study of entanglement generation is given through the calculation. The entanglement generation is based only on linear optical elements. There are some requirements in each following generation. The post-selection is also considered here. Finally, the entangled state is obtained to extend to the other applications.

8.1 Four-Photon Entanglement Generation using Linear Optical Elements

This study is about how to generate an entangled state, which is the entanglement of four-photon system. The basic idea is mentioned in Sec. 7.5. For four-photon entangled system, the basic idea and schematic setting are inspired by the work of Sheng *et al* (Sheng *et al.* 2008). The four-photon entangled states can be obtained by post-selection with the specific input state preparation. The proposed study in this thesis is an improvement of the setting of Sheng *et al* using a different initial input state. Additionally, the result of the proposed study is obtained with the higher efficiency and a distinguishability of states.

8.1.1 Schematic Diagram

The schematic diagram of the setup for generating four-photon entangled states is shown in Fig. 8.1. There are three symmetric polarization independent beam-splitters, 50-50 beam-splitters, and two half-waveplates (HWP) at two output modes, mode-7 and mode-8. The important thing is that this setup requires a specific initial input state. The initial input state is two arbitrary photons with horizontal polarization

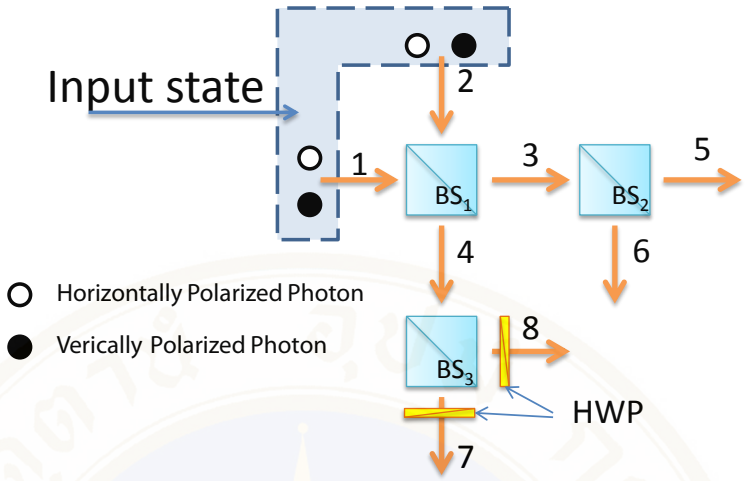

Figure 8.1: The schematic diagram of the setup for generating four-photon entangled states. There are three symmetric polarization-independent beam-splitters, 50-50 beam-splitters, and two half-waveplates (HWP) at mode-7 and mode-8. Four photons are inserted into mode-1 and mode-2, the input modes. Each input mode gets a horizontally polarized photon and a vertically polarized photon.

$|H\rangle$ and vertical polarization $|V\rangle$ at mode-1 and mode-2; this input state is denoted by $|1_H 1_V\rangle_1 |1_H 1_V\rangle_2$.

In this consideration, the beam-splitters are the plated type. The action on a beam-splitter can be described by the creation operators mentioned in Sec. 7.1. For example, the action of BS_1, following in Fig. 8.1, on H polarization is denoted by

$$\begin{aligned} a^\dagger_{1H} &= \frac{1}{\sqrt{2}}\left(a^\dagger_{3H} - a^\dagger_{4H}\right), \\ a^\dagger_{2H} &= \frac{1}{\sqrt{2}}\left(a^\dagger_{3H} + a^\dagger_{4H}\right). \end{aligned} \tag{8.1}$$

The action of BS_1 on V polarization is denoted by

$$\begin{aligned} a^\dagger_{1V} &= \frac{1}{\sqrt{2}}\left(a^\dagger_{3V} - a^\dagger_{4V}\right), \\ a^\dagger_{2V} &= \frac{1}{\sqrt{2}}\left(a^\dagger_{3V} + a^\dagger_{4V}\right). \end{aligned} \tag{8.2}$$

Similarly, the action of BS_2 and BS_3 on χ polarization are denoted by

$$\begin{aligned} a^\dagger_{3\chi} &= \frac{1}{\sqrt{2}}\left(a^\dagger_{5\chi} - a^\dagger_{6\chi}\right), \\ a^\dagger_{4\chi} &= \frac{1}{\sqrt{2}}\left(a^\dagger_{7\chi} + a^\dagger_{8\chi}\right), \end{aligned} \tag{8.3}$$

respectively, where χ polarization can be a set of orthogonal polarization such as H and V polarization.

The last step before photons left the system is the transformation of two HWPs at mode-7 and mode-8. The HWPs are aligned by $\frac{\pi}{4}$, thus the photon linear-polarization is rotated orthogonally comparing to the photon before the HWPs. The transformation on the HWP is denoted by

$$\begin{aligned} |H\rangle &\xrightarrow{HWP} |V\rangle \\ |V\rangle &\xrightarrow{HWP} -|H\rangle . \end{aligned} \tag{8.4}$$

8.1.2 Photon Evolution

According to the schematic diagram, the initial input state is $|1_H 1_V\rangle_1 |1_H 1_V\rangle_2$. The initial input state is injected into the system at BS_1. After BS_1, the input state evolves in the following.

$$\begin{aligned} |\text{output}\rangle_{3,4} =& U|\text{input}\rangle_{1,2} \\ =& U|1_H 1_V\rangle_1 |1_H 1_V\rangle_2 \\ =& U a^\dagger_{1H} a^\dagger_{1V} a^\dagger_{2H} a^\dagger_{2V} |0,0\rangle_1 |0,0\rangle_2 \\ =& U a^\dagger_{1H} U^\dagger U a^\dagger_{1V} U^\dagger U a^\dagger_{2H} U^\dagger U a^\dagger_{2V} U^\dagger U |0,0\rangle_1 |0,0\rangle_2 \\ =& \left(U a^\dagger_{1H} U^\dagger\right)\left(U a^\dagger_{1V} U^\dagger\right)\left(U a^\dagger_{2H} U^\dagger\right)\left(U a^\dagger_{2V} U^\dagger\right) U|0,0\rangle_1 |0,0\rangle_2 \\ =& \frac{1}{\sqrt{2}}\left(a^\dagger_{3H} - a^\dagger_{4H}\right)\frac{1}{\sqrt{2}}\left(a^\dagger_{3V} - a^\dagger_{4V}\right)\frac{1}{\sqrt{2}}\left(a^\dagger_{3H} + a^\dagger_{4H}\right) \\ & \times \frac{1}{\sqrt{2}}\left(a^\dagger_{3V} + a^\dagger_{4V}\right)|0,0\rangle_3 |0,0\rangle_4 \\ =& \frac{1}{4}\left(\left(a^\dagger_{3H}\right)^2 - \left(a^\dagger_{4H}\right)^2\right)\left(\left(a^\dagger_{3V}\right)^2 - \left(a^\dagger_{4V}\right)^2\right)|0,0\rangle_3 |0,0\rangle_4 \\ =& \frac{1}{2}\left(|2_H 2_V\rangle_3 |0\rangle_4 - |2_V\rangle_3 |2_H\rangle_4 - |2_H\rangle_3 |2_V\rangle_4 + |0\rangle_3 |2_H 2_V\rangle_4\right) \end{aligned} \tag{8.5}$$

In short description, the input state is transformed by BS_1 to be the state after BS_1,

$$\begin{aligned} &|1_H 1_V\rangle_1 |1_H 1_V\rangle_2 \\ &\xrightarrow{BS_1} \frac{1}{2}\left(|2_H 2_V\rangle_3 |0\rangle_4 - |2_V\rangle_3 |2_H\rangle_4 - |2_H\rangle_3 |2_V\rangle_4 + |0\rangle_3 |2_H 2_V\rangle_4\right). \end{aligned} \tag{8.6}$$

These output states after BS_1 are the input states for the rest of the system, which are BS_2, BS_3, and two HWPs. The final output is

$$\begin{aligned}
&\frac{1}{2}|2_H2_V\rangle_3|0\rangle_4-\frac{1}{2}|2_V\rangle_3|2_H\rangle_4-\frac{1}{2}|2_H\rangle_3|2_V\rangle_4+\frac{1}{2}|0\rangle_3|2_H2_V\rangle_4\\
&\xrightarrow{BS_2,BS_3,HWP}\\
&\quad\frac{1}{8}|2_H2_V\rangle_5|0\rangle_6|0\rangle_7|0\rangle_8-\frac{1}{4\sqrt{2}}|1_H2_V\rangle_5|1_H\rangle_6|0\rangle_7|0\rangle_8\\
&\quad+\frac{1}{8}|2_V\rangle_5|2_H\rangle_6|0\rangle_7|0\rangle_8-\frac{1}{8}|2_V\rangle_5|0\rangle_6|2_V\rangle_7|0\rangle_8\\
&\quad+\frac{1}{4\sqrt{2}}|2_V\rangle_5|0\rangle_6|1_V\rangle_7|1_V\rangle_8-\frac{1}{8}|2_V\rangle_5|0\rangle_6|0\rangle_7|2_V\rangle_8\\
&\quad-\frac{1}{4\sqrt{2}}|2_H1_V\rangle_5|1_V\rangle_6|0\rangle_7|0\rangle_8+\frac{1}{4}|1_H1_V\rangle_5|1_H1_V\rangle_6|0\rangle_7|0\rangle_8\\
&\quad-\frac{1}{4\sqrt{2}}|1_V\rangle_5|2_H1_V\rangle_6|0\rangle_7|0\rangle_8+\frac{1}{4\sqrt{2}}|1_V\rangle_5|1_V\rangle_6|2_H\rangle_7|0\rangle_8\\
&\quad-\frac{1}{4}|1_V\rangle_5|1_V\rangle_6|1_V\rangle_7|1_V\rangle_8+\frac{1}{4\sqrt{2}}|1_V\rangle_5|1_V\rangle_6|0\rangle_7|2_V\rangle_8\\
&\quad+\frac{1}{8}|2_H\rangle_5|2_V\rangle_6|0\rangle_7|0\rangle_8-\frac{1}{4\sqrt{2}}|1_H\rangle_5|1_H2_V\rangle_6|0\rangle_7|0\rangle_8\\
&\quad+\frac{1}{8}|0\rangle_5|2_H2_V\rangle_6|0\rangle_7|0\rangle_8-\frac{1}{8}|0\rangle_5|2_V\rangle_6|2_V\rangle_7|0\rangle_8\\
&\quad+\frac{1}{4\sqrt{2}}|0\rangle_5|2_V\rangle_6|1_V\rangle_7|1_V\rangle_8-\frac{1}{8}|0\rangle_5|2_V\rangle_6|0\rangle_7|2_V\rangle_8\\
&\quad-\frac{1}{8}|2_H\rangle_5|0\rangle_6|2_H\rangle_7|0\rangle_8+\frac{1}{4\sqrt{2}}|1_H\rangle_5|1_H\rangle_6|2_H\rangle_7|0\rangle_8\\
&\quad-\frac{1}{8}|0\rangle_5|2_H\rangle_6|2_H\rangle_7|0\rangle_8+\frac{1}{8}|0\rangle_5|0\rangle_6|2_H2_V\rangle_7|0\rangle_8\\
&\quad-\frac{1}{4\sqrt{2}}|0\rangle_5|0\rangle_6|2_H1_V\rangle_7|1_V\rangle_8-\frac{1}{8}|0\rangle_5|0\rangle_6|2_H\rangle_7|2_V\rangle_8\\
&\quad+\frac{1}{4\sqrt{2}}|2_H\rangle_5|0\rangle_6|1_H\rangle_7|1_H\rangle_8-\frac{1}{4}|1_H\rangle_5|1_H\rangle_6|1_H\rangle_7|1_H\rangle_8\\
&\quad+\frac{1}{4\sqrt{2}}|0\rangle_5|2_H\rangle_6|1_H\rangle_7|1_H\rangle_8-\frac{1}{4\sqrt{2}}|0\rangle_5|0\rangle_6|1_H2_V\rangle_7|1_H\rangle_8\\
&\quad+\frac{1}{4}|0\rangle_5|0\rangle_6|1_H1_V\rangle_7|1_H1_V\rangle_8-\frac{1}{4\sqrt{2}}|0\rangle_5|0\rangle_6|1_H\rangle_7|1_H2_V\rangle_8\\
&\quad-\frac{1}{8}|2_H\rangle_5|0\rangle_6|0\rangle_7|2_H\rangle_8+\frac{1}{4\sqrt{2}}|1_H\rangle_5|1_H\rangle_6|0\rangle_7|2_H\rangle_8\\
&\quad-\frac{1}{8}|0\rangle_5|2_H\rangle_6|0\rangle_7|2_H\rangle_8+\frac{1}{8}|0\rangle_5|0\rangle_6|2_V\rangle_7|2_H\rangle_8\\
&\quad-\frac{1}{4\sqrt{2}}|0\rangle_5|0\rangle_6|1_V\rangle_7|2_H1_V\rangle_8+\frac{1}{8}|0\rangle_5|0\rangle_6|0\rangle_7|2_H2_V\rangle_8. \qquad (8.7)
\end{aligned}$$

8.1.3 Post-Selection

According to Sec. 7.5, the bipartite entangled state is obtained by considering only two-folded coincidence of the output of leaving photon from the system. That is a post-selection of the system of Hong to generate the entanglement. Similarly, the post-selection in this thesis is considered here. The first consideration is the following: If only the events in which the distinguished photons come out from each mode are kept from Eq. 8.7, the output state will be

$$\begin{aligned}|\text{Select}_1\rangle =&\frac{1}{4}|1_H1_V\rangle_5|1_H1_V\rangle_6|0\rangle_7|0\rangle_8 - \frac{1}{4}|1_V\rangle_5|1_V\rangle_6|1_V\rangle_7|1_V\rangle_8 \\ &- \frac{1}{4}|1_H\rangle_5|1_H\rangle_6|1_H\rangle_7|1_H\rangle_8 + \frac{1}{4}|0\rangle_5|0\rangle_6|1_H1_V\rangle_7|1_H1_V\rangle_8. \end{aligned} \tag{8.8}$$

the selected state $|\text{Select}_1\rangle$ can be considered and separated by two parts: The first part is an entanglement of photon-number states (Fock-state entanglement), which are the first and the last term of Eq. 8.8. The second part also shows an entanglement of polarized states, which are the second and the third term of Eq. 8.8. When only the events with one photon at each mode are kept from Eq. 8.7, the output state will be

$$|\text{Select}_2\rangle = -\frac{1}{4}|1_H\rangle_5|1_H\rangle_6|1_H\rangle_7|1_H\rangle_8 - \frac{1}{4}|1_V\rangle_5|1_V\rangle_6|1_V\rangle_7|1_V\rangle_8, \tag{8.9}$$

which is the expected four-photon entangled state. The success probability of the four-photon entangled state generation is 1/8 with a perfect postselection. Comparing to the work of Sheng *et al* (Sheng *et al.* 2008), which has the state after their post-selection is

$$\begin{aligned}|G_4\rangle = &\frac{1}{8}|1_V\rangle_5|1_V\rangle_6|1_H\rangle_7|1_H\rangle_8 - \frac{1}{8}|1_H\rangle_5|1_V\rangle_6|1_H\rangle_7|1_V\rangle_8 \\ &-\frac{1}{8}|1_H\rangle_5|1_V\rangle_6|1_V\rangle_7|1_H\rangle_8 - \frac{1}{8}|1_V\rangle_5|1_H\rangle_6|1_H\rangle_7|1_V\rangle_8 \\ &-\frac{1}{8}|1_V\rangle_5|1_H\rangle_6|1_V\rangle_7|1_H\rangle_8 + \frac{1}{8}|1_H\rangle_5|1_H\rangle_6|1_V\rangle_7|1_V\rangle_8, \end{aligned} \tag{8.10}$$

and the efficiency is 3/32. Consequently, the state $|\text{Select}_2\rangle$ gives more efficiency by 1.33 times. Furthermore, this state is more practical for a practical implementation comparing to the state of Sheng *et al.* When a polarized state of a photon is known (by a measurement) on whatever mode a H (or V) polarized photon, this photon can

indicate that all other remaining modes give another H (or V) polarized photon at each remaining modes. For example, if a H polarized photon is obtained by mode-5, all other remaining modes (which are mode-6, mode-7, and mode-8) will obtain a H polarized photon. On the other hand for Eq. 8.10, when the polarized state of the first photon is known, it still cannot distinguish the states. It has to know at least another mode or another two modes to distinguish the states. Thus, the state of Sheng *et al* is not suitable in a practical implementation for sending the quantum information between network nodes, which is not applied to the state $|\text{Select}_2\rangle$.

8.1.4 Summary

The schematic setting for four-photon entangled-state generation is based on the system proposed by Sheng *et al* with changing the initial input state. In this study, the initial input state is two arbitrary photons with horizontal polarization and vertical polarization at both input modes (mode-1 and mode-2). Additionally, the scheme has only three beam-splitters and two HWPs. Thus, the generation requires only single-photon sources and linear optical elements. The generation is not necessary to concern about a small efficiency of a nonlinear optical process. Furthermore, by the modification of the initial input state, this scheme is improved from the work of Sheng *et al* to have 1.33 times more efficiency.

8.2 Heralded Generation of Bipartite Entangled States using Linear Optical Elements

This study is an expansion from the previous section to generate another GHZ-state. This generation of the GHZ-state will be a heralded generation of bipartite entangled states. The heralded generations allow us to know precisely when there is entanglement of photons, which cannot be achieved by a normal generation because each normal generation is random. The basic idea is mentioned in Sec. 7.3 and Sec.7.4. Certainly, the post-selecting process has to be performed. In this scheme, the post-selection is a small difference from normal post-selection, which is usually arrival photons

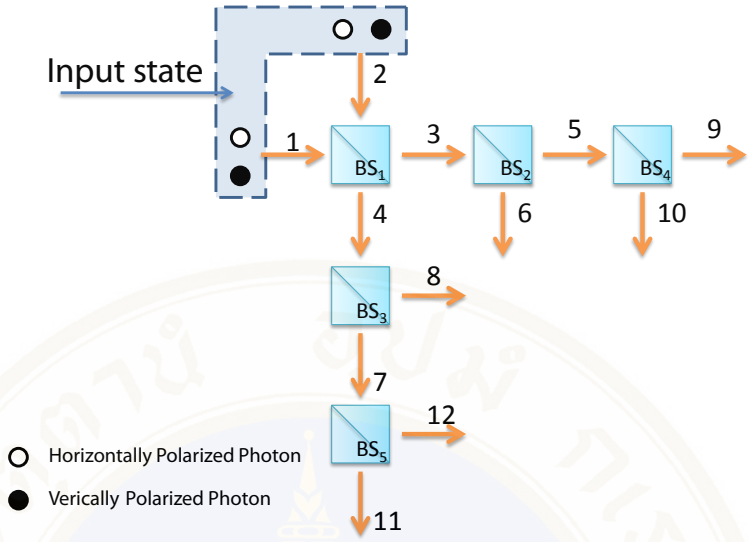

Figure 8.2: The schematic diagram of the setup for generating four-photon entangled states. There are five symmetric polarization-independent beam-splitters, 50-50 beam-splitters. Four photons are inserted into mode-1 and mode-2, the input modes. Each input mode gets a horizontally polarized photon and a vertically polarized photon.

to detection systems or N-folded coincidence. The difference is a post-selection with the combination of null-states and two-folded coincidence.

8.2.1 Schematic Diagram

The idea is similar to Sec. 8.1.1. The schematic diagram of the proposed setup for generating heralded entangled states, expanded from the work of Sheng *et al* (Sheng *et al.* 2008), is shown in Fig. 8.2. In the system, five symmetric beam-splitters, 50-50 beam-splitters, are located. All beamsplitters are polarization-independent. In this schematic setup, the initial input state must be a horizontally polarized (H) photon and a vertically polarized (V) photon into both input modes, mode-1 and mode-2. The input state is denoted by $|1_H 1_V\rangle_1 |1_H 1_V\rangle_2$, where the subscripts are the numbers of modes. The rest is the evolution of photons in the system of beam-splitters.

8.2.2 Photon Evolution

The first step of evolution in the system is similar to Eq. 8.6. These output states after BS_1 are the input states for the rest of the system, which are BS_2, BS_3,

BS_4, and BS_5. The final output is

$$\begin{aligned}
&\frac{1}{2}|2_H2_V\rangle_3|0\rangle_4-\frac{1}{2}|2_V\rangle_3|2_H\rangle_4-\frac{1}{2}|2_H\rangle_3|2_V\rangle_4+\frac{1}{2}|0\rangle_3|2_H2_V\rangle_4\longrightarrow\\
&\quad\frac{1}{8}|2_H2_V\rangle_6|0\rangle_8|0\rangle_9|0\rangle_{10}|0\rangle_{11}|0\rangle_{12}-\frac{1}{8}|2_V\rangle_6|2_H\rangle_8|0\rangle_9|0\rangle_{10}|0\rangle_{11}|0\rangle_{12}\\
&-\frac{1}{8}|2_H\rangle_6|2_V\rangle_8|0\rangle_9|0\rangle_{10}|0\rangle_{11}|0\rangle_{12}+\frac{1}{8}|0\rangle_6|2_H2_V\rangle_8|0\rangle_9|0\rangle_{10}|0\rangle_{11}|0\rangle_{12}\\
&-\frac{1}{8}|1_H2_V\rangle_6|0\rangle_8|1_H\rangle_9|0\rangle_{10}|0\rangle_{11}|0\rangle_{12}+\frac{1}{8}|1_H\rangle_6|2_V\rangle_8|1_H\rangle_9|0\rangle_{10}|0\rangle_{11}|0\rangle_{12}\\
&+\frac{1}{16}|2_V\rangle_6|0\rangle_8|2_H\rangle_9|0\rangle_{10}|0\rangle_{11}|0\rangle_{12}-\frac{1}{16}|0\rangle_6|2_V\rangle_8|2_H\rangle_9|0\rangle_{10}|0\rangle_{11}|0\rangle_{12}\\
&-\frac{1}{8}|2_H1_V\rangle_6|0\rangle_8|1_V\rangle_9|0\rangle_{10}|0\rangle_{11}|0\rangle_{12}+\frac{1}{8}|1_V\rangle_6|2_H\rangle_8|1_V\rangle_9|0\rangle_{10}|0\rangle_{11}|0\rangle_{12}\\
&+\frac{1}{8}|1_H1_V\rangle_6|0\rangle_8|1_H1_V\rangle_9|0\rangle_{10}|0\rangle_{11}|0\rangle_{12}-\frac{1}{16}|1_V\rangle_6|0\rangle_8|2_H1_V\rangle_9|0\rangle_{10}|0\rangle_{11}|0\rangle_{12}\\
&+\frac{1}{16}|2_H\rangle_6|0\rangle_8|2_V\rangle_9|0\rangle_{10}|0\rangle_{11}|0\rangle_{12}-\frac{1}{16}|0\rangle_6|2_H\rangle_8|2_V\rangle_9|0\rangle_{10}|0\rangle_{11}|0\rangle_{12}\\
&-\frac{1}{16}|1_H\rangle_6|0\rangle_8|1_H2_V\rangle_9|0\rangle_{10}|0\rangle_{11}|0\rangle_{12}+\frac{1}{32}|0\rangle_6|0\rangle_8|2_H2_V\rangle_9|0\rangle_{10}|0\rangle_{11}|0\rangle_{12}\\
&+\frac{1}{8}|1_H2_V\rangle_6|0\rangle_8|0\rangle_9|1_H\rangle_{10}|0\rangle_{11}|0\rangle_{12}-\frac{1}{8}|1_H\rangle_6|2_V\rangle_8|0\rangle_9|1_H\rangle_{10}|0\rangle_{11}|0\rangle_{12}\\
&-\frac{1}{8\sqrt{2}}|2_V\rangle_6|0\rangle_8|1_H\rangle_9|1_H\rangle_{10}|0\rangle_{11}|0\rangle_{12}+\frac{1}{8\sqrt{2}}|0\rangle_6|2_V\rangle_8|1_H\rangle_9|1_H\rangle_{10}|0\rangle_{11}|0\rangle_{12}\\
&-\frac{1}{8}|1_H1_V\rangle_6|0\rangle_8|1_V\rangle_9|1_H\rangle_{10}|0\rangle_{11}|0\rangle_{12}+\frac{1}{8\sqrt{2}}|1_V\rangle_6|0\rangle_8|1_H1_V\rangle_9|1_H\rangle_{10}|0\rangle_{11}|0\rangle_{12}\\
&+\frac{1}{16}|1_H\rangle_6|0\rangle_8|2_V\rangle_9|1_H\rangle_{10}|0\rangle_{11}|0\rangle_{12}-\frac{1}{16\sqrt{2}}|0\rangle_6|0\rangle_8|1_H2_V\rangle_9|1_H\rangle_{10}|0\rangle_{11}|0\rangle_{12}\\
&+\frac{1}{16}|2_V\rangle_6|0\rangle_8|0\rangle_9|2_H\rangle_{10}|0\rangle_{11}|0\rangle_{12}-\frac{1}{16}|0\rangle_6|2_V\rangle_8|0\rangle_9|2_H\rangle_{10}|0\rangle_{11}|0\rangle_{12}\\
&-\frac{1}{16}|1_V\rangle_6|0\rangle_8|1_V\rangle_9|2_H\rangle_{10}|0\rangle_{11}|0\rangle_{12}+\frac{1}{32}|0\rangle_6|0\rangle_8|2_V\rangle_9|2_H\rangle_{10}|0\rangle_{11}|0\rangle_{12}\\
&+\frac{1}{8}|2_H1_V\rangle_6|0\rangle_8|0\rangle_9|1_V\rangle_{10}|0\rangle_{11}|0\rangle_{12}-\frac{1}{8}|1_V\rangle_6|2_H\rangle_8|0\rangle_9|1_V\rangle_{10}|0\rangle_{11}|0\rangle_{12}\\
&-\frac{1}{8}|1_H1_V\rangle_6|0\rangle_8|1_H\rangle_9|1_V\rangle_{10}|0\rangle_{11}|0\rangle_{12}+\frac{1}{16}|1_V\rangle_6|0\rangle_8|2_H\rangle_9|1_V\rangle_{10}|0\rangle_{11}|0\rangle_{12}\\
&-\frac{1}{8\sqrt{2}}|2_H\rangle_6|0\rangle_8|1_V\rangle_9|1_V\rangle_{10}|0\rangle_{11}|0\rangle_{12}+\frac{1}{8\sqrt{2}}|0\rangle_6|2_H\rangle_8|1_V\rangle_9|1_V\rangle_{10}|0\rangle_{11}|0\rangle_{12}\\
&+\frac{1}{8\sqrt{2}}|1_H\rangle_6|0\rangle_8|1_H1_V\rangle_9|1_V\rangle_{10}|0\rangle_{11}|0\rangle_{12}-\frac{1}{16\sqrt{2}}|0\rangle_6|0\rangle_8|2_H1_V\rangle_9|1_V\rangle_{10}|0\rangle_{11}\\
&+\frac{1}{8}|1_H1_V\rangle_6|0\rangle_8|0\rangle_9|1_H1_V\rangle_{10}|0\rangle_{11}|0\rangle_{12}-\frac{1}{8\sqrt{2}}|1_V\rangle_6|0\rangle_8|1_H\rangle_9|1_H1_V\rangle_{10}|0\rangle_{11}|0\rangle_{12}\\
&-\frac{1}{8\sqrt{2}}|1_H\rangle_6|0\rangle_8|1_V\rangle_9|1_H1_V\rangle_{10}|0\rangle_{11}|0\rangle_{12}+\frac{1}{16}|0\rangle_6|0\rangle_8|1_H1_V\rangle_9|1_H1_V\rangle_{10}|0\rangle_{11}|0\rangle_{12}\\
&+\frac{1}{16}|1_V\rangle_6|0\rangle_8|0\rangle_9|2_H1_V\rangle_{10}|0\rangle_{11}|0\rangle_{12}-\frac{1}{16\sqrt{2}}|0\rangle_6|0\rangle_8|1_V\rangle_9|2_H1_V\rangle_{10}|0\rangle_{11}|0\rangle_{12}\\
&+\frac{1}{16}|2_H\rangle_6|0\rangle_8|0\rangle_9|2_V\rangle_{10}|0\rangle_{11}|0\rangle_{12}-\frac{1}{16}|0\rangle_6|2_H\rangle_8|0\rangle_9|2_V\rangle_{10}|0\rangle_{11}|0\rangle_{12}
\end{aligned}$$

$$
\begin{aligned}
&-\frac{1}{16}|1_H\rangle_6|0\rangle_8|1_H\rangle_9|2_V\rangle_{10}|0\rangle_{11}|0\rangle_{12}+\frac{1}{32}|0\rangle_6|0\rangle_8|2_H\rangle_9|2_V\rangle_{10}|0\rangle_{11}|0\rangle_{12}\\
&+\frac{1}{16}|1_H\rangle_6|0\rangle_8|0\rangle_9|1_H2_V\rangle_{10}|0\rangle_{11}|0\rangle_{12}-\frac{1}{16\sqrt{2}}|0\rangle_6|0\rangle_8|1_H\rangle_9|1_H2_V\rangle_{10}|0\rangle_{11}|0\rangle_{12}\\
&+\frac{1}{32}|0\rangle_6|0\rangle_8|0\rangle_9|2_H2_V\rangle_{10}|0\rangle_{11}|0\rangle_{12}+\frac{1}{8}|2_V\rangle_6|1_H\rangle_8|0\rangle_9|0\rangle_{10}|1_H\rangle_{11}|0\rangle_{12}\\
&-\frac{1}{8}|0\rangle_6|1_H2_V\rangle_8|0\rangle_9|0\rangle_{10}|1_H\rangle_{11}|0\rangle_{12}-\frac{1}{8}|1_V\rangle_6|1_H\rangle_8|1_V\rangle_9|0\rangle_{10}|1_H\rangle_{11}|0\rangle_{12}\\
&+\frac{1}{16}|0\rangle_6|1_H\rangle_8|2_V\rangle_9|0\rangle_{10}|1_H\rangle_{11}|0\rangle_{12}+\frac{1}{8}|1_V\rangle_6|1_H\rangle_8|0\rangle_9|1_V\rangle_{10}|1_H\rangle_{11}|0\rangle_{12}\\
&-\frac{1}{8\sqrt{2}}|0\rangle_6|1_H\rangle_8|1_V\rangle_9|1_V\rangle_{10}|1_H\rangle_{11}|0\rangle_{12}+\frac{1}{16}|0\rangle_6|1_H\rangle_8|0\rangle_9|2_V\rangle_{10}|1_H\rangle_{11}|0\rangle_{12}\\
&-\frac{1}{16}|2_V\rangle_6|0\rangle_8|0\rangle_9|0\rangle_{10}|2_H\rangle_{11}|0\rangle_{12}+\frac{1}{16}|0\rangle_6|2_V\rangle_8|0\rangle_9|0\rangle_{10}|2_H\rangle_{11}|0\rangle_{12}\\
&+\frac{1}{16}|1_V\rangle_6|0\rangle_8|1_V\rangle_9|0\rangle_{10}|2_H\rangle_{11}|0\rangle_{12}-\frac{1}{32}|0\rangle_6|0\rangle_8|2_V\rangle_9|0\rangle_{10}|2_H\rangle_{11}|0\rangle_{12}\\
&-\frac{1}{16}|1_V\rangle_6|0\rangle_8|0\rangle_9|1_V\rangle_{10}|2_H\rangle_{11}|0\rangle_{12}+\frac{1}{32}|1_V\rangle_9|1_V\rangle_{10}|1_H\rangle_{11}{}^2|0\rangle_{12}\\
&-\frac{1}{32}|0\rangle_6|0\rangle_8|0\rangle_9|2_V\rangle_{10}|2_H\rangle_{11}|0\rangle_{12}+\frac{1}{8}|2_H\rangle_6|1_V\rangle_8|0\rangle_9|0\rangle_{10}|1_V\rangle_{11}|0\rangle_{12}\\
&-\frac{1}{8}|0\rangle_6|2_H1_V\rangle_8|0\rangle_9|0\rangle_{10}|1_V\rangle_{11}|0\rangle_{12}-\frac{1}{8}|1_H\rangle_6|1_V\rangle_8|1_H\rangle_9|0\rangle_{10}|1_V\rangle_{11}|0\rangle_{12}\\
&+\frac{1}{16}|0\rangle_6|1_V\rangle_8|2_H\rangle_9|0\rangle_{10}|1_V\rangle_{11}|0\rangle_{12}+\frac{1}{8}|1_H\rangle_6|1_V\rangle_8|0\rangle_9|1_H\rangle_{10}|1_V\rangle_{11}|0\rangle_{12}\\
&-\frac{1}{8\sqrt{2}}|0\rangle_6|1_V\rangle_8|1_H\rangle_9|1_H\rangle_{10}|1_V\rangle_{11}|0\rangle_{12}+\frac{1}{16}|0\rangle_6|1_V\rangle_8|0\rangle_9|2_H\rangle_{10}|1_V\rangle_{11}|0\rangle_{12}\\
&+\frac{1}{8}|0\rangle_6|1_H1_V\rangle_8|0\rangle_9|0\rangle_{10}|1_H1_V\rangle_{11}|0\rangle_{12}-\frac{1}{16}|0\rangle_6|1_V\rangle_8|0\rangle_9|0\rangle_{10}|2_H1_V\rangle_{11}|0\rangle_{12}\\
&-\frac{1}{16}|2_H\rangle_6|0\rangle_8|0\rangle_9|0\rangle_{10}|2_V\rangle_{11}|0\rangle_{12}+\frac{1}{16}|0\rangle_6|2_H\rangle_8|0\rangle_9|0\rangle_{10}|2_V\rangle_{11}|0\rangle_{12}\\
&+\frac{1}{16}|1_H\rangle_6|0\rangle_8|1_H\rangle_9|0\rangle_{10}|2_V\rangle_{11}|0\rangle_{12}-\frac{1}{32}|0\rangle_6|0\rangle_8|2_H\rangle_9|0\rangle_{10}|2_V\rangle_{11}|0\rangle_{12}\\
&-\frac{1}{16}|1_H\rangle_6|0\rangle_8|0\rangle_9|1_H\rangle_{10}|2_V\rangle_{11}|0\rangle_{12}+\frac{1}{16\sqrt{2}}|0\rangle_6|0\rangle_8|1_H\rangle_9|1_H\rangle_{10}|2_V\rangle_{11}|0\rangle_{12}\\
&-\frac{1}{32}|0\rangle_6|0\rangle_8|0\rangle_9|2_H\rangle_{10}|2_V\rangle_{11}|0\rangle_{12}-\frac{1}{16}|0\rangle_6|1_H\rangle_8|0\rangle_9|0\rangle_{10}|1_H2_V\rangle_{11}|0\rangle_{12}\\
&+\frac{1}{32}|0\rangle_6|0\rangle_8|0\rangle_9|0\rangle_{10}|2_H2_V\rangle_{11}|0\rangle_{12}-\frac{1}{8}|2_V\rangle_6|1_H\rangle_8|0\rangle_9|0\rangle_{10}|0\rangle_{11}|1_H\rangle_{12}\\
&+\frac{1}{8}|0\rangle_6|1_H2_V\rangle_8|0\rangle_9|0\rangle_{10}|0\rangle_{11}|1_H\rangle_{12}+\frac{1}{8}|1_V\rangle_6|1_H\rangle_8|1_V\rangle_9|0\rangle_{10}|0\rangle_{11}|1_H\rangle_{12}\\
&-\frac{1}{16}|0\rangle_6|1_H\rangle_8|2_V\rangle_9|0\rangle_{10}|0\rangle_{11}|1_H\rangle_{12}-\frac{1}{8}|1_V\rangle_6|1_H\rangle_8|0\rangle_9|1_V\rangle_{10}|0\rangle_{11}|1_H\rangle_{12}\\
&+\frac{1}{8\sqrt{2}}|0\rangle_6|1_H\rangle_8|1_V\rangle_9|1_V\rangle_{10}|0\rangle_{11}|1_H\rangle_{12}-\frac{1}{16}|0\rangle_6|1_H\rangle_8|0\rangle_9|2_V\rangle_{10}|0\rangle_{11}|1_H\rangle_{12}\\
&+\frac{1}{8\sqrt{2}}|2_V\rangle_6|0\rangle_8|0\rangle_9|0\rangle_{10}|1_H\rangle_{11}|1_H\rangle_{12}-\frac{1}{8\sqrt{2}}|0\rangle_6|2_V\rangle_8|0\rangle_9|0\rangle_{10}|1_H\rangle_{11}|1_H\rangle_{12}\\
&-\frac{1}{8\sqrt{2}}|1_V\rangle_6|0\rangle_8|1_V\rangle_9|0\rangle_{10}|1_H\rangle_{11}|1_H\rangle_{12}+\frac{1}{16\sqrt{2}}|0\rangle_6|0\rangle_8|2_V\rangle_9|0\rangle_{10}|1_H\rangle_{11}|1_H\rangle_{12}
\end{aligned}
$$

$$+\frac{1}{8\sqrt{2}}|1_V\rangle_6|0\rangle_8|0\rangle_9|1_V\rangle_{10}|1_H\rangle_{11}|1_H\rangle_{12}-\frac{1}{16}|0\rangle_6|0\rangle_8|1_V\rangle_9|1_V\rangle_{10}|1_H\rangle_{11}|1_H\rangle_{12}$$
$$+\frac{1}{16\sqrt{2}}|0\rangle_6|0\rangle_8|0\rangle_9|2_V\rangle_{10}|1_H\rangle_{11}|1_H\rangle_{12}-\frac{1}{8}|0\rangle_6|1_H1_V\rangle_8|0\rangle_9|0\rangle_{10}|1_V\rangle_{11}|1_H\rangle_{12}$$
$$+\frac{1}{8\sqrt{2}}|0\rangle_6|1_V\rangle_8|0\rangle_9|0\rangle_{10}|1_H1_V\rangle_{11}|1_H\rangle_{12}+\frac{1}{16}|0\rangle_6|1_H\rangle_8|0\rangle_9|0\rangle_{10}|2_V\rangle_{11}|1_H\rangle_{12}$$
$$-\frac{1}{16\sqrt{2}}|0\rangle_6|0\rangle_8|0\rangle_9|0\rangle_{10}|1_H2_V\rangle_{11}|1_H\rangle_{12}-\frac{1}{16}|2_V\rangle_6|0\rangle_8|0\rangle_9|0\rangle_{10}|0\rangle_{11}|2_H\rangle_{12}$$
$$+\frac{1}{16}|0\rangle_6|2_V\rangle_8|0\rangle_9|0\rangle_{10}|0\rangle_{11}|2_H\rangle_{12}+\frac{1}{16}|1_V\rangle_6|0\rangle_8|1_V\rangle_9|0\rangle_{10}|0\rangle_{11}|2_H\rangle_{12}$$
$$-\frac{1}{32}|0\rangle_6|0\rangle_8|2_V\rangle_9|0\rangle_{10}|0\rangle_{11}|2_H\rangle_{12}-\frac{1}{16}|1_V\rangle_6|0\rangle_8|0\rangle_9|1_V\rangle_{10}|0\rangle_{11}|2_H\rangle_{12}$$
$$+\frac{1}{16\sqrt{2}}|0\rangle_6|0\rangle_8|1_V\rangle_9|1_V\rangle_{10}|0\rangle_{11}|2_H\rangle_{12}-\frac{1}{32}|0\rangle_6|0\rangle_8|0\rangle_9|2_V\rangle_{10}|0\rangle_{11}|2_H\rangle_{12}$$
$$-\frac{1}{16}|0\rangle_6|1_V\rangle_8|0\rangle_9|0\rangle_{10}|1_V\rangle_{11}|2_H\rangle_{12}+\frac{1}{32}|0\rangle_6|0\rangle_8|0\rangle_9|0\rangle_{10}|2_V\rangle_{11}|2_H\rangle_{12}$$
$$-\frac{1}{8}|2_H\rangle_6|1_V\rangle_8|0\rangle_9|0\rangle_{10}|0\rangle_{11}|1_V\rangle_{12}+\frac{1}{8}|0\rangle_6|2_H1_V\rangle_8|0\rangle_9|0\rangle_{10}|0\rangle_{11}|1_V\rangle_{12}$$
$$+\frac{1}{8}|1_H\rangle_6|1_V\rangle_8|1_H\rangle_9|0\rangle_{10}|0\rangle_{11}|1_V\rangle_{12}-\frac{1}{16}|0\rangle_6|1_V\rangle_8|2_H\rangle_9|0\rangle_{10}|0\rangle_{11}|1_V\rangle_{12}$$
$$-\frac{1}{8}|1_H\rangle_6|1_V\rangle_8|0\rangle_9|1_H\rangle_{10}|0\rangle_{11}|1_V\rangle_{12}+\frac{1}{8\sqrt{2}}|0\rangle_6|1_V\rangle_8|1_H\rangle_9|1_H\rangle_{10}|0\rangle_{11}|1_V\rangle_{12}$$
$$-\frac{1}{16}|0\rangle_6|1_V\rangle_8|0\rangle_9|2_H\rangle_{10}|0\rangle_{11}|1_V\rangle_{12}-\frac{1}{8}|0\rangle_6|1_H1_V\rangle_8|0\rangle_9|0\rangle_{10}|1_H\rangle_{11}|1_V\rangle_{12}$$
$$+\frac{1}{16}|0\rangle_6|1_V\rangle_8|0\rangle_9|0\rangle_{10}|2_H\rangle_{11}|1_V\rangle_{12}+\frac{1}{8\sqrt{2}}|2_H\rangle_6|0\rangle_8|0\rangle_9|0\rangle_{10}|1_V\rangle_{11}|1_V\rangle_{12}$$
$$-\frac{1}{8\sqrt{2}}|0\rangle_6|2_H\rangle_8|0\rangle_9|0\rangle_{10}|1_V\rangle_{11}|1_V\rangle_{12}-\frac{1}{8\sqrt{2}}|1_H\rangle_6|0\rangle_8|1_H\rangle_9|0\rangle_{10}|1_V\rangle_{11}|1_V\rangle_{12}$$
$$+\frac{1}{16\sqrt{2}}|0\rangle_6|0\rangle_8|2_H\rangle_9|0\rangle_{10}|1_V\rangle_{11}|1_V\rangle_{12}+\frac{1}{8\sqrt{2}}|1_H\rangle_6|0\rangle_8|0\rangle_9|1_H\rangle_{10}|1_V\rangle_{11}|1_V\rangle_{12}$$
$$-\frac{1}{16}|0\rangle_6|0\rangle_8|1_H\rangle_9|1_H\rangle_{10}|1_V\rangle_{11}|1_V\rangle_{12}+\frac{1}{16\sqrt{2}}|0\rangle_6|0\rangle_8|0\rangle_9|2_H\rangle_{10}|1_V\rangle_{11}|1_V\rangle_{12}$$
$$+\frac{1}{8\sqrt{2}}|0\rangle_6|1_H\rangle_8|0\rangle_9|0\rangle_{10}|1_H1_V\rangle_{11}|1_V\rangle_{12}-\frac{1}{16\sqrt{2}}|0\rangle_6|0\rangle_8|0\rangle_9|0\rangle_{10}|2_H1_V\rangle_{11}|1_V\rangle_{12}$$
$$+\frac{1}{8}|0\rangle_6|1_H1_V\rangle_8|0\rangle_9|0\rangle_{10}|0\rangle_{11}|1_H1_V\rangle_{12}-\frac{1}{8\sqrt{2}}|0\rangle_6|1_V\rangle_8|0\rangle_9|0\rangle_{10}|1_H\rangle_{11}|1_H1_V\rangle_{12}$$
$$-\frac{1}{8\sqrt{2}}|0\rangle_6|1_H\rangle_8|0\rangle_9|0\rangle_{10}|1_V\rangle_{11}|1_H1_V\rangle_{12}+\frac{1}{16}|0\rangle_6|0\rangle_8|0\rangle_9|0\rangle_{10}|1_H1_V\rangle_{11}|1_H1_V\rangle_{12}$$
$$+\frac{1}{16}|0\rangle_6|1_V\rangle_8|0\rangle_9|0\rangle_{10}|0\rangle_{11}|2_H1_V\rangle_{12}-\frac{1}{32}|1_V\rangle_{11}|1_H\rangle_{12}{}^2|1_V\rangle_{12}$$
$$-\frac{1}{16}|2_H\rangle_6|0\rangle_8|0\rangle_9|0\rangle_{10}|0\rangle_{11}|2_V\rangle_{12}+\frac{1}{16}|0\rangle_6|2_H\rangle_8|0\rangle_9|0\rangle_{10}|0\rangle_{11}|2_V\rangle_{12}$$
$$+\frac{1}{16}|1_H\rangle_6|0\rangle_8|1_H\rangle_9|0\rangle_{10}|0\rangle_{11}|2_V\rangle_{12}-\frac{1}{32}|0\rangle_6|0\rangle_8|2_H\rangle_9|0\rangle_{10}|0\rangle_{11}|2_V\rangle_{12}$$
$$-\frac{1}{16}|1_H\rangle_6|0\rangle_8|0\rangle_9|1_H\rangle_{10}|0\rangle_{11}|2_V\rangle_{12}+\frac{1}{16\sqrt{2}}|0\rangle_6|0\rangle_8|1_H\rangle_9|1_H\rangle_{10}|0\rangle_{11}|2_V\rangle_{12}$$
$$-\frac{1}{32}|0\rangle_6|0\rangle_8|0\rangle_9|2_H\rangle_{10}|0\rangle_{11}|2_V\rangle_{12}-\frac{1}{16}|0\rangle_6|1_H\rangle_8|0\rangle_9|0\rangle_{10}|1_H\rangle_{11}|2_V\rangle_{12}$$

$$+\frac{1}{32}|0\rangle_6|0\rangle_8|0\rangle_9|0\rangle_{10}|2_H\rangle_{11}|2_V\rangle_{12}+\frac{1}{16}|0\rangle_6|1_H\rangle_8|0\rangle_9|0\rangle_{10}|0\rangle_{11}|1_H2_V\rangle_{12}$$
$$-\frac{1}{16\sqrt{2}}|0\rangle_6|0\rangle_8|0\rangle_9|0\rangle_{10}|1_H\rangle_{11}|1_H2_V\rangle_{12}+\frac{1}{32}|0\rangle_6|0\rangle_8|0\rangle_9|0\rangle_{10}|0\rangle_{11}|2_H2_V\rangle_{12} \tag{8.11}$$

Finally, six output modes after all parts of the system are mode-6, mode-8, mode-9, mode-10, mode-11, and mode-12. At this point, the interesting part comes up by the post-selection applied to these output states.

8.2.3 Post-Selection

This consideration is divided the post-selection into two levels:

Case I

The first one is a distinguish photon in each output mode with the absence of mode-6 and mode-8. This is a selection of null-states on mode-6 and mode-8. The condition filters the output states to be

$$\begin{aligned}|\text{CaseI}\rangle =&\frac{1}{16}|0\rangle_6|0\rangle_8|1_H1_V\rangle_9|1_H1_V\rangle_{10}|0\rangle_{11}|0\rangle_{12}\\ &-\frac{1}{16}|0\rangle_6|0\rangle_8|1_V\rangle_9|1_V\rangle_{10}|1_H\rangle_{11}|1_H\rangle_{12}\\ &-\frac{1}{16}|0\rangle_6|0\rangle_8|1_H\rangle_9|1_H\rangle_{10}|1_V\rangle_{11}|1_V\rangle_{12}\\ &+\frac{1}{16}|0\rangle_6|0\rangle_8|0\rangle_9|0\rangle_{10}|1_H1_V\rangle_{11}|1_H1_V\rangle_{12}.\end{aligned} \tag{8.12}$$

According to $|\text{CaseI}\rangle$, the states are divided to be a trigger and a working output. Two-folded coincidences are chosen as a trigger in our consideration. If mode-9 and mode-10 are chosen to be a trigger, the remainder is

$$|\text{CaseI}_{9,10}\rangle=\frac{1}{\sqrt{3}}\left(|0\rangle_{11}|0\rangle_{12}-|1_H\rangle_{11}|1_H\rangle_{12}-|1_V\rangle_{11}|1_V\rangle_{12}\right). \tag{8.13}$$

Similarly, if mode-11 and mode-12 are chosen to be a trigger, the remainder will be

$$|\text{CaseI}_{11,12}\rangle=\frac{1}{\sqrt{3}}\left(|0\rangle_{9}|0\rangle_{10}-|1_V\rangle_{9}|1_V\rangle_{10}-|1_H\rangle_{9}|1_H\rangle_{10}\right). \tag{8.14}$$

The other combinations of the trigger are mode-9 and mode-11, mode-10 and mode-12, mode-9 and mode-12, and mode-10 and mode-11. The remainder will be

$$
\begin{aligned}
|\text{CaseI}_{9,11}\rangle &= \frac{1}{\sqrt{2}}\left(|1_V\rangle_{10}|1_H\rangle_{12} + |1_H\rangle_{10}|1_V\rangle_{12}\right), \\
|\text{CaseI}_{10,12}\rangle &= \frac{1}{\sqrt{2}}\left(|1_V\rangle_{9}|1_H\rangle_{11} + |1_H\rangle_{9}|1_V\rangle_{11}\right), \\
|\text{CaseI}_{9,12}\rangle &= \frac{1}{\sqrt{2}}\left(|1_V\rangle_{10}|1_H\rangle_{11} + |1_H\rangle_{10}|1_V\rangle_{11}\right), \\
|\text{CaseI}_{10,11}\rangle &= \frac{1}{\sqrt{2}}\left(|1_V\rangle_{9}|1_H\rangle_{12} + |1_H\rangle_{9}|1_V\rangle_{12}\right),
\end{aligned} \tag{8.15}
$$

respectively.

From Eq.(8.13) to Eq.(8.15), bipartite-entangled states are presented here through the triggers as heralded parts. However, the obtaining states are divided into two cases by the selected efficiency after heralding. In Eq.(8.13) and Eq.(8.14), impure-bipartite-entangled states are obtained with 2/3 selected efficiency because of the first term, the vacuum state. On the other hand, by the other combinations of the trigger, pure-bipartite-entangled states are certainly obtained.

Case II

Next, the second condition is only a photon in each output mode. Therefore, the filtering output states are

$$
\begin{aligned}
|\text{CaseII}\rangle =& \frac{\sqrt{2}}{6}|0\rangle_6|0\rangle_8|1_V\rangle_9|1_V\rangle_{10}|1_H\rangle_{11}|1_H\rangle_{12} - \frac{\sqrt{2}}{6}|0\rangle_6|0\rangle_8|1_H\rangle_9|1_H\rangle_{10}|1_V\rangle_{11}|1_V\rangle_{12} \\
&-\frac{1}{3}|0\rangle_6|1_H\rangle_8|1_V\rangle_9|1_V\rangle_{10}|1_H\rangle_{11}|0\rangle_{12} - \frac{1}{3}|0\rangle_6|1_V\rangle_8|1_H\rangle_9|1_H\rangle_{10}|1_V\rangle_{11}|0\rangle_{12} \\
&+\frac{1}{8}|1_V\rangle_6|1_H\rangle_8|0\rangle_9|1_V\rangle_{10}|1_H\rangle_{11}|0\rangle_{12} - \frac{1}{8}|1_V\rangle_6|1_H\rangle_8|0\rangle_9|1_V\rangle_{10}|0\rangle_{11}|1_H\rangle_{12} \\
&+\frac{1}{8}|1_H\rangle_6|1_V\rangle_8|0\rangle_9|1_H\rangle_{10}|1_V\rangle_{11}|0\rangle_{12} + \frac{1}{3}|0\rangle_6|1_H\rangle_8|1_V\rangle_9|1_V\rangle_{10}|0\rangle_{11}|1_H\rangle_{12} \\
&-\frac{1}{8}|1_H\rangle_6|1_V\rangle_8|1_H\rangle_9|0\rangle_{10}|1_V\rangle_{11}|0\rangle_{12} - \frac{1}{8}|1_H\rangle_6|1_V\rangle_8|0\rangle_9|1_H\rangle_{10}|0\rangle_{11}|1_V\rangle_{12} \\
&+\frac{1}{3}|0\rangle_6|1_V\rangle_8|1_H\rangle_9|1_H\rangle_{10}|0\rangle_{11}|1_V\rangle_{12} + \frac{1}{8}|1_H\rangle_6|1_V\rangle_8|1_H\rangle_9|0\rangle_{10}|0\rangle_{11}|1_V\rangle_{12} \\
&-\frac{1}{3}|1_H\rangle_6|0\rangle_8|1_H\rangle_9|0\rangle_{10}|1_V\rangle_{11}|1_V\rangle_{12} - \frac{1}{3}|1_V\rangle_6|0\rangle_8|1_V\rangle_9|0\rangle_{10}|1_H\rangle_{11}|1_H\rangle_{12} \\
&+\frac{1}{3}|1_H\rangle_6|0\rangle_8|0\rangle_9|1_H\rangle_{10}|1_V\rangle_{11}|1_V\rangle_{12} + \frac{1}{3}|1_V\rangle_6|0\rangle_8|0\rangle_9|1_V\rangle_{10}|1_H\rangle_{11}|1_H\rangle_{12}
\end{aligned}
$$

$$-\frac{1}{8}|1_V\rangle_6|1_H\rangle_8|1_V\rangle_9|0\rangle_{10}|1_H\rangle_{11}|0\rangle_{12}+\frac{1}{8}|1_V\rangle_6|1_H\rangle_8|1_V\rangle_9|0\rangle_{10}|0\rangle_{11}|1_H\rangle_{12}. \tag{8.16}$$

Furthermore, the states are selected as a heralded state by combinations between two-folded coincidence and two absent modes. Thus, it can be shown that the bipartite-entangled states can be obtained. For example, the combination between the absence of modes 6 and 8 and two-folded coincidence of modes 9 and 10 as heralded states are chosen. The selecting states are

$$\left|\text{CaseII}_{\bar{6},\bar{8},9,10}\right\rangle = \frac{1}{\sqrt{2}}\left(|1_H\rangle_{11}|1_H\rangle_{12}+|1_V\rangle_{11}|1_V\rangle_{12}\right). \tag{8.17}$$

The other results can also be obtained by the other combinations of states. These selecting states are

$$|\text{CaseII}_\alpha\rangle = \frac{1}{\sqrt{2}}\left(|1_H\rangle_i|1_H\rangle_j+|1_V\rangle_i|1_V\rangle_j\right), \tag{8.18}$$

$$|\text{CaseII}_\beta\rangle = \frac{1}{\sqrt{2}}\left(|1_H\rangle_i|1_V\rangle_j+|1_V\rangle_i|1_H\rangle_j\right), \tag{8.19}$$

when i and j denote modes of the states and $i \neq j$. Eq. 8.18 and Eq. 8.19 are consistent with the Bell's states, $|\Psi^+\rangle$ and $|\Phi^+\rangle$, respectively. All of 54 combinations from Eq. 8.16 can be obtained the Bell's states. All states are pure-bipartite-entangled states by this condition.

8.2.4 Summary

This study is an extended idea from the generation of four-photon entanglement in Sec. 8.1. A simple schematic setup, which is made up by five beam-splitters and single-photon sources, is shown. Similarly, the specific input state, which is not an entangled state, is required. The initial input state is also two single-photons state into each mode. Two single-photons state is a horizontally polarized photon and a vertically polarized photon. By considering the combination of two absent modes (null-states) and two-folded coincidence, the output states are post-selected. These considerations divide the output states into heralded states and remainder states. The heralded states act as

a trigger to indicate the remainder states. The remainder states are shown by two conditions. The first condition is a distinguished photon in each output mode with the absence of mode-6 and mode-8. The second condition is only a photon in each output mode. The first condition gives impure-bipartite-entangled states and pure-bipartite-entangled states depending on the combination of the heralded state. The second condition gives only pure-bipartite-entangled states through all combinations between two-folded coincidence and two absent modes. Thus, bipartite entangled states with heralded generation can be obtained by linear-optical elements and single-photon sources.

CHAPTER IX

SUMMARY OF THE PROJECT II

Two schematic settings for entangled-state generation are shown. These schemes are based on linear-optical elements. The basic idea comes from the system proposing by Sheng *et al.* The modification of the initial input state is considered to generate four-photon entangled states. The modification is improved efficiency 1.33 times from the work of Sheng *et al.* Additionally, the extended idea from the four-photon scheme is shown to heralded generation of bipartite entangled states. The heralded states act as a trigger to indicate the remainder states in GHZ-states be considering the combination between null-states and two-folded coincidence. These two schemes are not necessarily depend on any nonlinear-optical process. They use only single-photon sources and linear-optical elements. This kind of entanglement is in term of position-time of particles. Thus, all generations can achieve more efficiency than the system basing on a nonlinear-optical process.

REFERENCES

Barnett, S., 2009 *Quantum Information (Oxford Master Series in Physics: Atomic, Optical, and Laser Physics)* (Oxford University Press, USA).

Barz, S., Cronenberg, G., Zeilinger, A. & Walther, P., 2010 "Heralded generation of entangled photon pairs," *Nature Photonics* **4**, 553–556.

Bennett, C. H. & DiVincenzo, D. P., 2000 "Quantum information and computation," *Nature* **404**, 247–255.

Boschi, D., Branca, S., De Martini, F., Hardy, L. & Popescu, S., 1998 "Experimental realization of teleporting an unknown pure quantum state via dual classical and einstein-podolsky-rosen channels," *Phys. Rev. Lett.* **80**, 1121–1125.

Bouwmeester, D., Pan, J., Daniell, M., Weinfurter, H. & Zeilinger, A., 1999 "Observation of Three-Photon Greenberger-Horne-Zeilinger entanglement," *Phys. Rev. Lett.* **82**, 1345.

Bouwmeester, D., Pan, J., Mattle, K., Eibl, M., Weinfurter, H. & Zeilinger, A., 1997 "Experimental quantum teleportation," *Nature* **390**, 575–579.

Bromberg, Y., Katz, O. & Silberberg, Y., 2009 "Ghost imaging with a single detector," *Phys. Rev. A* **79**, 053840.

Cai, Y. & Zhu, S.-Y., 2005 "Ghost imaging with incoherent and partially coherent light radiation," *Phys. Rev. E* **71**, 056607.

Cao, D.-Z., Xiong, J. & Wang, K., 2005 "Geometrical optics in correlated imaging systems," *Phys. Rev. A* **71**, 013801.

Dirac, P. A. M., 1982 *The Principles of Quantum Mechanics (International Series of Monographs on Physics)* (Oxford University Press, USA).

Einstein, A., Podolsky, B. & Rosen, N., 1935 "Can quantum-mechanical description of physical reality be considered complete?" *Phys. Rev.* **47**, 777–780.

Ekert, A. K., 1991 "Quantum cryptography based on bell's theorem," *Phys. Rev. Lett.* **67**, 661–663.

Erkmen, B. I. & Shapiro, J. H., 2008 "Unified theory of ghost imaging with gaussian-state light," *Phys. Rev. A* **77**, 043809.

Furusawa, A., Sorensen, J. L., Braunstein, S. L., Fuchs, C. A., Kimble, H. J. & Polzik, E. S., 1998 "Unconditional quantum teleportation," *Science* **282**, 706–709.

Gatti, A., Brambilla, E., Bache, M. & Lugiato, L. A., 2004a "Correlated imaging, quantum and classical," *Phys. Rev. A* **70**, 013802.

Gatti, A., Brambilla, E., Bache, M. & Lugiato, L. A., 2004b "Ghost imaging with thermal light: Comparing entanglement and classical correlation," *Phys. Rev. Lett.* **93**, 093602.

Gisin, N., Ribordy, G., Tittel, W. & Zbinden, H., 2002 "Quantum cryptography," *Rev. Mod. Phys.* **74**, 145–195.

Greenberger, D. M., Horne, M. A. & Zeilinger, A., 2007 "Going beyond bell's theorem," *eprint arXiv:0712.0921* In: 'Bell's Theorem, Quantum Theory, and Conceptions of the Universe', M. Kafatos (Ed.), Kluwer, Dordrecht, 69-72 (1989).

Hamilton, M. W., 2000 "Phase shifts in multilayer dielectric beam splitters," *Am. J. Phys.* **68**, 186.

Hong, C. K., Ou, Z. Y. & Mandel, L., 1987 "Measurement of subpicosecond time intervals between two photons by interference," *Phys. Rev. Lett.* **59**, 2044.

Jennewein, T., Simon, C., Weihs, G., Weinfurter, H. & Zeilinger, A., 2000 "Quantum cryptography with entangled photons," *Phys. Rev. Lett.* **84**, 4729–4732.

Kwiat, P. G., Mattle, K., Weinfurter, H., Zeilinger, A., Sergienko, A. V. & Shih, Y., 1995 "New High-Intensity source of Polarization-Entangled photon pairs," *Phys. Rev. Lett.* **75**, 4337.

Kwiat, P. G., Waks, E., White, A. G., Appelbaum, I. & Eberhard, P. H., 1999 "Ultrabright source of polarization-entangled photons," *Phys. Rev. A* **60**, R773.

Nielsen, M. & Chuang, I., 2000 *Quantum computation and quantum information*, Cambridge Series on Information and the Natural Sciences (Cambridge University Press).

Pan, J.-W., Daniell, M., Gasparoni, S., Weihs, G. & Zeilinger, A., 2001 "Experimental demonstration of four-photon entanglement and high-fidelity teleportation," *Phys. Rev. Lett.* **86**, 4435–4438.

Pittman, T. B., Shih, Y. H., Strekalov, D. V. & Sergienko, A. V., 1995 "Optical imaging by means of two-photon quantum entanglement," *Phys. Rev. A* **52**, R3429–R3432.

Podoshvedov, S. A., 2006 "Conditional preparation of x (2) macroscopic entangled states," *J. Exp. Theo. Phys.* **102**, 537–546.

Scarcelli, G., Berardi, V. & Shih, Y. H., 2007 "Scarcelli, berardi, and shih reply:," *Phys. Rev. Lett.* **98**, 039302.

Śliwa, C. & Banaszek, K., 2003 "Conditional preparation of maximal polarization entanglement," *Phys. Rev. A* **67**, 030101.

Sheng, Y., Deng, F. & Zhou, H., 2008 "Generation of multiphoton entangled states with linear optical elements," *Chinese Physics Letters* **25**, 3558–3561.

Shih, Y., 2007 "Quantum imaging," *Selected Topics in Quantum Electronics, IEEE Journal of* **13**, 1016–1030.

Shih, Y., 2008 "The physics of ghost imaging," *eprint arXiv:0805.1166* .

Shih, Y. H. & Alley, C. O., 1988 "New type of Einstein-Podolsky-Rosen-Bohm experiment using pairs of light quanta produced by optical parametric down conversion," *Phys. Rev. Lett.* **61**, 2921–2924.

Walther, P., Aspelmeyer, M. & Zeilinger, A., 2007 "Heralded generation of multiphoton entanglement," *Phys. Rev. A* **75**, 012313.

Wang, K. & Cao, D.-Z., 2004 "Subwavelength coincidence interference with classical thermal light," *Phys. Rev. A* **70**, 041801.

Wolfram Research, I., 2011 "Correlation - wolfram mathematica 8 documentation," `http://reference.wolfram.com/mathematica/ref/Correlation.html`.

APPENDICES

APPENDIX A

LIST OF ABBREVIATIONS

BBO Beta barium borate

CI Conventional Imaging

CW Continuous wave

EPR Einsten, Podosky, and Rosen

FWHM Full width at half maximum

GHZ Greenberger, Horne, and Zeilinger

GI Ghost Imaging

GSI Ghost Shadow Imaging

HOM Hong-Ou-Mandel

HWP Half-waveplates

PBS Polarizing beam-splitter

SPDC Spontaneous parametric down-conversion

APPENDIX B

CORRELATION FUNCTION

The correlation function calculates the relationship of two functions. In this thesis, the correlation means the cross-correlation of statistical function. The correlation function is given by, (Wolfram Research 2011),

$$\mathrm{Corr}_{X,Y}(x_1, y_1) = \frac{\mathrm{cov}_{X,Y}(x_1, y_1)}{\sqrt{\mathrm{var}(X)\mathrm{var}(Y)}}, \tag{B.1}$$

where $\mathrm{cov}_{X,Y}(x_1, y_1)$ is covariance between data X at point x_1 and data Y at point y_1, $\mathrm{var}(X)$ is variance of data X, and $\mathrm{var}(Y)$ is variance of data Y. The value of correlation lies between -1 to 1. The function are uncorrelated when the correlation value is 0, and they are correlated when the absolute of correlation is 1. (1 means absolute correlated and -1 means anti-correlated.)

APPENDIX C

SOURCE CODE

Code I

The following code was written in Mathematica 7.0.1. It is used to study a simulation of GSI.

```
(* Set Object *)
doubleSlit := Module[{aperture,i},
aperture:=If[1600<= i<= 1613|| 1671<= i<= 1684,1,0];

Table[aperture,{i,size1DDetector}]];
(* ListLinePlot[doubleSlit] *)

(* Light source profile function*)
profile1D [size1DDetector0_,point0_,sizeSpeckle0_]:=Module[ {
    randPoint,out,kern},

randPoint = Table[{RandomInteger[{1,size1DDetector0}],
    RandomReal[]},{i,1,point0}];

rawProfile1D = ConstantArray[0,size1DDetector0];
rawProfile1D = ReplacePart[rawProfile1D,Table[randPoint[[i
    ,1]]->randPoint[[i,2]],{i,1,point0}]];

kern =  Table[N[E^(-(i)^2/(2sizeSpeckle0^2))],{i,-
    size1DDetector0,size1DDetector0}];
out = ListConvolve[kern,rawProfile1D,1];


out];


ghostImage[size1DDetector0_,point0_,sizeSpeckle0_,
    sizeIteration0_]:= Module[
{result,sourceProfile,profileAfterObject,bucketDetector},

(* Light source profile *)
sourceProfile = Table[profile1D[size1DDetector0,point0,
    sizeSpeckle0],{sizeIteration0}];
(*
```

```
MatrixPlot[sourceProfile]
ListLinePlot[sourceProfile[[1]]]
*)

(* Measurement *)

profileAfterObject = Transpose[sourceProfile]*doubleSlit;
(* MatrixPlot[Transpose[profileAfterObject ]] *)
bucketDetector = Total[profileAfterObject];
(* ListLinePlot[bucketDetector] *)

(* Image reconstruction *)
jointDetection = sourceProfile*(bucketDetector-Mean[
    bucketDetector]);
(* MatrixPlot[jointDetection] *)

image= Total[jointDetection]/Max[Total[jointDetection]];
(*
ListLinePlot[{image},PlotRange->All]
ListLinePlot[{image,doubleSlit},PlotRange->All]
*)

(* Analysis part *)
similarity = Correlation[doubleSlit,image];
(* Print["Similarity = ",similarity*100,"%"] *)

backGround = SBarChart3D[ob,ChartLayout->"Grid"]BarChart3D[ob,
    ChartLayout->"Grid"]ort[(image-(image*doubleSlit)),Abs[#1]<
    Abs[#2]&][[29;;All]];
meanBackGround = Mean[backGround];
errorBackGround = StandardDeviation[backGround]/Sqrt[Dimensions
    [backGround][[1]]];

imageLevel = Sort[image*doubleSlit];
imageLevel = imageLevel[[Max[Position[imageLevel,0]]+1;;All]];
meanImageLevel = Mean[imageLevel];
errorImageLevel = StandardDeviation[imageLevel]/Sqrt[Dimensions
    [imageLevel][[1]]];

visibility = (meanBackGround+errorBackGround)/((meanImageLevel-
    errorImageLevel)-(meanBackGround+errorBackGround))100;
(* Print["Visibility = ",visibility,"%"] *)


{sizeSpeckle0,similarity*100,visibility,Total[jointDetection]}]
file = "D:\\Users\\Chronos\\Documents\\@Work\\Research\\OQPL\\
    Report_&_Present\\Present_and_Fullpaper_STT36_GShadow_sim\\
    Mathematica__simulation\\10point_per_speckle\\calc2";
```

```
sizeIteration = 300;
size1DDetector = 3000;
point = 500;
loopPerStep = 10;
sizeSpeckleStart=22;
sizeSpeckleEnd=25;
Timing[Table[{
result = Table[ghostImage[size1DDetector,point,sizeSpeckle,
    sizeIteration],{loopPerStep}];
Print[result[[All,1;;3]]];

Save[file<>"_"<>ToString[sizeSpeckle]<>".txt",{sizeIteration,
    size1DDetector,point,result}];

NotebookSave[];
Speak["Finished loop"<>ToString[sizeSpeckle]];
},{sizeSpeckle,sizeSpeckleStart,sizeSpeckleEnd}]][[1]]

NotebookSave[];
Speak["Jobs finished"]
In[273]:= size1DDetector=3000;

file = "D:\\Users\\Chronos\\Documents\\@Work\\Research\\OQPL\\
    My Paper\\LaTeX - 02 - GShadowSimulation\\Mathematica
    simulation\\simulation_result\\10point\\calc2";
In[275]:= (* Set Object *)
doubleSlit := Module[{aperture,i},
aperture:=If[1600<= i<= 1613|| 1671<= i<= 1684,1,0];

Table[aperture,{i,size1DDetector}]];
ListLinePlot[doubleSlit,PlotRange->{{1400,1900},{-0.6,1.2}},
    PlotStyle->Black,
Frame->True
(*,PlotLabel->Style["Double slits"],AxesLabel->{"x(Pixel)",""}
    *)
]
In[298]:= (* Retrieve parameters manual*)
fileNO =1;
Get[file<>"_"<>ToString[fileNO]<>".txt"];
result[[All,1;;3]]
ListLinePlot[result[[1,4]],PlotRange->{{1400,1900},All},
Frame->True
(*,PlotLabel->Style["Constructed image"],AxesLabel->{"x(Pixel)
    ","G(x)"}*)
]
ListLinePlot[{doubleSlit,result[[1,4]]/Max[result[[1,4]]]},
    PlotRange->{{1400,1900},All},PlotStyle->{{Black,Dashed},{Red
    }}
(*,Frame->True*)
```

```
,PlotLabel->Style["Constructed image (\[Sigma]=1)"],AxesLabel
    ->{"x(Pixel)","G(x)"}
]
In[796]:= (* Reanalyze visibility *)
(* This part combines calc2 and calc7 together *)
noiseRatio[inputImage_,loopPerStep0_,doubleSlit_]:=Module[{out,
    image2,backGround,meanBackGround,errorBackGround,imageLevel,
    meanImageLevel,errorImageLevel},

image2 = inputImage;

backGround = Table[Sort[(image2[[k]]-(image2[[k]]*doubleSlit)),
    Abs[#1]<Abs[#2]&][[29;;All]],{k,loopPerStep0}];
meanBackGround = Mean[Transpose[backGround]];
errorBackGround = StandardDeviation[Transpose[backGround]]/Sqrt
    [Dimensions[Transpose[backGround]][[1]]];
imageLevel = Table[Sort[image2[[k]]*doubleSlit],{k,loopPerStep0
    }];
imageLevel = Table[imageLevel[[k,Max[Position[imageLevel[[k
    ]],0]]+1;;All]],{k,loopPerStep0}];
meanImageLevel = Mean[Transpose[imageLevel]];
errorImageLevel = StandardDeviation[Transpose[imageLevel]]/Sqrt
    [Dimensions[Transpose[imageLevel]][[1]]];

(*out =Abs[(meanBackGround+Abs[errorBackGround])/((
    meanImageLevel+Abs[errorImageLevel])-(meanBackGround-Abs[
    errorBackGround]))];*)
out =Abs[(Abs[errorBackGround])/(meanImageLevel)];

out];

reanalyze[size1DDetector0_,file0_,file2_,fileNOStart0_,
    fileNOEnd0_,step0_,loopPerStep0_] := Module[{out,result1,
    result2,jointDetection2,similarity2,meanSimilarity,
    errorSimilarity,NR,meanNR,errorNR,discrepancyLevel,
    meanDiscrepancyLevel,errorDiscrepancyLevel},

(* Set Object *)
doubleSlit := Module[{aperture,k},
aperture:=If[1600<= k<= 1613|| 1671<= k<= 1684,1,0];

Table[aperture,{k,size1DDetector0}]];
(* ListLinePlot[doubleSlit] *)



Table[
Get[file0<>"_"<>ToString[fileNO]<>".txt"];
result1=result;
Get[file2<>"_"<>ToString[fileNO]<>".txt"];
```

```
result2=result;
If[fileNO==fileNOStart0,
jointDetection2 = {Join[result1[[All,4]],result2[[All,4]]]};
similarity2 = {Join[Abs[result1[[All,2]]/100],Abs[result2[[All
    ,2]]]/100]};
meanSimilarity = {Mean[Join[Abs[result1[[All,2]]/100],Abs[
    result2[[All,2]]/100]]]};
errorSimilarity = {StandardDeviation[Join[Abs[result1[[All
    ,2]]/100],Abs[result2[[All,2]]]]/100]/Sqrt[loopPerStep0]};
discrepancyLevel= {Join[1-Abs[result1[[All,2]]/100],1-Abs[
    result2[[All,2]]]/100]};
meanDiscrepancyLevel = {Mean[Join[(1-Abs[result1[[All,2]]/100])
    ,(1-Abs[result2[[All,2]]/100])]]};
errorDiscrepancyLevel = {StandardDeviation[Join[1-Abs[result1
    [[All,2]]/100],1-Abs[result2[[All,2]]]]/100]/Sqrt[
    loopPerStep0]};

NR = Join[noiseRatio[result1[[All,4]],10,doubleSlit],noiseRatio
    [result2[[All,4]],10,doubleSlit]];
meanNR = {Mean[NR]};
errorNR = {StandardDeviation[NR]};
,
jointDetection2=Join[jointDetection2,{Join[result1[[All,4]],
    result2[[All,4]]]}];
similarity2=Join[similarity2,{Join[Abs[result1[[All,2]]/100],
    Abs[result2[[All,2]]/100]]}];
meanSimilarity=Join[meanSimilarity,{Mean[Join[Abs[result1[[All
    ,2]]/100],Abs[result2[[All,2]]/100]]]}];
errorSimilarity=Join[errorSimilarity,{StandardDeviation[Join[
    Abs[result1[[All,2]]/100],Abs[result2[[All,2]]]]/100]/Sqrt[
    loopPerStep0]}];
discrepancyLevel=Join[discrepancyLevel,{Join[1-Abs[result1[[All
    ,2]]/100],1-Abs[result2[[All,2]]/100]]}];
meanDiscrepancyLevel = Join[meanDiscrepancyLevel,{Mean[Join[1-
    Abs[result1[[All,2]]/100],1-Abs[result2[[All,2]]/100]]]}];
errorDiscrepancyLevel = Join[errorDiscrepancyLevel,{
    StandardDeviation[Join[1-Abs[result1[[All,2]]/100],1-Abs[
    result2[[All,2]]]]/100]/Sqrt[loopPerStep0]}];

NR = Join[noiseRatio[result1[[All,4]],10,doubleSlit],noiseRatio
    [result2[[All,4]],10,doubleSlit]];
meanNR=Join[meanNR, {Mean[NR]}];
errorNR=Join[errorNR, {StandardDeviation[NR]}];

];
,{fileNO,fileNOStart0,fileNOEnd0,step0}];

out = {meanSimilarity,errorSimilarity,meanNR,errorNR,
    meanDiscrepancyLevel,errorDiscrepancyLevel};
```

```
out]
In[333]:= Needs["ErrorBarPlots`"]
In[808]:= file = "D:\\Users\\Chronos\\Documents\\@Work\\
    Research\\OQPL\\My Paper\\LaTeX - 02 - GShadowSimulation\\
    Mathematica  simulation\\simulation_result\\10point\\calc2";
file2 = "D:\\Users\\Chronos\\Documents\\@Work\\Research\\OQPL\\
    My Paper\\LaTeX - 02 - GShadowSimulation\\Mathematica
    simulation\\simulation_result\\20point\\calc7";
size1DDetector=3000;
fileNOStart = 1;
fileNOEnd = 40;
step = 1;
loopPerStep = 30;
Print["{meanSimilarity,errorSimilarity,meanNR,errorNR,
    meanDiscrepancyLevel,errorDiscrepancyLevel}"]
output = Transpose[reanalyze[size1DDetector,file,file2,
    fileNOStart,fileNOEnd,step,loopPerStep]]

Speak["Calculation completed!"]
In[350]:= ListPlot[1-output[[All,1]],PlotRange->All,PlotLabel->
    Style["Discrepancy level"],AxesLabel->{"\[Sigma]","
    Discrepancy level"}]
ListPlot[output[[All,3]],PlotRange->All,PlotLabel->Style["Noise
    ratio"],AxesLabel->{"\[Sigma]","Noise ratio"}]
ErrorListPlot[Transpose[{1-output[[All,1]],output[[All,2]]}],
    PlotRange->{All,{0,1}},AxesOrigin->{0,0},PlotStyle->Blue,
PlotLabel->Style["Discrepancy level"],AxesLabel->{"Peak size \[
    Sigma] (Pixels)","Discrepancy level"}
]
ErrorListPlot[output[[All,{3,4}]],PlotRange->All,AxesOrigin
    ->{0,0},PlotStyle->Blue,
PlotLabel->Style["Noise ratio"],AxesLabel->{"Peak size \[Sigma]
    (Pixels)","Noise ratio"}
]
In[366]:= Print["Max Err Sim = ",Max[output[[All,2]]]," @ ",
    Position[output[[All,2]],Max[output[[All,2]]]]]
Print["Min Err Sim = ",Min[output[[All,2]]]," @ ",Position[
    output[[All,2]],Min[output[[All,2]]]]]
Print["Max Err NR = ",Max[output[[All,4]]]," @ ",Position[
    output[[All,4]],Max[output[[All,4]]]]]
Print["Min Err NR = ",Min[output[[All,4]]]," @ ",Position[
    output[[All,4]],Min[output[[All,4]]]]]

Position[output[[All,1]],Max[output[[All,1]]]]
Position[output[[All,3]],Min[output[[All,3]]]]
In[602]:= numberOfPoint = fileNOEnd-fileNOStart+1;
pointStyle = Table[Graphics[{ColorData["RustTones",n/
    numberOfPoint*0.8],Opacity[0.5],Disk[{0,0}]}],{n,
    numberOfPoint}];
```

```
pointStyleShow = Table[Graphics[{ColorData["RustTones",n/
    numberOfPoint*0.8],Opacity[0.65],Disk[{0,0}]},ImageSize->
    Scaled[0.8]],{n,numberOfPoint}];
GraphicsGrid[Partition[Flatten[Table[{n,Show[pointStyleShow[[n
    ]],ImageSize->15]},{n,numberOfPoint}]],20],Frame->All
]
plotOutPut = Table[{output[[n,1]],output[[n,3]]},{n,
    numberOfPoint}];
ListPlot[plotOutPut,PlotRange->{{0,1},{0,0.005}},AxesOrigin
    ->{0,0},PlotMarkers->Table[{s,.03},{s,pointStyle}],
ImageSize->350,
PlotLabel->Style["Noise-ratio vs Discrepancy level"],AxesLabel
    ->{"Discrepancy level","Noise-ratio"}
]
In[537]:= plotOutPut2 = Table[{output[[n,1]],output[[n,3]]},{n
    ,40}];

rangeFrom = Table[Norm[plotOutPut2[[n]]-{1,0}],{n,40}];
Min[rangeFrom]
Position[rangeFrom,Min[rangeFrom]]
ListPlot[rangeFrom,PlotRange->{All,{0,1}},AxesOrigin->{0,0},
    PlotStyle->Brown,
PlotLabel->Style["Magnitude relative to the absolute value"],
    AxesLabel->{"Peak size \[Sigma] (Pixels)","Magnitude"}]
```

Code II

The following code was written in Mathematica 8.0. It is used to study a generation of photon-entangled states.

```
(*
[Ref: Chin.Phys.Lett.25, 3558, 2008]
"Generation of Multiphoton Entangled states with Linear Optical
    Elements"
*)
(* "input = |1h1vSubscript[>, 1] |1h1vSubscript[>, 2]" *)
(* port 1,2 -> port 3,4 with non-pol BS1 *)
(* def *)
Clear[ah3,av3,ah4,av4]

ah1 := 1/Sqrt[2] (ah3 - ah4)
av1 := 1/Sqrt[2] (av3 - av4)
ah2 := 1/Sqrt[2] (ah3 + ah4)
av2 := 1/Sqrt[2] (av3 + av4)

sol = Expand[(ah1)(av1) (ah2)(av2)];
```

```
Print["sol = ",sol];
sol = (ah3^2 av3^2)/4-(ah4^2 av3^2)/4-(ah3^2 av4^2)/4+(ah4^2
   av4^2)/4
(*
port 3 -> port 5,6 with BS2,
port 4 -> port 7,8 with BS3
*)
ah3 := 1/Sqrt[2] (ah5 - ah6)
av3 := 1/Sqrt[2] (av5 - av6)
ah4 := 1/Sqrt[2] (ah7 - ah8)
av4 := 1/Sqrt[2] (av7 - av8)

port = {{ah5,av5},{ah6,av6},{ah7,av7},{ah8,av8}};

sol2 = Expand[sol];
Print["sol2 = ",sol2];
sol2 = (ah5^2 av5^2)/16-1/8 ah5 ah6 av5^2+(ah6^2 av5^2)/16-(ah7
   ^2 av5^2)/16+1/8 ah7 ah8 av5^2-(ah8^2 av5^2)/16-1/8 ah5^2
   av5 av6+1/4 ah5 ah6 av5 av6-1/8 ah6^2 av5 av6+1/8 ah7^2 av5
   av6-1/4 ah7 ah8 av5 av6+1/8 ah8^2 av5 av6+(ah5^2 av6^2)
   /16-1/8 ah5 ah6 av6^2+(ah6^2 av6^2)/16-(ah7^2 av6^2)/16+1/8
   ah7 ah8 av6^2-(ah8^2 av6^2)/16-(ah5^2 av7^2)/16+1/8 ah5 ah6
   av7^2-(ah6^2 av7^2)/16+(ah7^2 av7^2)/16-1/8 ah7 ah8 av7^2+(
   ah8^2 av7^2)/16+1/8 ah5^2 av7 av8-1/4 ah5 ah6 av7 av8+1/8
   ah6^2 av7 av8-1/8 ah7^2 av7 av8+1/4 ah7 ah8 av7 av8-1/8 ah8
   ^2 av7 av8-(ah5^2 av8^2)/16+1/8 ah5 ah6 av8^2-(ah6^2 av8^2)
   /16+(ah7^2 av8^2)/16-1/8 ah7 ah8 av8^2+(ah8^2 av8^2)/16
posHigherOrder = Position[sol2, _^_Integer][[All,1]];
posHigherOrder = DeleteDuplicates[posHigherOrder];

Print["!! Filter out higer orders !!"];

sol2Pure1stOrder = Delete[sol2,Partition[posHigherOrder,1]];
Print["sol2Pure1stOrder = "sol2Pure1stOrder]
!! Filter out higer orders !!
sol2Pure1stOrder =  (1/4 ah5 ah6 av5 av6-1/4 ah7 ah8 av5 av6
   -1/4 ah5 ah6 av7 av8+1/4 ah7 ah8 av7 av8)
(*
Select positions of terms to delete
*)
pos =
Union[
Intersection[
Position[sol2Pure1stOrder,ah5 ][[All,1]],
Position[sol2Pure1stOrder,av5 ][[All,1]]
],
Intersection[
Position[sol2Pure1stOrder,ah6 ][[All,1]],
Position[sol2Pure1stOrder,av6 ][[All,1]]
```

```
],
Intersection[
Position[sol2Pure1stOrder,ah7 ][[All,1]],
Position[sol2Pure1stOrder,av7 ][[All,1]]
],
Intersection[
Position[sol2Pure1stOrder,ah8 ][[All,1]],
Position[sol2Pure1stOrder,av8 ][[All,1]]
]
];

Print["!! Exclude photons in same ports !!"];

selectedState = Delete[sol2Pure1stOrder,Partition[pos,1]];

Print["selectedState = ",selectedState];
!! Exclude photons in same ports !!
selectedState = -(1/4) ah7 ah8 av5 av6-1/4 ah5 ah6 av7 av8
```

Code III

The following code was written in Mathematica 8.0. It is used to study a heralded generation of bipartite entanglement.

```
(*
[Ref: Chin.Phys.Lett.25, 3558, 2008]
"Generation of Multiphoton Entangled states with Linear Optical
    Elements"
*)
(* "input = |hv> |hv>" *)
(* port 1,2 -> port 3,4 with non-pol BS1 *)
(* def *)
ClearAll["Global`*"]

in := (ah1)(av1) (ah2)(av2);

ah1 := 1/Sqrt[2] (ah3 - ah4)
av1 := 1/Sqrt[2] (av3 - av4)
ah2 := 1/Sqrt[2] (ah3 + ah4)
av2 := 1/Sqrt[2] (av3 + av4)

sol = Expand[in];

Print["sol = ",sol];
sol = (ah3^2 av3^2)/4-(ah4^2 av3^2)/4-(ah3^2 av4^2)/4+(ah4^2
   av4^2)/4
(*
```

```
port 3 -> port 5,6 with BS2,
port 4 -> port 7,8 with BS3
*)
ah3 := 1/Sqrt[2] (ah5 - ah6)
av3 := 1/Sqrt[2] (av5 - av6)
ah4 := 1/Sqrt[2] (ah7 - ah8)
av4 := 1/Sqrt[2] (av7 - av8)

ah5 := 1/Sqrt[2] (ah9 - ah10)
av5 := 1/Sqrt[2] (av9 - av10)
ah7 := 1/Sqrt[2] (ah11 - ah12)
av7 := 1/Sqrt[2] (av11 - av12)

port = {{ah6,av6},{ah8,av8},{ah9,av9},{ah10,av10},{ah11,av11},{
   ah12,av12}};

outAllposible = Expand[sol];
Print["outAllposible = ",outAllposible];
(* This last one is all out! *)
posHigherOrder = Position[outAllposible, _^_Integer][[All,1]];
posHigherOrder = DeleteDuplicates[posHigherOrder];

Print["!! Filter out higer orders !!\n"];

sol2Pure1stOrder = Delete[outAllposible, Partition[
   posHigherOrder,1]];
Print["sol2Pure1stOrder = "sol2Pure1stOrder]
!! Filter out higer orders !!

sol2Pure1stOrder =  (1/16 ah11 ah12 av11 av12+(ah10 ah6 av11
   av12)/(8 Sqrt[2])+(ah11 ah8 av11 av12)/(8 Sqrt[2])-(ah12 ah8
    av11 av12)/(8 Sqrt[2])-1/16 ah10 ah9 av11 av12-(ah6 ah9
   av11 av12)/(8 Sqrt[2])+(ah11 ah12 av10 av6)/(8 Sqrt[2])+1/8
   ah10 ah6 av10 av6+1/8 ah11 ah8 av10 av6-1/8 ah12 ah8 av10
   av6-(ah10 ah9 av10 av6)/(8 Sqrt[2])-1/8 ah6 ah9 av10 av6+(
   ah11 ah12 av11 av8)/(8 Sqrt[2])+1/8 ah10 ah6 av11 av8+1/8
   ah11 ah8 av11 av8-1/8 ah12 ah8 av11 av8-(ah10 ah9 av11 av8)
   /(8 Sqrt[2])-1/8 ah6 ah9 av11 av8-(ah11 ah12 av12 av8)/(8
   Sqrt[2])-1/8 ah10 ah6 av12 av8-1/8 ah11 ah8 av12 av8+1/8
   ah12 ah8 av12 av8+(ah10 ah9 av12 av8)/(8 Sqrt[2])+1/8 ah6
   ah9 av12 av8-1/16 ah11 ah12 av10 av9-(ah10 ah6 av10 av9)/(8
   Sqrt[2])-(ah11 ah8 av10 av9)/(8 Sqrt[2])+(ah12 ah8 av10 av9)
   /(8 Sqrt[2])+1/16 ah10 ah9 av10 av9+(ah6 ah9 av10 av9)/(8
   Sqrt[2])-(ah11 ah12 av6 av9)/(8 Sqrt[2])-1/8 ah10 ah6 av6
   av9-1/8 ah11 ah8 av6 av9+1/8 ah12 ah8 av6 av9+(ah10 ah9 av6
   av9)/(8 Sqrt[2])+1/8 ah6 ah9 av6 av9)
(* CASEI: Absence port6 and 8 *)
port68 =  Flatten[ {{ah6,av6},{ah8,av8}} ];
```

```
posAB68 = Union[
Flatten[
Table[
Position[sol2Pure1stOrder,port68[[i]] ][[All,1]]
,{i,Dimensions[port68][[1]]}
]
]
];

Print["\n!! CASEI: Absence port6 and 8 !! \n"];

stateAB68 = Delete[sol2Pure1stOrder,Partition[posAB68,1]];
Print["stateAB68 = ",stateAB68];

!! CASEI: Absence port6 and 8 !!

stateAB68 = 1/16 ah11 ah12 av11 av12-1/16 ah10 ah9 av11 av12
   -1/16 ah11 ah12 av10 av9+1/16 ah10 ah9 av10 av9



(* CASEII: the condition is only a photon in each output mode
   *)
(*
Select positions of terms to delete
*)
pos =
Union[
Flatten[
Table[
Intersection[
Position[sol2Pure1stOrder,port[[i,1]] ][[All,1]],
Position[sol2Pure1stOrder,port[[i,2]] ][[All,1]]
]
,{i,Dimensions[port][[1]]}]
]
];

Print["!! Exclude photons in same ports !!"];

state1PEP = Delete[sol2Pure1stOrder,Partition[pos,1]];

Print["state1PhotonEachPort = ",state1PEP];
!! Exclude photons in same ports !!
state1PhotonEachPort = (ah10 ah6 av11 av12)/(8 Sqrt[2])-1/16
   ah10 ah9 av11 av12-(ah6 ah9 av11 av12)/(8 Sqrt[2])+(ah11
   ah12 av10 av6)/(8 Sqrt[2])+1/8 ah11 ah8 av10 av6-1/8 ah12
   ah8 av10 av6+1/8 ah10 ah6 av11 av8-(ah10 ah9 av11 av8)/(8
   Sqrt[2])-1/8 ah6 ah9 av11 av8-1/8 ah10 ah6 av12 av8+(ah10
```

```
    ah9 av12 av8)/(8 Sqrt[2])+1/8 ah6 ah9 av12 av8-1/16 ah11
    ah12 av10 av9-(ah11 ah8 av10 av9)/(8 Sqrt[2])+(ah12 ah8 av10
     av9)/(8 Sqrt[2])-(ah11 ah12 av6 av9)/(8 Sqrt[2])-1/8 ah11
    ah8 av6 av9+1/8 ah12 ah8 av6 av9
posAB68L2 = Union[
Flatten[
Table[
Position[state1PEP,port68[[i]] ][[All,1]]
,{i,Dimensions[port68][[1]]}]
]
];

Print["!! AB68 !!"];

stateAB68L2 = Delete[state1PEP,Partition[posAB68L2,1]];

Print["state1PhotonEachPortAB68 = ",stateAB68L2];
!! AB68 !!
state1PhotonEachPortAB68 = -(1/16) ah10 ah9 av11 av12-1/16 ah11
    ah12 av10 av9
(* HERALDED by 11 and 12 *)
port1112 = {{ah11,av11},{ah12,av12}};

portHerald = Tuples[port1112];

posHerald =
Union[
Flatten[
Table[
Intersection[
Position[stateAB68L2,portHerald[[i,1]] ][[All,1]],
Position[stateAB68L2,portHerald[[i,2]] ][[All,1]]
]
,{i,Dimensions[portHerald][[1]]}]
]
];

Print["!! AFTER HERALDED !!"];

stateFinal = stateAB68L2[[posHerald]];

Print["stateFinal = ",stateFinal];
!! AFTER HERALDED !!
state1PhotonEachPort = -(1/16) ah10 ah9 av11 av12-1/16 ah11
    ah12 av10 av9
```

BIOGRAPHY

NAME	Mr. Theeraphot Sriarunothai
DATE OF BIRTH	August 11, 1987
PLACE OF BIRTH	Bangkok, Thailand
INSTITUTIONS ATTENDED	Mahidol University, 2005–2008 Bachelor of Science (Physics) Mahidol University, 2009–2012 Master of Science (Physics)
SCHOLARSHIPS	Development and Promotion of Science and Technology Talent Project, 2005–present Teaching assistant, Mahidol University, 2009–2011
HOME ADDRESS	652, Sintorn village, Happyland RD, Klongjan, Bangkapi, Bangkok, THAILAND, 10240
E-MAIL	T.Sriarunothai@gmail.com

PRESENTATION

- **"Four-Photon Entanglement Generation using Linear Optics"**

  The 37th Congress on Science and Technology of Thailand (STT37), Bangkok, Thailand
  (October 10 – 12, 2011)

- **"The Influence of the Characteristics of Light Source Profiles in Ghost Shadow Imaging"**

School and Workshop on New Trends in Quantum Dynamics and Entanglement, The Abdus Salam International Centre for Theoretical Physics (ICTP), Trieste, Italy
(February 14 – 25, 2011)
The 6th Siam Physics Congress 2011, Chonburi, Thailand
(March 23 – 26, 2011)

- **"Gaussian Convolution Model Simulation for Light Source Profile Generation in Ghost Shadow Imaging"**
The 36th Congress on Science and Technology of Thailand (STT36), Bangkok, Thailand
(October 26 – 28, 2010)

- **"Ghost Shadow Imaging using a Single-pixel Detector"**
The 5th Siam Physics Congress 2010, Kanchanaburi, Thailand
(March 24 – 27, 2010)

PROCEEDING

- Sriarunothai, T. and Singhsomroje, W. *"Four-Photon Entanglement Generation using Linear Optics"*, The 37th Congress on Science and Technology of Thailand, 2011. (Extended abstract submitted)

- Sriarunothai, T., Singhsomroje, W., Sinsarp, A., Chunwachirasiri, W., Wangsuya, S. *"Gaussian Convolution Model Simulation for Light Source Profile Generation in Ghost Shadow Imaging"*, The 36th Congress on Science and Technology of Thailand, 2010. (Extended abstract submitted)